Gadjah Mada University – Shizuoka University Joint Workshop on Telecommunications
Gadjah Mada University, Yogyakarta, Indonesia, December 2–7, 2013

A Study of Cooperative Sensing based on Energy Detection

Shunsuke FUJIMAKI†, Tadahiro WADA†, and Kaiji MUKUMOTO‡

†Graduate School of Engineering,
Shizuoka University
3-5-1 Johoku, Hamamatsu, 432-8561, JAPAN
Email: {f0230135,tetwada}@ipc.shizuoka.ac.jp

‡Faculity of Engineering,
Shizuoka University
3-5-1 Johoku, Hamamatsu, 432-8561, JAPAN

Abstract

For cognitive radio systems, one of important keys to make it possible to effectively utilize of frequency band is detection of the primary system. The energy detection is one of candidate of signal detection technologies. It is known that cooparating with other terminals makes performance better. In this paper we evaluate an effect of cooperative sensing. We show results of performance in cases that the number of cooperative terminals is fixed and is poisson distributed.

Index Terms—cognitive radio, cooperative sensing, energy detection

1. Introduction

Recently, a shortage of available frequency band by widely spreading of wireless apparatus is very serious problem all over the world. Since the frequency band which can be used by wireless communication is limited, it is possible that the frequency band which can be used is drained. However in some cases, since communication is not perfomed continuously with respect to time-course, there are a lot of vacant channels. If such vacant channels with respect to time-course can be used effectively, it is possible to increase efficiency of frequency use.

A cognitive wireless technology is one of candidates enabling to effectively use of frequency. The cognitive radio technology is an intelligent radio that can be programmed and configured dynamically. Its transceiver is designed to use the best wireless channels in its vicinity. This radio system automatically detects available channels in wireless spectrum, then changes its transmission or reception parameters to allow simultaneous transmissions in a given frequency band. Researches of the cognitive radio system sharing frequency are done briskly.

The terminal which can use a certain frequency band preferentially is defined as Primary Terminal(PT). The terminal which can not use a certain frequency band preferentially but can temporary use is defined as Secondary Terminal(ST). ST allows to use the frequency band, unless it interferes to the wireless system of PT. However PT will be affected if ST mistakenly communicates while PT is communicating. Therefore, it is important for ST to investigate whether PT is communicating or not in advance. One of the methods for judging whether communicating is performed in a certain frequency band is energy detection[1][2]. Energy detection is the method of judging whether PT communicating or not and compares the electric signal power at ST with a predetermind threshold value.

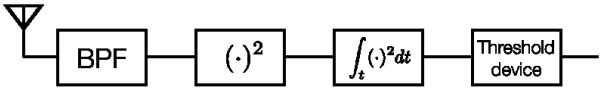

Figure 1: Structure of energy detection

In usual ST investigates signal power. However it is thought that a sensing by only one terminal, namely individual sensing, might be inaccurate because of fading, shadowing and so on. Then, it is expectable that the accuracy improves by sensing in cooperation with two or more terminals[3][4]. The sensing method by coorperation with plural terminals is called "Cooperative Sensing".

In this paper we evaluate an effect of cooperative sensing. We obtain results of performance evaluation in cases that the number of cooperative terminals is fixed and is poisson distributed.

2. Energy Detection

2.1. Procedures of Energy Detection

Figure 1 shows the receiver structure of energy detection. The energy detection is one of signal detection methodes. As compared with other methods, the energy detection has following merits:

· ST needs not to know PT modulation scheme, and

· Structure of energy detection is easy and low cost.

From Fig.1, the energy detection is performed by the following procedures:

1. The energy detection circuit receives a signal.
2. The signal is then band-pass-filtered whose band width is W. The filterd signal, $s(t)$, can be expressed as,

$$s(t) = \begin{cases} n(t) & \cdots H_0 \\ hs_{PT}(t) + n(t) & \cdots H_1 \end{cases} \quad (1)$$

where H_0 means the hypothesis that PT is not communicating and H_1 means that PT is communicating. h and $n(t)$ mean a chennel cofficient and an addictive noise, respectively.

3. The signal is then squared, $s(t)^2$.
4. After that, the signal is integrated over the interval T, i.e.,

$$\int_T s(t)^2 dt \simeq \sum_{i=1}^{2TW} a_i. \quad (2)$$

TW is a important parameter for the energy detection and called as the "degree of freedom".

5. Finally the signal is compared with the threshold δ.

If it higher than δ, ST decides PT is communicating. On the other hand, if it is lower than δ, ST decides PT is not communicating.

2.2. Issues of Detection Errors

The energy detection essentialy has two types of errors, "false alarm" and "miss detection". The "false alarm" means that ST mistakenly decides PT is communicating in spite of PT is not communicating. The "miss detection" means that ST mistakenly decides PT is not communicating in spite of PT is communicating. Probabilities of the "false alarm" and the "miss detection" under AWGN channels are expressed as[1],

$$P_{fa} = \frac{\Gamma(TW, \frac{\delta}{2})}{\Gamma(TW)}, \quad (3)$$

$$P_{md} = 1 - Q_{TW}(\sqrt{2TW\gamma}, \sqrt{\delta}), \quad (4)$$

where $\Gamma(,)$ denotes incomplete Gamma function and γ means SNR. The false alarm rate and miss detection rate are important factors for evaluating the performance of the energy detection.

3. Cooperative Sensing based on Energy Detection

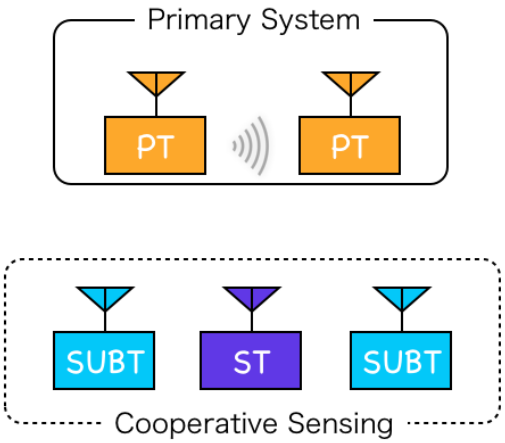

Figure 2: System model of cooperative sensing

3.1. System Model

Figure 2 shows a system model of cooperative sensing. SUBTs mean cooperative terminals for ST.
In this paper, since ST and SUBTs are assumed to be located at almost the same position relative to PT, SNR of all received signal by ST and SUBTs is considered to be the same. And to simplify the discussion, these terminals have the same degree of freedom of energy detection. ST reveives information of the energy detection from SUBTs and performs a synthetic decision.

3.2. Decision Rules for Cooperative Sensing

There are many decision rules for cooperative sensing. The following methods have been mainly considered as a synthetic decision method for cooperative sensing,

· Averaging-rule,

· AND-rule,

· OR-rule, and

· Majority-rule.

In this maniscript, we forcus on Averaging-rule. In Anveraging-rule, ST takes the average of all sensing values of ST and SUBTs, and compares it with a threshold δ. Firstly, ST and SUBTs perform energy detection and have a sensing value. Then, each SUBT transmits each sensing value to ST and ST calculates an average of all sensing values including the value obtained by ST itself. Finally, ST compares it with a threshold δ and decides judgement of cooperative sensing. The false alarm rate using Average-rule is denoted as,

$$P_{fa} = \frac{\Gamma((N+1)TW, \frac{(N+1)\delta}{2})}{\Gamma((N+1)TW)}, \quad (5)$$

Table 1: Assumptions

SNR	2.0[dB]
degree of freedom	5.0
Channel	AWGN
Number o trials	100000

where N means the number of SUBTs. The miss detection probability using Averaging-rule is denoted as,

$$P_{md} = 1 - Q_{(N+1)TW}(\sqrt{2(N+1)TW\gamma}, \sqrt{(N+1)\delta}). \quad (6)$$

AND-rule places importance on "false alarm". Firstly, ST and SUBTs perform energy detection. Then ST and all SUBTs individually make a decision whether PT is communicating or not. Next, ST collects all decisions from SUBTs. By AND-rule, ST finally decides PT is transmitting if ST and all SUBTs decide that PT is transmmitting.

OR-rule places importance on "miss detection". Firstly, similar to AND-rule, ST and SUBTs perform energy detection and they individually make a decision. By OR-rule, ST finally decides PT is transmitting if ST and all SUBTs decide that PT transmmitting.

Majority-rule is also simillar to AND-rule and OR-rule. Majoruty-rule takes majority of collected individual dicisions by ST.

4. Numerical Examples

In this section, we give some numerical exapmles to evaluate effect of cooperative sensing. We consider two cases as listed below:

- Case 1: cooperative sensing with fixed number of SUBTs
- Case 2: cooperative sensing when the number of SUBTs is Poisson distributed

Table 1 shows assumptions for numerical examples.

Figure 3 shows the performance of cooprative sensing with respect to the number of SUBTs. The vartical line shows the probability of miss detection and the horizontal line is the probability of false alarm. These lines can be obtained by changing theshold value, δ. From this figure, theotical analysys is rightly confirmed by the results of computer simulations. We can also find that characteristic of cooperating with larger number of terminals is better.

Figure 4 shows the effect of the number of SUBTs is not fixed and is distributed. From this figure, a characteristic of Case 2 is worse than a characteristic of Case 1 with $N = 2$. Both of Case 1 with $N = 2$ and Case 2 have the same average of SUBTs. It is because that, in Case 2, probability that the number of SUBTs is less than two is not so small, and the performance of the case is significantly affected by situation of small number of terminals. Therefore, we can consider that the performance is more strongly subject to the influence of the situation with few terminals.

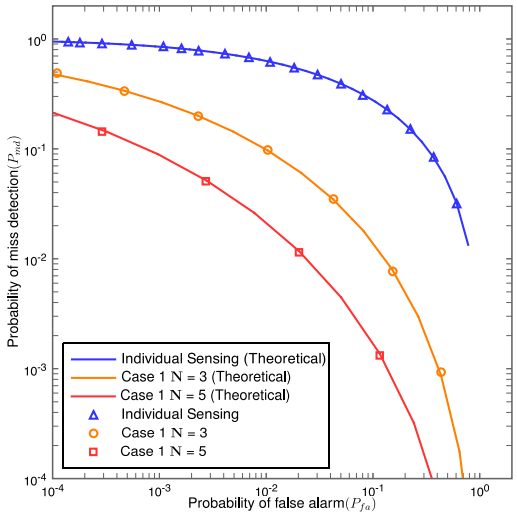

Figure 3: The effect of cooperative sensing with respect to the number of SUBTs.

5. Conclusion

We have shown the effect of cooperative sensing. We firstly introduced energy detection and dicision rules of cooperative sensing. Then we have evaluated the performance of cooperative sensing in cases that the number of SUBTs is fixed and Poisson distributed. As a result, we have shown that cooperative sensing with fixed number of SUBTs exhibits better performance.

References

[1] H.Urknowitz, "Energy Detection of Unknown Deterministic Signals," Proceedings of the IEEE Vol.55, No.4, pp.523-531, 1967

[2] F. Digham, M. Alouini, and M. Simon, "On the energy detection of unknown signals over fading channels," Proceedings the IEEE International Conference on Communications 2003(ICC2003), Vol.5, pp.3575-3579, 2003

[3] S.Kyperountas, et.al, "Performance Analysis of Cooperative Spectrum Sensing in Suzuki Fading

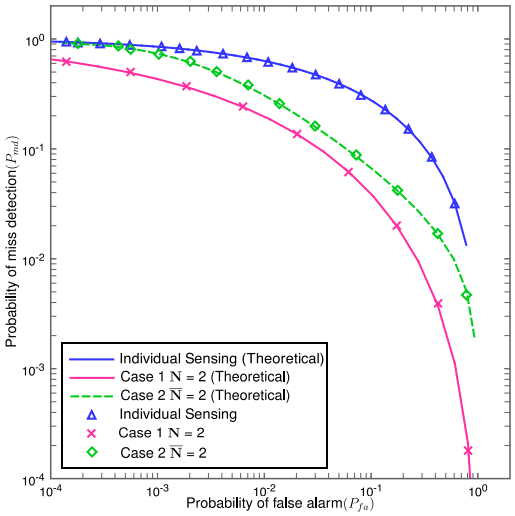

Figure 4: The effect of coopertive sensing when the number of SUBTs is Poisson distributed.

Channels," Cognitive Radio Oriented Wireless Networks and Communications 2007, pp.428-432, 2007

[4] Jayakrishnan Unnikrishnan, "Cooperative Sensing for Primary Detection in Cognitive Radio," Proceedings of the IEEE Vol.2, No.1, pp.18-27, 2008

Gadjah Mada University – Shizuoka University Joint Workshop on Telecommunications
Gadjah Mada University, Yogyakarta, Indonesia, December 2–7, 2013

Introduction to Controller Area Network Communication

Junya WATANABE†, Tadahiro WADA†, Kaiji MUKUMOTO‡

†Faculty of Engineering,
Shizuoka University
3-5-1 Johoku, Hamamatsu, 432-8561, JAPAN
Email:{f0011149, tetwada} @ipc.shizuoka.ac.jp

‡Division of Technical Services,
Shizuoka University
3-5-1 Johoku, Hamamatsu, 432-8561, JAPAN

Abstract

In this paper, we introduce Controller Area Network(CAN) used as the standard of in-vehicle networks. And we describe the partial protocol of CAN. In particular, we explain an arbitration which is one of the important characteristic structures in CAN.

1. Introduction

In the second half of the 1970s to the 1980s, electronization of cars started as backgrounds of the emission control and fuel regulation on cars. From those days, electronic control of cars has been developed instead of mechanical control. By using the electric control, precise controls of the mixture ratio of air and fuel, and the optimal engine ignition timing can be achieved. However, while control facilities of cars increase, electronic components increase and weight and a space of wiring also increase. An in-vehicle network, which can reduce wiring cost, is a system which controls broadly cars such as a power train system, a body system, and a comfortable equipment system. The network also improves safety, reliability, tolerance to external factors, cost for driving cars.

There are various protocols of in-vehicle networks. Controller Aria Network(CAN) is a serial bus system developed for in-vehicle networks, and it is widely spread as an in-vehicle network protocol. CAN can realize reduction of wiring cost and the weight saving of cars by adopting bus communication between two or more Electric Control Units (ECUs) instead of wire harness.

Nowadays, with the increase in functions we ask for, the number of ECUs is increasing every year. The electronic control system of cars, therefore, becomes complicated and large-scaled. To realize the control having additional functions such as car navigation systems, parking assists, etc, and to improve the basic movement of cars about a run or a drive such as engine control, the brakes assistance, etc, large number of ECUs should be required. In particular, high real-time nature is required in the control system concerning a run or a drive. However, with increase in number of the deployment of ECUs, communication capacity of CAN may be short. Especially, an electronic control system for a hybrid fuel cars and an electric vehicle requires high transmission capability.

In this study, we aim to recognize the protocols of CAN to improve the capability of communications.

2. The protocol of CAN

In this chapter, we briefly introduce features of CAN.

2.1. Line type structure

Generally, communications equipment connected to network is called a node. In the case of an in-vehicle network, an ECU becomes a node. CAN is adopted a line type. Since the line type can constitute a network from connecting each node to bus simply, the network becomes simple and the design of it is easy.

2.2. Multi-master system

CAN is adopted the "multi-master method" which can realize equal bus access priority for every node connected to the bus. If the bus is vacant, every node can start transmission of data.

2.3. Access method

Usually, if data is freely transmitted by two or more nodes, a collision of data will occur.

However, this cannot be prevented when data is simultaneously transmitted to bus from two or more nodes.

CAN adopts the media access method similar to CSMA/CD which is adopted by Ethernet. The difference between CAN and Ethernet comes from that real-time nature is more important for CAN. From the structure of CSMA/CD, transmissions are interrupted if a collision is detected, and after having waited at a certain random time, the node retransmits the message. In this case, however, communication delay occurs and causes degradation of communication performance.

On the other hand, in CAN, a concept of a priority of frame is applied. If frames are simultaneously transmitted from two or more nodes, a high priority of a frame can continue transmission. By applying such the structure, a frame with a high priority can be transmitted to bus without being delayed.

2.4. ID(Idetifier)

In Ethernet, origin of transmission address and destination address are included the transmitted frame. On the other hand, there is no such concept in CAN. Instead, CAN is applied a concept of the identifier(ID). An ID is added to the transmitted frame, and this ID shows the kind of contents of data and the priority of frame. When frames are simultaneously transmitted from two or more nodes, the node which continues transmission and the node which should wait for transmission are determined by comparing their IDs. This operation is called "arbitration".

2.5. Arbitration

2.5.1. Bus level

In CAN, frames consist of binary digits. Signals of 0s and 1s are called as "Dominant"and "Recessive", respectively. Dominant means "being preferential", and the value of a bus will become dominant if this value is outputted from at least one node. On the other hand, Recessive means "being receptive", and the value of a bus will become recessive if the output from all the nodes is recessive.

2.5.2. Frame structure

In CAN, there are four kinds of frames as listed below:

- **Data frame**
- **Remote frame**
- **Error frame**
- **Overload frame**

In the data frame and the remote frame, there are two kinds of formats, a standard format and an expansion format. A standard format has 11 bits of the ID, and an expansion format has 29 bits of the ID. In this paper, we take up a standard format for examples.

1. Data frame

A data frame is used in order to transmit data. This frame consists of seven fields. The structure of a data frame is shown in Fig.1.

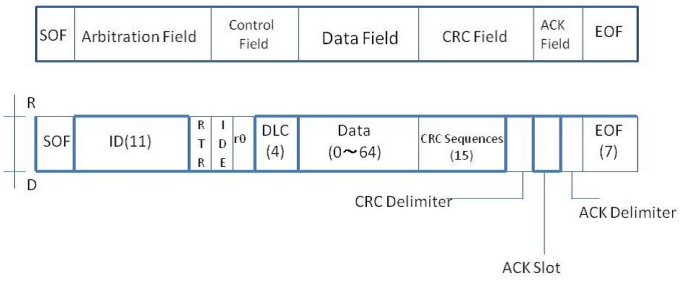

Figure 1: The structure of a data frame

The seven fields in a data frame is listed below.

- SOF(Start of frame)
- Arbitration field
- Control field
- Data field
- CRC[1] field
- ACK field
- EOF(End of frame)

SOF shows the start of a frame. SOF serves as a 1-bit dominant bit.

The arbitration field consists of an identifier (ID) and a RTR (Remote Transmission Request) bit[2].

Here, the length of the identifier is specified as 11 bits by the standard format. An identifier is transmitted from the Most Significant Bit(MSB). It is forbidden that all of top 7 bits are recessive. Moreover, the identifier must be unique, that is, different roles of frames have different IDs.

The control field consists of 6 bits. 4 bits out of 6 bits are a data length code(DLC0∼DLC3), and remaining 2 bits are used as reservation for future extension. A data length code determines the length (0 to 8 bytes) of the data field.

A data field consists of data to transmit and it is transmitted from most significant bit. As explained, the number of bytes of data varies 0 to 8 bytes.

[1]Cyclic Redundancy Check

[2]RTR expresses distinction between a data frame and a remote frame. In the case of a data frame, the value of a RTR bit is Dominant. In contrast, the value of a RTR bit becomes Recessive for a remote frame.

The CRC field is a field to check errors in the frame and it consists of 15 bits CRC sequence and a 1-bit CRC delimiter which is the bits as distinction with the ACK field.

The ACK field is the field for reporting that the transmitted message is rightly received by receivers. It consists of 2 bits: 1 bit for ACK slot and 1-bit for ACK delimiter.

EOF shows the end of a frame.

2. Remote frame

A remote frame is a frame for requesting transmission of a data frame for other nodes. Difference between the data frame and remote frame is only the existence of a data field or not. The structure of a remote frame is shown below.

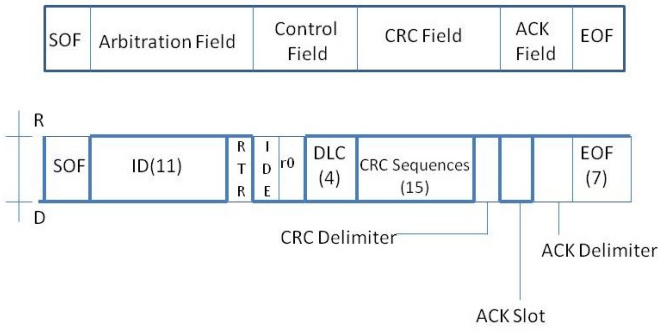

Figure 2: The structure of remote frame

- SOF(Start of frame)
- Arbitration field
- Control field
- CRC field
- ACK field
- EOF(End of frame)

The contents of each field are fundamentally the same as the data frame, except for the value of RTR.

3. Error frame

The error frame is a format in the case that a node detects an error and it notifies the error.

4. Overload frame

An overload frame is transmitted in the cases that:

- when the internal state of a receiving node requires delay of the following data frame or a remote frame and,
- when the bit which becomes dominant is detected in inter-frame space. [3]

2.5.3. The process of the arbitration

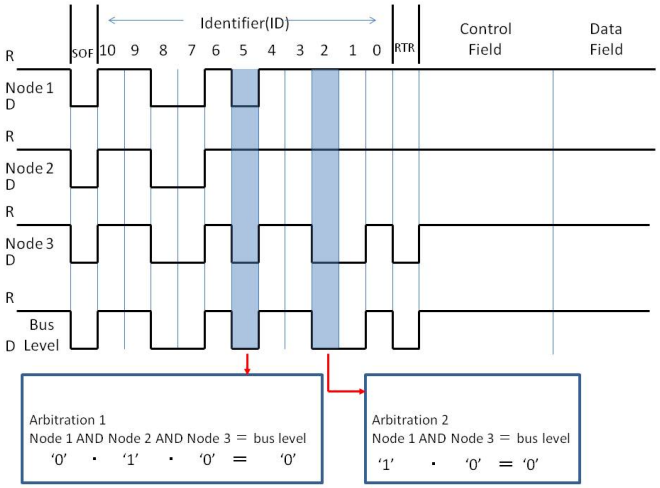

Figure 3: An arbitration of CAN

Figure 3 shows the state diagram that three nodes connected to the network try to transmit their messages simultaneously. Their message frames of CAN start with SOF and the bus level at this time is dominant.

Then, the identifier of the arbitration field is transmitted. The arbitration begins from the MSB of this identifier.

Every node can monitor the bus level. In the case shown in Fig.3, the 10th bit of ID is the same, i.e., Recessive, for all nodes.

Thus , the bus level corresponds to the 10th bit is recessive.

In this figure, from 10th to 6th bits, all nodes have the same bit level. Thus by monitoring the bus line, all nodes judge that they can continue transmission.

At the 5th bit in arbitration field, we can see that Nodes 1 and 3 transmits Dominant signal and Node 2 transmits Recessive signal. While having transmitted the identifier, a logical product (AND) is taken for every bit, and the arbitration is performed.

The logical product at the 5th bit is "0" because at least one node sends Dominant signal, "0". As a

[3] Between a certain data frame and the data frame (or remote frame) which comes to the next, it is specified that the space more than a triplet is provided and it dissociates, and this is called inter-frame space.

result, the bus level at the 5th bit becomes Dominant. By monitoring the bus level, Node 2 can find that the bit which Node 2 transmits is different from the bus level. In this case, Node 2 stops its transmission.

Similarly, Node 1 stops transmission at the 2nd bit in the arbitration field. Finally Node 3 can transmit its frame by this arbitration.

3. A micro computer system modeling CAN

Figure 4: PIC-CAN 360 Evaluation Board

Fig.4 shows the PIC-CAN 360 Evaluation Board, made by Micro Application Laboratory, Inc. Three nodes are put on this board. One of three nodes becomes CAN communication monitor. Furthermore, we can see a CAN bus by connecting USB and a PC.

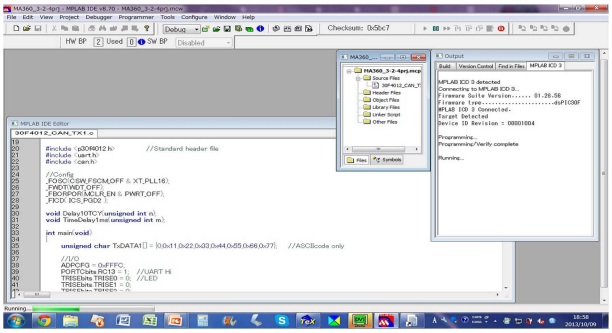

Figure 5: MPLAB IDE

Fig.5 shows the screen shot of programming software, MPLAB IDE. It is provided by Microchip Technology, Inc, and is used for writing a program.

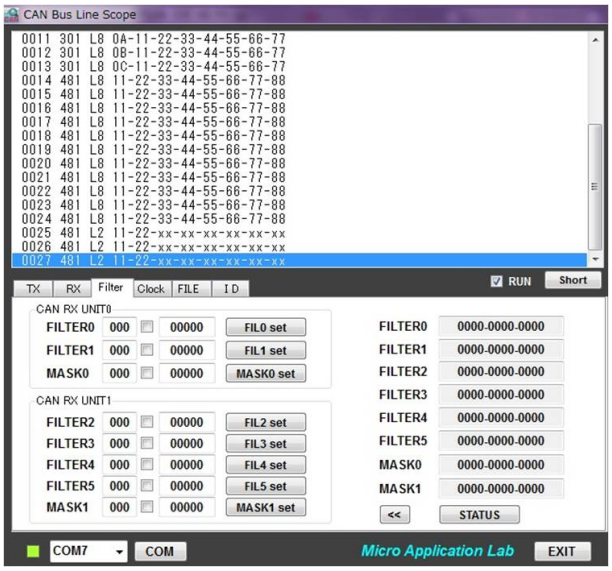

Figure 6: CAN Bus Line Scope

Fig.6 shows a screen shot of CAN Bus Line Scope. We can monitor a data flowing through a bus.

4. Conclusion

We have described the outline of CAN and explained that CAN is required for high transmission capacity by electronization of cars.

And then, we have explained the structure of the arbitration of CAN.

Finally, we have introduced the environment equipment for understanding structure of CAN.

References

[1] S. Igarashi, M. Sato, R. Tamashiro, "CAN introduction lecture, The CAN protocol and programming which are studied with an inclusion microcomputer", Dempa Shimbun, 2008.

[2] M. Sato, "In-vehicle network system thoroughness description, The protocol of CAN, LIN, and FlexRay, and mounting " , CQ publishing company, 2005.

[3] A. Ogawa, 「PIC CAN Technical Guide」, Micro Application Laboratory Inc..

[4] "What is CSMA/CA ?, IT glossary binary",
`http://www.sophia-it.com/content/CSMA/CA`

[5] "What is CSMA/CD ?, IT glossary binary",
`http://www.sophia-it.com/content/CSMA/CD`

[6] "Insider's Computer Dictionary:CSMA/CD",
http://www.atmarkit.co.jp/icd/root/96/5787296.html

[7] "MPLAB®ICD 3 In circuit debugger User's guide", Microchip Technology Inc.,
http://akizukidenshi.com/download/ds/microchip/DS51766A_JP.pdf

[8] Dr.Conal Watterson, "Application Note, The mounting guide of CAN application （Japanese version）",
http://www.analog.com/static/imported-files/jp/application_notes/AN-1123_jp.pdf

[9] "The outline of CAN, and the feature of FUJITSU CAN",
http://edevice.fujitsu.com/jp/catalog/find/18-1j/pdf/j18-1-2.pdf

[10] "First CAN", Vector Japan Inc.,
http://download.vector-japan.co.jp/portal/medien/cmc/beginners/For_Beginners_CAN.pdf

Gadjah Mada University – Shizuoka University Joint Workshop on Telecommunications
Gadjah Mada University, Yogyakarta, Indonesia, December 2–7, 2013

Studies on Performance Evaluation of a Remote Monitoring System Using Meteor Burst Communications

Yasuhiro TAKEUCHI[†], Kaiji MUKUMOTO[‡], and Tadahiro WADA[†]

[†]Graduate School of Engineering,
Shizuoka University
3-5-1 Johoku, Hamamatsu, 432-8561, JAPAN
Email: f0330121@ipc.shizuoka.ac.jp

[‡]Division of Technical Service, Shizuoka University.
3-5-1 Johoku, Hamamatsu, 432-8561, JAPAN

Abstract

Meteor Burst Communications(MBC) is one of beyond line of sight communication modes, which is known to have many advantages for systems with delay tolerance and low data transmission rate. This paper considers a remote monitoring system collecting fixed-length monitored data in a fixed period from many remote stations deployed in large area to one master station by using MBC. In this paper, we propose a data transmission protocol for this system, named random transmission scheme, and evaluate the performance of the scheme by numerical analyses and computer simulations. Optimization of the transmission probability is also investigated.

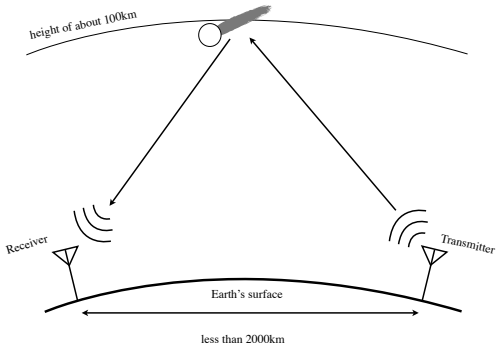

Figure 1: Meteor burst communication

1. Introduction

Meteors are space dust particles entering the earth's atmosphere. Although most of the meteors cannot be seen by naked eyes, billions of tiny meteors enter the earth's atmosphere daily. When a meteor enters the earth's atmosphere, an ionized gas column (meteor burst) is generated at the height of about 100 kilo meters. The typical length of a meteor burst is several tens kilo meters. Meteor bursts disappear in a few seconds due to diffuse. However, during its brief existence, a meteor burst works as good reflection medium of radio waves in low VHF band (30-100MHz) and enables over-the-horizon communication between two stations within 2,000 kilo meters. (See Figure 1).

Meteor bursts are roughly classified into two categories: "under-dense burst" and "overdense burst" according to the reflection properties. The typical received signal level variations reflected from an underdense burst and an overdense burst are shown in Figures 2 and 3, respectively. The received signal level from an underdense burst exhibits abrupt increment at the instance of the meteor burst occurrence and attenuates exponentially with time. The overdense burst is characterized by relatively long duration time.

Defference of the reflection properties depends on electron line density of the meteor burst. The boundary value is about 2×10^{12}[electrons/m] and the value corresponds to a meteor burst generated by a space dust particle of several milligrams. The number of meteors is inversely proportional to the weight of space dust particles. Therefore, most of the meteor bursts are underdense burst.

Among a great number of meteors entering the earth's atmosphere, only those entering at proper location and correct orientation support communication between two specific points. From past experiments, it is known that the generation interval depends on exponential distribution with the average of several tens seconds.

Duration time of a meteor burst differs from burst to burst. It is known that the duration time also depends on exponential distribution with the average of several hundreds milli seconds.

This paper considers an MBC network which collects monitoring data from many remote stations to one master station in a fixed time period.

The rest of this paper is organized as follows: In Section 2, we describe a meteor burst channel model, ON-OFF channel, assumed throughout the paper. We

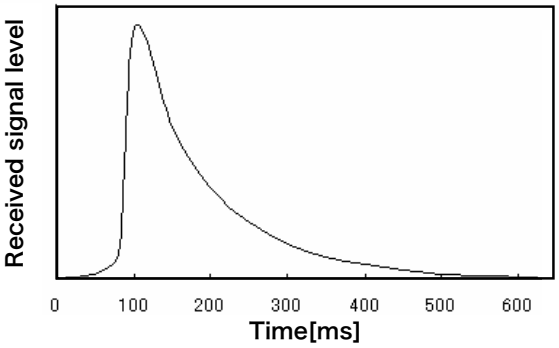

Figure 2: Underdense burst

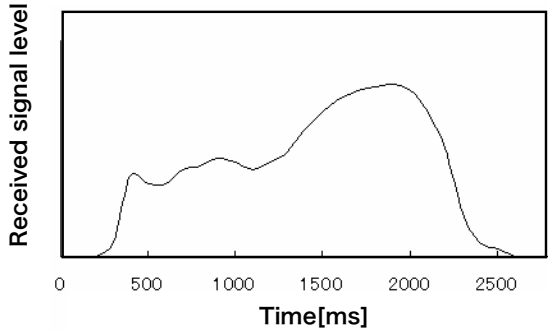

Figure 3: Overdense burst

briefly descirbe a remote monitoring system using MBC and propose our transmission protocol for the system in Section 3. In addtion, Section 3 gives the performance analysis of the protocol. In Section 4, the performance of the transmission protocol is evaluated by numerical results. Finally, in Section 5, we conclude this paper.

2. Channel model

Generation of a meteor burst channel and its duration time are probabilistic. Both generation interval and duration time of the meteor burst channel for two stations follow exponential distributions as stated previously. Here, we denote the averages of generation interval and duration time by $1/l_0$ and $1/m_0$, respectively. The values of $1/l_0$ and $1/m_0$ depend on various factors, such as system transmit power, frequency, antenna beam width, and communication range. Moreover, as for $1/l_0$, there are significant diurnal and seasonal variations.

For the purposes of analysis and/or simulations, various channel models are proposed. In this paper, in order to evaluate the fundamental performance of the MBC network, we adopt the simplest model called ON-OFF channel model.

In the ON-OFF channel model, the state of the channel for two stations is supposed to be one of two states:

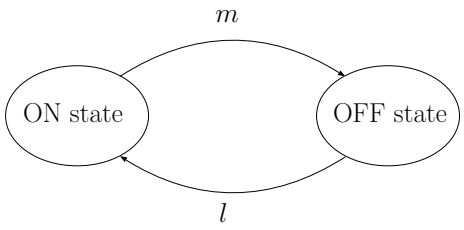

Figure 4: The state transition diagram of the ON-OFF model

open state (ON state) and closed state (OFF state), as shown in Figure 4. A packet transmitted in ON state is supposed to be succeeded in transmission, if there is no collision with other packets. The signal transmitted in OFF state is not received at all. The state of the channel is assumed to change according to a Markov process, and the state transition rate m from ON state to OFF state and the state transition rate l from OFF state to ON state are set constant. That is, the channel in OFF state will be in ON state after the time exponentially distributed with the average of $1/l$ seconds, and the channel in ON state will be in OFF state after the exponentially distributed time with the average of $1/m$ seconds. Due to the noise of the receiver circumference, the value of $1/l$ is bigger than the abovementioned $1/l_0$, and the typical value will be about several minutes from tens of seconds. However, it is known that the average duration time of meteor bursts hardly changes even if the detection threshold value changes and typical value of $1/m$ is hundreds of milli seconds which are almost the same typical as $1/m_0$.

3. The remote monitoring system using MBC

In this paper, we consider an MBC network which collects monitoring data periodically generated in many remote stations to one master station in a fixed time T, called observation period. Let us denote the total number of remote stations as M. Each remote station is assumed to generate monitoring data simultaneously. Generated monitoring data are contained in a fixed length packet. If the packet can not succeed in transmission within the observation period T, it is discarded.

As the transmission protocol of such an MBC data acquisition system, various schemes such as repetition transmission scheme[3], polling scheme, and power control scheme[5] have been proposed. Polling scheme can further be classified into individual polling, group

polling , and global polling schemes. In the literature [4], numerical analysis and computer simulations are performed to compare the performance of such polling schemes and it is shown that the group polling scheme outperforms other schemes. However, in order to keep the number of remote stations in a group optimal, the group polling scheme requires group reorganization, which may become a heavy burden. In this paper, we thus propose another approach, random access type global polling scheme, as is explained below.

3.1. The random transmission scheme

In the random access type global polling scheme, the master station transmits polling packets addressing to all the remote stations. A remote station transmits its data packet responding to the polling packet when it has a packet to be transmitted. Polling packets in global polling scheme are always addressed to all the remote stations and the role is to examine the existence of the meteor burst channel. Therefore, global polling packet is also called probe packet (PP). Since remote stations which received PP always return their data packets (DP), collision may occurs when more than one remote stations transmit DP simultaneously. Thus, in this paper, we propose random transmission scheme in which a remote station received PP sends DP by probability p to reduce the packet collision. When the master station receives the data packet, it returns an Ack (acknowledge) packet (AP) including the remote station ID. The remote station which succeeded in reception of the AP will be in hibernation and does not respond to PP till the next observation period.

3.2. Performance analysis

Figure 5 shows an example of data collection process in the random transmission scheme. The PP length, the DP length, the AP length, and the waiting time of DP response are denoted by d_{P}, d_{D}, d_{A}, and d_{W}, respectively. Let us consider the case where n remote stations are left in not receiving AP, i.e., $(M-n)$ remote stations are in sleeping state. The average time until any one of n remote stations succeeds in DP transmission and it receives the AP is represented by $\bar{\mathrm{T}}_{\mathrm{s}}(n)$. The average time until all of n remote stations succeed in AP reception is expressed by $\bar{\mathrm{T}}_{all}(n)$. Then, the following recurrence equation obviously holds.

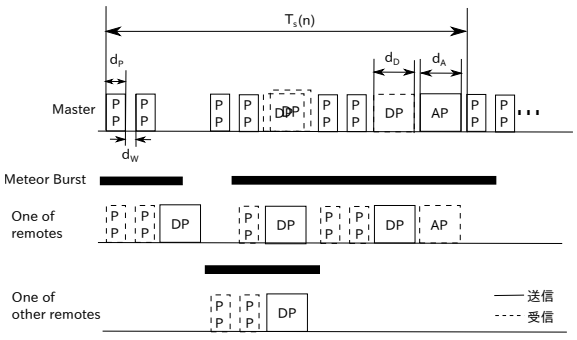

Figure 5: The example of data collection process in the random transmission scheme

$$\bar{\mathrm{T}}_{all}(n) = \bar{\mathrm{T}}_{all}(n-1) + \bar{\mathrm{T}}_{\mathrm{S}}(n) \tag{1}$$

Therefore, the average time until all M stations succeed in reception of AP is obtained by the next equation.

$$\bar{\mathrm{T}}_{all}(M) = \sum_{n=1}^{M} \bar{\mathrm{T}}_{\mathrm{S}}(n) \tag{2}$$

In the following, we show the calculation of $\bar{\mathrm{T}}_{\mathrm{s}}(n)$. The average number of DPs responded to a PP is called traffic and denoted by $G(n)$ when the remaining number of remote stations is n. Moreover, the traffic per remote station is denoted by $g(n)$. Then, the average transmission interval of PP, $\bar{\mathrm{T}}_{\mathrm{P}}(n)$, is calculated by the next equation.

$$\bar{\mathrm{T}}_{\mathrm{P}}(n) = d_{\mathrm{P}} + d_{\mathrm{W}} + d_{\mathrm{D}} \cdot \mathrm{S}_{\mathrm{D}}(n) + d_{\mathrm{A}} \cdot \mathrm{S}_{\mathrm{DS}}(n) \cdot \exp(-m d_{\mathrm{D}}) \tag{3}$$

Here, $\mathrm{S}_{\mathrm{D}}(n)$ is the probability that at least one DP is transmitted corresponding to a PP, and is given by the next equation.

$$\mathrm{S}_{\mathrm{D}}(n) = 1 - (1 - g(n))^n \tag{4}$$

$\mathrm{S}_{\mathrm{DS}}(n)$ is the probability that AP is transmitted, that is, the probability that transmission of the DP is successful and it is given by the next equation.

$$\mathrm{S}_{\mathrm{DS}}(n) = n g(n)(1 - g(n))^{n-1} \cdot \exp(-m d_{\mathrm{D}}) \tag{5}$$

If $\bar{\mathrm{T}}_{\mathrm{P}}(n)$ is given, the traffic per remote station, $g(n)$, can be estimated as follows. The period until the channel state between one remote station and the master station changes from OFF state to ON state and returns to the OFF state again is called channel cycle. From the assumption of the ON-OFF channel model, the average number of the PP transmissions within one channel cycle is given by $(1/l + 1/m)/\bar{\mathrm{T}}_{\mathrm{P}}(n)$. Therefore, if the average number $\bar{N}_{\mathrm{D}}$ of DP transmitted from the remote station within one channel cycle is found, the DP transmission probability, or $g(n)$, will be given by the next equation.

$$g(n) = \frac{\bar{\mathrm{T}}_{\mathrm{P}}(n) \cdot \bar{\mathrm{N}}_{\mathrm{D}}(n)}{1/l + 1/m} \tag{6}$$

Here, $\bar{N}_{\mathrm{D}}(n)$ can be calculated using the next expression.

$$\bar{N}_{\mathrm{D}}(n) = \sum_{i=0}^{\infty} \Pr(N_{\mathrm{D}} > i) \tag{7}$$

Each remote station succeeds in PP reception when the channel state to the master station is in ON-state. Therefore, the probability $\Pr(k)$ that the number of PP receptions within a channel cycle is k can be estimated by the next equation, where X is a random variable expressing the duration time of the ON state.

$$\begin{aligned} \Pr(k) &= \Pr\{k\bar{\mathrm{T}}_{\mathrm{P}}(n) < X < (k+1)\bar{\mathrm{T}}_{\mathrm{P}}(n)\} \\ &= \exp(-mk\bar{\mathrm{T}}_{\mathrm{P}}(n))\{1 - \exp(-m\bar{\mathrm{T}}_{\mathrm{P}}(n))\} \end{aligned} \tag{8}$$

The probability that the remote station transmits DP more than once in this channel cycle is given by the next equation.

$$\mathrm{P}_{\mathrm{DT}\bar{0}}(k) = 1 - (1-p)^k \tag{9}$$

Next, let us calculate the probability of transmitting DP twice or more. Since PP is not received during the DP transmission, if DP is transmitted, the number of the PP reception will decrease. The decreased number of PP reception, h, is estimated by

$$h = \frac{d_{\mathrm{D}}}{\bar{\mathrm{T}}_{\mathrm{P}}(n)}. \tag{10}$$

The probability that the remote station transmits DP exactly once within the channel cycle is given by

$$\mathrm{P}_{\mathrm{DT1}}(k) = \begin{cases} 1 - (1-p)^k & (k \le h) \\ (k-h)p(1-p)^{k-h} & (k > h). \end{cases} \tag{11}$$

Since the probability that the remote station transmits DP twice or more in the channel cycle is obtained by subtracting the probability that the remote station sends DP just once from the probability of DP transmitting two or more times in the case of $k > h$ and multiplying the probability that the first transmission is failure, it is given by the next equation.

$$\mathrm{P}_{\mathrm{DT}\bar{0}\bar{1}}(k) = (\mathrm{P}_{\mathrm{DT}\bar{0}}(k) - \mathrm{P}_{\mathrm{DT1}}(k)) \cdot \{1 - (1 - g(n))^{n-1}\} \tag{12}$$

Therefore, in the equation (7), if the probability that the DP is transmitted three or more times within one channel cycle is ignored and $g(n)$ is calculated using the equation (6), the next equation is obtained.

$$\begin{aligned} g(n) &= \frac{\bar{\mathrm{T}}_{\mathrm{P}}(n)}{1/l + 1/m} \cdot \left\{ \sum_{k=1}^{\infty} \mathrm{P}_{\mathrm{DT}\bar{0}}(k) \cdot \Pr(k) \right. \\ &\quad \left. + \sum_{k=h+1}^{\infty} \mathrm{P}_{\mathrm{DT}\bar{0}\bar{1}}(k) \cdot \Pr(k) \right\} \\ &= \frac{\bar{\mathrm{T}}_{\mathrm{P}}(n)}{1/l + 1/m} \left[\frac{p \cdot \exp(-m\bar{\mathrm{T}}_{\mathrm{P}}(n))}{1 - (1-p) \cdot \exp(-m\bar{\mathrm{T}}_{\mathrm{P}}(n))} \right. \\ &\quad \left. + \frac{p^2 \cdot \exp(-m(h+2)\bar{\mathrm{T}}_{\mathrm{P}}(n))\{1 - (1 - g(n))^{n-1}\}}{\{1 - (1-p) \cdot \exp(-m\bar{\mathrm{T}}_{\mathrm{P}}(n))\}^2} \right] \end{aligned} \tag{13}$$

The final value of $g(n)$ and $\bar{\mathrm{T}}_{\mathrm{P}}(n)$ are numerically calculated from simultaneous equations (3) and (13). If $g(n)$ is found, the probability that the master station succeeds in reception of DP and the AP is received in the remote station is given by the next equation.

$$\mathrm{S}_{\mathrm{A}}(n) = ng(n)(1-g(n))^{n-1} \cdot \exp(-m(d_{\mathrm{D}} + d_{\mathrm{A}})) \tag{14}$$

Therefore, when the remaining number of remote stations are n, the average time needed for arbitrary remote station to receive AP is found as follow.

$$\bar{\mathrm{T}}_{\mathrm{S}}(n) = \frac{\bar{\mathrm{T}}_{\mathrm{P}}(n)}{\mathrm{S}_{\mathrm{A}}(n)} + d_{\mathrm{D}} + d_{\mathrm{A}} \tag{15}$$

3.2.1. The optimal value of DP transmission probability

Let denote the optimal DP transmission probability which minimizes the average time $\bar{\mathrm{T}}_{\mathrm{S}}(n)$ of equation (15) as p_{opt}. The system traffic $G(n)$ is given by

$$G(n) = ng(n) \tag{16}$$

The equation (14) can be simplified when $G(n) \gg md_{\mathrm{D}}, md_{\mathrm{A}}$ by using the approximation of $(1 - g(n))^{n-1} \simeq \exp(-G)$. Then, the equation (15) becomes a function only depending on G as follows:

$$\bar{\mathrm{T}}_{\mathrm{S}}(n) \simeq \frac{d_{\mathrm{P}} + d_{\mathrm{W}} + d_{\mathrm{D}} \cdot \{1 - \exp(-G)\}}{G \cdot \exp(-G)} + d_{\mathrm{D}} + d_{\mathrm{A}} \tag{17}$$

The next equation is given by differentiating the equation (17) with G and putting it to 0.

$$\frac{d_{\mathrm{D}}}{d_{\mathrm{P}} + d_{\mathrm{W}} + d_{\mathrm{D}}} = (1 - G) \cdot \exp(G) \tag{18}$$

The G which satisfies the equation (18) is the optimal traffic G_{opt} and G_{opt} does not depend on the number of remaining remote stations. The optimal traffic g_{opt} per remote station is given by substituting G_{opt} for the

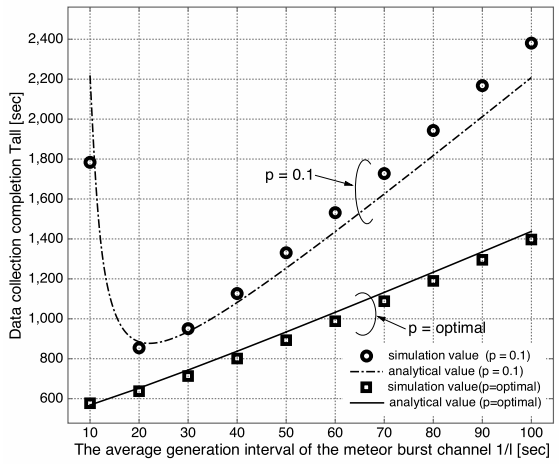

Figure 6: $\bar{\mathrm{T}}_{all}$ VS. $1/l$ (in the random transmission scheme)

equation (16). The corresponding average PP transmission interval is approximated by the next equation from the equation (3).

$$\bar{\mathrm{T}}_{\mathrm{P}opt} = d_{\mathrm{P}} + d_{\mathrm{D}} \cdot \{1 - \exp(-G_{opt})\} + d_{\mathrm{A}} \cdot G_{opt} \cdot \exp(-G_{opt}) \tag{19}$$

The optimal value p_{opt} of the DP transmission probability can be calculated by substituting g_{opt} and $\bar{\mathrm{T}}_{\mathrm{P}opt}$ to the equation (13) and solving it for p. By assuming that PP is transmitted at random, it can also be approximated as follows.

$$p_{opt}(n) \simeq g_{opt}(n) \cdot \left(1 + \frac{m}{l}\right) \cdot \exp(m d_{\mathrm{P}}) \tag{20}$$

4. Performance evaluation

In this chapter, we show the performance evaluation of the random transmission scheme by using a numerical example. In the followings, we set the total number M of remote stations at 2000 stations, and $d_{\mathrm{P}} = 0.01$ [sec], $d_{\mathrm{W}} = 0.02$ [sec], $d_{\mathrm{D}} = 0.03$ [sec], and $d_{\mathrm{A}} = 0.03$ [sec], respecvtively. Moreover, the average duration time of meteor bursts is set at 0.3[sec]. In a simulation, transmission-and-reception swichover time s and the radio wave propagation time a are taken into consideration as $s = 0.003$ [sec] and $a = 0.0063$ [sec].

Figure 6 shows $\bar{\mathrm{T}}_{all}$ versus $1/l$. The dashed line in the figure expresses the analytical value when the DP transmission probability p is fixed at 0.1. The solid line expresses the analytical value when p is controlled to the optimal value which is given by the equation (20). Marks ∘ and □ are simulation results for the cases of $p = 0.1$ and p_{opt}, respectively.

The figure shows that both simulation results are well approximated by their the analytical curves. In the case of $p = 0.1$, the time required to collect monitoring data from all the remote stations when $1/l = 10$ [sec] is longer than that when $1/l = 20$ [sec]. This is caused by increment of DP collisions. However, by controlling the DP transmission probability p to the optimal value using equation (20), the data collection completion time is kept in short.

5. Conclusion

In this paper, we have proposed a data transmission protocol suitable for a remote monitoring system using MBC network named random transmission scheme. We also have shown the optimal control method for DP transmission probability in the random transmission scheme.

By introducing random transmission in global polling scheme, we have succeeded to mitigate the DP collision problem. We evaluate the delay time required to collect monitoring data from all the remote stations by numerical analysis and computer simulations. By controlling the DP transmission probability at the optimal value, the probability of the DP collision is further reduced and thus the performance improvement is acheived.

References

[1] J.Z.Schanker, Meteor Burst Communication, Artech House, Boston 1990.

[2] A. Fukuda, Meteor burst communications, Corona Publishing, Tokyo, 1997 (in Japanese).

[3] K. Mukumoto, A. Fukuda, "Data Collecting System with Unattended Sensors via Meteor Burst Channel, " IEICE Trans. (B), vol.J68-B, no.6, pp.670-677, June 1985 (in Japanese).

[4] M. Nagasawa, K. Mukumoto, A. Fukuda, "Analysis of Data Collection System via Meteor Burst Channel, "IEICE Trans.(B-I), vol.79-B-I, no.6, pp.424-435, June 1996 (in Japanese).

[5] M. Nagasawa, K. Mukumoto, A. Fukuda, "Properties of Meteor Burst Channel and Power Controlled Probe, " IEICE Trans.(B-II), vol.J81-B-II, no.11, pp.1038-1047, Nov. 1998 (in Japanese).

Study on Go-Back-i-symbol ARQ Scheme Joint Workshops

Shotaro ITOH[†], Kaiji MUKUMOTO[‡], and Tadahiro WADA[†]

[†]Faculty of Engineering,
Shizuoka University
3-5-1 Johoku, Hamamatsu, 432-8561, JAPAN

[‡]Division of Technical Services,
Shizuoka University
3-5-1 Johoku, Hamamatsu, 432-8561, JAPAN

Abstract

In this paper, we introduce of Go-Back-i-symbol-ARQ scheme which is symbol-wise retransmission. The GBi-ARQ scheme is proposed in MBC, and the GBi-ARQ scheme exhibits better performance than the GBN-ARQ scheme.

1. Introduction

Today, wireless communications are used in various scenes. However, compared to wired communication links, wireless communication channels suffer from a number of problems such as ambient noise, fadings, interferences, etc. Thus, in general, we cannot use wireless communications without error control. Error control schemes can be classified into three categories: Forward Error Correction (FEC), Automatic Repeat reQuest (ARQ), and their combination, i.e., Hybrid-ARQ (HARQ). The schemes in each of these categories are actively studied for various communication systems.

In this paper, we present a sort of HARQ scheme named Go-Back-i-symbol ARQ (GBi-ARQ), which was proposed by our laboratory[1]. In conventional ARQ schemes, data are transmitted in block manner and block-wise retransmission is performed when error is detected. In the GBi-ARQ scheme, transmission data are sequentially encoded by a convolutional encoder and symbol-wise retransmission is achieved by evaluating the reliability of decoded data using modified Viterbi Algorithm(VA) [3].

The GBi-ARQ scheme was proposed for Meteor Burst Communications (MBC)[2]. MBC is one of beyond line of sight communication techniques which uses reflections from ionized meteor trails called meteor bursts. In MBC, channels open randomly and the received signal power passed through the channel mostly exponentially decays with time. Due to intermittent nature of the meteor burst channel, errors tend to occur in the tail part of a packet. Therefore, the GBi-ARQ scheme, which can evaluate the reliability of received data and perform symbol-wise retransmission if the reliability is not enough, is very suitable for MBC.

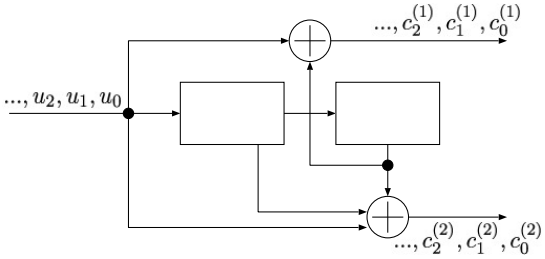

Figure 1: Example of the convolutional encoder, R=3,K=3

The rest of this paper is organized as follows. Section 2 describes convolutional code, Section 3 describes Viterbi algorithm. Section 4 explains GBi-ARQ scheme and shows the algorithm for GBi-ARQ scheme by Viterbi algorithm modified. Secotion 5 shows the performance of GBi-ARQ shceme in MBC. Finaly, Section 6 concludes the paper.

2. Convolutional Code

In this section, we briefly explain the forward error correcting code used in the GBi-ARQ scheme, i.e., convolutional code. An encoder for a non-recursive binary convolutional code consists of m shift-registers and v modulo-2 adders. Input bits are shifted along the registers one bit at a time. Output bits are obtained by adding the current input value and/or values in specified registers. The maximum number of input symbols affecting the current output value is called constraint length K and it is given by m+1. Code rate for a convolutional code, R, is defined as the number of input bits divided by the number of output bits at each time step.

Figure 1 shows an example of the encoder for a convolutional code with R=1/2 and K=3. Input bit sequence $\boldsymbol{u} = (u_0, u_1, u_2, ...)$ is fed into the leftmost register. Then, the elements of the output bit sequence

$\boldsymbol{c} = (c_0^{(1)}, c_0^{(2)}, c_1^{(1)}, c_1^{(2)}, ...)$ are obtained by the following equations:

$$c_i^{(1)} = u_i \oplus u_{i-2} \quad (1)$$

$$c_i^{(2)} = u_i \oplus u_{i-1} \oplus u_{i-2} \quad (2)$$

It is convenient to denote the input and output sequences as polynomials:

$$U(D) = u_0 + u_1 D + u_2 D^2 + \cdots \quad (3)$$

and

$$C^{(j)}(D) = c_0^{(j)} + c_1^{(j)} D + c_2^{(j)} D^2 + \cdots \quad (4)$$

Then, by using generator polinomials

$$g^{(1)}(D) = 1 + D^2, g^{(2)}(D) = 1 + D^1 + D^2, \quad (5)$$

we can express the above operations as

$$C^{(j)}(D) = g^{(j)}(D)U(D). \quad (6)$$

Note that the convolutional encoder in Figure1 is specified by the generator matrix

$$G(D) = [g^{(1)}(D), g^{(2)}] = [1 + D^2, 1 + D + D^2]. \quad (7)$$

3. Viterbi Algorithm

The GBi-ARQ scheme uses modified VA explained in the next section. We thus review ordinary VA in this section. The VA was proposed by Andrew J. Viterbi as a maximum likelihood decoding algorithm for convolutional codes.

In the followings, we explain the algorithm by using a simple example. Transmitted data are assumed to be encoded by a convolutional encoder in Figure1. Usually, the registers start with all zero state and a code sequence is terminated at all zero state by sending m dummy zeros. The trellis diagram corresponding the encoder is shown in Figure 2. In the figure, nodes S_0, S_1,S_2, and S_3 correspond to internal states of the encoder. Branches expressed by solid and broken lines correspond to code elements produced by input bit 0 and 1, respectively. The corresponding input bit and code symbol are shown beside each branch. For example, 1/01 represents that a code symbol 01 is produced by an input bit 0.

Each branch in the trellis diagram has a value called branch metric. Branch metric expresses a log likelihood of the code symbol of the branch for the received symbol. Path metric is calculated by adding the branch metrics along the path. At each node at each level, VA selects the path having the largest metric and discards the other paths. The selected paths are called survivors. The decoder repeats the same operation until the final level. Since codes are assumed to be terminated at all zero state, there is only one survivor at the final level. The final survivor is clearly the path having the largest metric, so that the code sequence corresponding to the final survivor is the maximum likelihood estimate for the received sequence.

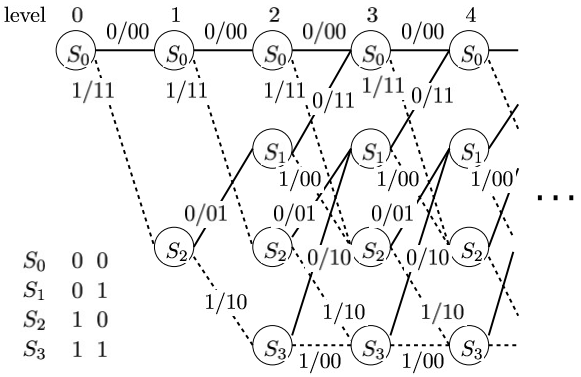

Figure 2: Trellis diagrom for Viterbi algorithm

Here, we consider the Viterbi decoder in a practical application. The code sequence is assumed to be modulated by the binary phase shift keying (BPSK) and transmitted over additive white Gaussian noise (AWGN) channel with one sided noise spectral density N_0. Let us denote the i-th channel symbol by x_i which takes values $+1$ or -1 corresponding to a code symbol element 1 and 0, respectively. In this case, the normalized output r_i of the i-th received symbol from the optimum receiver is given by

$$r_i = \sqrt{2E/N_0} + n_i \quad (8)$$

where E is a signal energy per symbol and n_i is a Gaussian random variable with zero mean and unit variance. It is known that $x_i r_i$ serves as a sufficient measure for the log likelihood function. Thus, we can use $x_i r_i$ instead of $\ln Pr(ri|xi)$.

In the example of Figure 2, the i-th code symbol is constructed by two elements,$c_i^{(1)}, c_i^{(2)}$.

Therefore, denoting the corresponding channel symbol as $\boldsymbol{x}_i = (x_i^{(1)}, x_i^{(2)})$ and its receiver output as ,$\boldsymbol{r}_i = (r_i^{(1)}, r_i^{(2)})$ the branch metric corresponding to is given by

$$m_i(\boldsymbol{c}_i) = \boldsymbol{x}_i \cdot \boldsymbol{r}_i = x_i^{(1)} y_i^{(1)} + x_i^{(2)} y_i^{(2)}. \quad (9)$$

4. GBi-ARQ scheme

The GBi-ARQ scheme was proposed by our laboratory as a symbol-wise HARQ scheme. In conventional ARQ schemes such as GBN-ARQ scheme, data are transmitted in block manner and block-wise retransmission is performed when error is detected. On

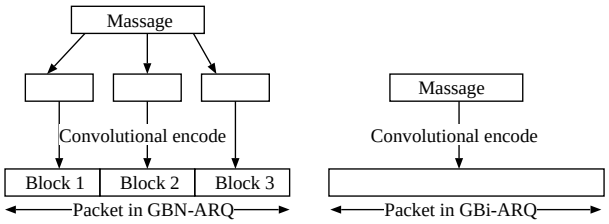

Figure 3: Packet structure in GBN-ARQ and GBi-ARQ schemes.

the other hand, in the GBi-ARQ scheme, transmission data are sequentially encoded by a convolutional encoder and symbol-wise retransmission is achieved by evaluating the reliability of decoded data using modified VA as described below.

The modified VA is also explained by a trellis diagram. Similar to the ordinary VA, at each node on the trellis diagram, a path with the largest metric among the paths merging into the node is selected as a survivor. However, it is different from the ordinary VA that the survivor survives with label X if the difference between the metrics of the survivor and the others is smaller than a threshold U, a predetermined positive constant. Label X indicates that the path is unreliable and it is not removed as long as the path survives.

This procedure is continued until the best survivor, i.e., the survivor with the largest metric at the current level, is labeled X, then the receiver stops decoding process at that level. Since the VA decoding is truncated on the way of processing, the decoder needs to determine a node terminating the VA to decide the received data symbols in this transmission. After that, the receiver requests the transmitter to send the remaining data symbols in the next transmission. In the GBi-ARQ scheme, the termination node is determined by the following procedure: After stopping the VA at some level, say t, the decoder firstly goes back d levels, where d is a predetermined integer, and then trace back all survivors from the nodes at level $t-d$ to their common node. If the value d is properly selected, we can expect that the correct path is survived at level $t-d$, so that the common node is connected to the correct path with high probability. Note that U and d are the parameters to optimize the performance of the GBi-ARQ scheme.

5. Performance of GBi-ARQ scheme in MBC

MBC is one of beyond line of sight communication techniques which uses reflections from ionized meteor trails called meteor bursts. In MBC, channels open randomly and the received signal power passed through the channel mostly exponentially decays with time.

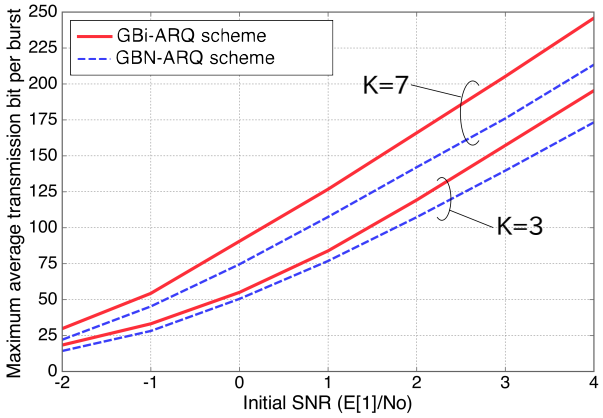

Figure 4: Performance coparison between GBi-ARQ and GBN-ARQ schemes.

Due to intermittent nature of the meteor burst channel, errors tend to occur in the tail part of a packet. Therefore, the GBi-ARQ scheme is very suitable for MBC.

In this section, we compare the performance of the GBi-ARQ scheme with that of the GBN-ARQ scheme proposed in MBC. The difference in the packet constructions of the GBi-ARQ and the GBN-ARQ schemes is described in Figure 3.

Figure 4 shows throughput performances of the GBi-ARQ and the GBN-ARQ schemes. The curves indicate the maximum achievable average transmitted bits per burst as a function of initial SNR of a meteor burst channel. The decay time constant for a meteor burst is assumed to be 0.15 [s]. The packet is assumed to be encoded by a convolutional code with R=1/2,K=5,7 and BPSK modulated with symbol rate 2400[baud]. The parameters, U and d, in the GBi-ARQ scheme and block length in the GBN-ARQ scheme are optimized for each initial SNR. We can see from the figure that the GBi-ARQ scheme exhibits better performance than the GBN-ARQ scheme. Since the GBi-ARQ scheme employs symbol-wise retransmission, it can use MBC channel more effectively.

6. Conclusions

In this paper, we present GBi-ARQ scheme proposed by our laboratory. In the GBi-ARQ scheme, transmission data are sequentially encoded by a convolutional encoder and symbol-wise retransmission is achieved by evaluating the reliability of decoded data using modified VA. The paper explains the modified VA used in the GBi-ARQ scheme together with general convolutional codes and ordinary VA. The performance of the GBi-ARQ scheme in MBC is compared with that of the GBN-scheme. Then, it is shown that the

GBi-ARQ scheme has better throughput performance than the GBi-ARQ scheme. However, other than MBC, there are many wireless communication systems which suffer from unexpected disconnections due to sudden noise increment, abrupt signal fading, interference and so on. Thus, in the future study, I am thinking to apply the GBi-ARQ scheme to such communication systems and evaluate the performances.

References

[1] K.Mukumoto, N.Ngashima, and A.Fukuda : Centralized data collection systems via meteor burst, *IEEE Trans.*, vol.J67-B,no.5,pp.489-496,May 1984.

[2] J.Z.Schanker : Meteor Burst Communicatioins (in japanese), Tokyo:Corona Publishing Co., 1997.

[3] H.Yamamoto and K.Itoh, : Viterbi decoding algorithm for convolutional codes with repeat request, *IEEE Trans.Inf.Theory*, vol.26, no.5,pp.540-547,Sep.1980

Gadjah Mada University – Shizuoka University Joint Workshop on Telecommunications
Gadjah Mada University, Yogyakarta, Indonesia, December 2–7, 2013

Parallel Transmission Wireless Visible Light Communication Systems using Color Shift Keying

Haruki Furukawa†, Tadahiro Wada †, Kaiji Mukumoto‡

†Graduate School of Engineering,
Shizuoka University
3-5-1 Johoku, Hamamatsu, 432-8561, JAPAN
Email: {f0330134,tetwada}@ipc.shizuoka.ac.jp

‡Division of Technical Service,
Shizuoka University
3-5-1 Johoku, Hamamatsu, 432-8561, JAPAN
Email: tekmuku@ipc.shizuoka.ac.jp

Abstract

In this paper, we show an effect of Color-Shift Keying (CSK) on parallel-transmission wireless visible light communication (PT-VLC) systems. The CSK scheme can improve information transmission rate of PT-VLC systems compared with that using mono-color. In this study, we construct a prototype of a PT-VLC system using a liquid crystal display as a transmitter and experimentally evaluate an effect of the CSK. We also show an effect of a forward error correction code for PT-VLC.

1. Introduction

Visible light communication(VLC) is a communication system using the visible light as a carrier. VLC has many advantages. It has little influence to human bodies or precision instruments compared with other wireless radio communications [1–3]. It can perform secure communication because it has a visible irradiation range. VLC allows to use a light source as not only the illumination but also the transmitter. There are many devices used for transmitter of VLC. Liquid Crystal Display(LCD) is one of candidates . The LCD is widely used on various situations, such as a computer, a television, a smart phone, and a tablet PC. Furthermore the LCD can easily control strength of luminescence and use many colors.

For VLC systems, there are two standard devices for receivers, photo-diodes (PD) and image-sensors (IS). PDs are popular devices and have quick electronic response, hence they allow fast communications. However, PDs have wide field of view, therefore VLCs using PDs are seriously affected by optical disturbance. On the other side, VLCs using ISs (ISC) restore information by image processing. This characteristic enables to clear optical disturbance. Moreover, since ISs are implemented as a digital camera in various devices such as cellular phones today, systems employing ISC and IC together (ISIC systems) are expected to be utilized easily.

Table 1: Product Specifications of the LCD

Name of product	FTD-G722AS2
Display size	17[inch]
Resolution	1280×768
Input signal	analog RGB
Power consumption	23[W]

One disadvantage of the ISIC systems is that popular ISs have very low frame rate such as 30-60[fps], which limits a transmission rate. In order to overcome this problem, parallel transmissions are quite effective. The parallel transmissions can be achieved by using the LCD. At the receiving side, parallely transmitted data can be obtained by image processing.

Color Shift Keying(CSK) is alternative technique to increase transmission rate. If ON-OFF keying is used for VLC, one light source can transmit only 1 bit. However, if we can use 3 colors, Red, Green, and Blue, one light source can transmit more information.

In this paper, we construct a prototype of a parallel transmission ISC system using an LCD and a USB camera, and evaluate the performance of this system by experiments. Especially, the effectiveness of CSK is evaluate by experiments.

2. System Construction

This section describes the structure of the transmitter and receiver of our ISC system. Fig. 1 shows the constructed ISC system. This ISC system transmits digital information by controlling brightness of the LCD, then restores the information by capturing the brightness of the LCD and image processing.

2.1. transmitter

This system uses an LCD shown in Fig. 2(a) as a transmitter. The specification of the LCD is described in Table 1.

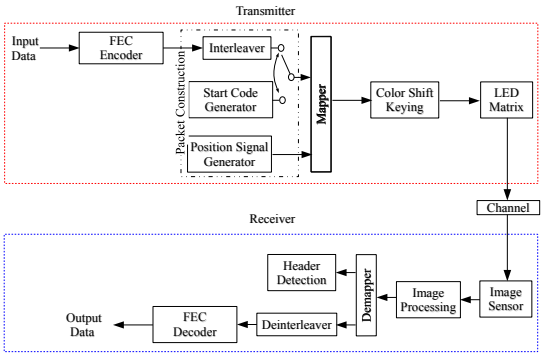

Figure 1: Block Diagram of the PT-ISC System

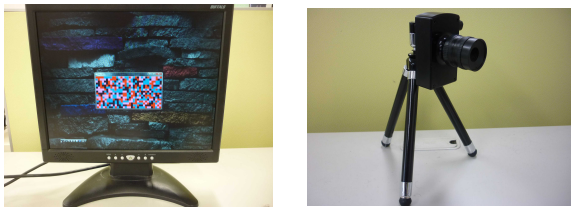

(a) LCD (b) USB camera

Figure 2: Experimental Equipments

An example of the transmission pattern of information by an LCD is shown in Fig. 3. As shown in Fig. 3, the information is transmitted by $M \times N$ boxes, and each box consists of some liquid crystal pixels and displays a color according to the information bits. The area of $M \times N$ is called as a frame in this paper. Here, two variables, m and n, indicate the coordinate of each box, where m and n are integers and satisfy $0 \leq m < M$ and $0 \leq n < N$, respectively. For example, the BOX in the 3rd column at the 0th row is represented as $\mathrm{BOX}_{(0,3)}$.

The LCD is used by this research consists of three primary colors of red, green, and blue on one liquid-crystal pixel. Three variables, r, g and b, denote light intensity of the LCD and have a range from 0 to 255 (8 bits). By using the three primary colors, we can express various colors by mixing these three colors.

In this manuscript, we only use two colors, red and blue. Futhermore, we set the light intensity of two colors, r and b, at 0 or 255. Therefore, each box is expressed by 4 colors, black, blue, purple, and red. The sets of light intensity, (r, b) are $(0, 0)$, $(0, 255)$, $(255, 255)$ and $(255, 0)$, respectively.

Moreover, M-sequence is used for the signal of the position detection of the information area on the LCD [3]. Because M-sequence is expected for reliable position detection, it has the very excellent auto-correlation characteristic. The signal of $\mathrm{BOX}_{(1,1)}$, $\mathrm{BOX}_{(1,N)}$, $\mathrm{BOX}_{(M,1)}$ and $\mathrm{BOX}_{(M,N)}$ located in four corners of the frame is made into the signal for position detection.

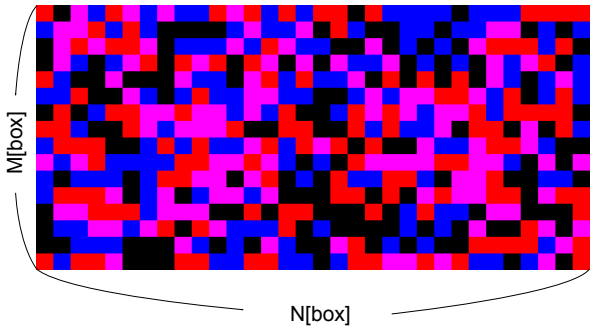

Figure 3: An Example of a frame

Table 2: Specification of the USB Camera

Name of product	Lumenera Lu75C
Resolution of images	640×480
Gradation	8[bit]
Frame rate	60.0[fps]

2.2. Receiver

In this ISC system, a USB camera (as an IS) shown in Fig. 2(b) is used a receiver. The specification of this camera is shown in Table 2. We adopt the camera whose specification is approximately the same as popular cameras. The captured image is then fed to a personal computer for image processing.

3. Restoration Algorithm

Fig. 4 shows the flowchart of the information restoration algorithm at the receiving side of this system.

3.1. Capture

In the first step, the receiver captures an image with height $I^{(0)}$ and width $J^{(0)}$ involving the LCD named $IMG^{(0)}$. Fig. 5(a) is an example of $IMG^{(0)}$, whose $I^{(0)}$ =480[pixel] and $J^{(0)}$ = 640[pixel], respectively. In this paper, the pixel in the j^{th} column of the i^{th} row of $IMG^{(\alpha)}$ is represented as $P_{i,j}^{(\alpha)}$, where the variables i and j satisfy $0 \leq i < I^{(\alpha)}$ and $0 \leq j < J^{(\alpha)}$, respectively. Since $IMG^{(0)}$ is the color image, $P_{i,j}^{(0)}$ has 3-color channels, RED, GREEN, and BLUE, of which

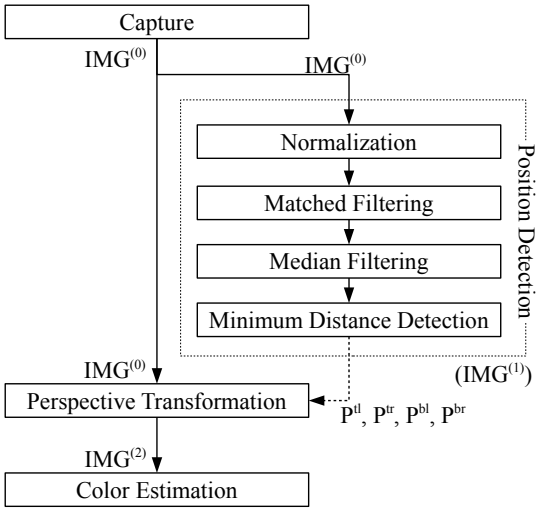

Figure 4: Flowchart of the Restoration Algorithm

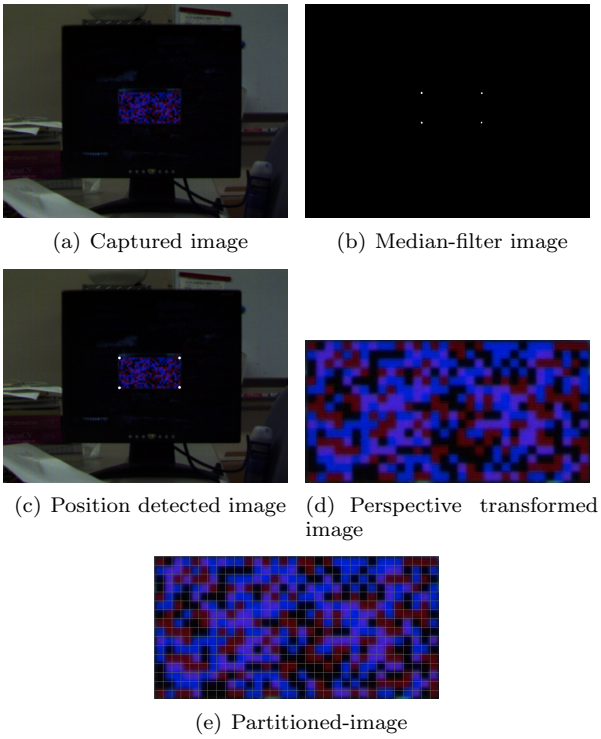

(a) Captured image (b) Median-filter image

(c) Position detected image (d) Perspective transformed image

(e) Partitioned-image

Figure 5: Sample Images on the Restoration Process

the received light intensities are represented as $R_{(i,j)}$, $G_{(i,j)}$, and $B_{(i,j)}$, respectively.

3.2. Position Detection

Next, the position of information area, which is frame, in the captured image should be determined. As mentioned earlier, M-sequence is used for the detection of the information area. The detection algorithm is almost the same as shown in Ref. [3].

3.3. Perspective Transformation

The shape, location and size of the information area on $\mathrm{IMG}^{(0)}$ depend on relative position of the LCD and the USB camera, that is, the region of the information area is not constant on $\mathrm{IMG}^{(0)}$. In order to easily detect transmitted information, the region of information transforms to a fixed size rectangle. Perspective Transformation is adopted for this transformation, as show in Ref. [3]. The transformed image, $\mathrm{IMG}^{(2)}$, is described as Fig. 5(d), whose size, $I^{(2)} \times J^{(2)}$, is 640×480 in this study.

3.4. Color Estimation

As the final process of the information restoration, the transmitted symbols are estimated by detecting colors of the boxes. In order to identify all boxes, $\mathrm{IMG}^{(2)}$ is evenly partitioned into $M \times N$ areas as shown in Fig. 5(e). Each partitioned area is named a "cell". The height of a cell, c_h, and the width of it, c_w, are given by

$$c_\mathrm{h} = \frac{I^{(2)}}{M} \text{ and } c_\mathrm{w} = \frac{J^{(2)}}{N}, \tag{1}$$

respectively. The cell of (m, n) is written as $\mathrm{CELL}_{(m,n)}$. The transmitted light intensities, r and b, of boxes can be estimated from the internal state of $\mathrm{CELL}_{(m,n)}$. Here, we define received light intensities, $R_{(m,n)}$ and $B_{(m,n)}$, which is derived as,

$$R_{(m,n)} \equiv \sum_{i=c_\mathrm{h}(m-1)}^{c_\mathrm{h}m} \sum_{j=c_\mathrm{w}(n-1)}^{c_\mathrm{w}n} R^{(2)}_{(i,j)}, \text{and} \tag{2}$$

$$B_{(m,n)} \equiv \sum_{i=c_\mathrm{h}(m-1)}^{c_\mathrm{h}m} \sum_{j=c_\mathrm{w}(n-1)}^{c_\mathrm{w}n} B^{(2)}_{(i,j)}, \tag{3}$$

where $R^{(2)}_{(i,j)}$ and $B^{(2)}_{(i,j)}$ are light intensities of $\mathrm{IMG}^{(2)}$.

In order to perform the color estimation of each symbol, the Euclid distance d on a color space is defined. The Euclid distance on the color space is found from Eq.(4). The receiver detects the color having the smallest Euclid distance. The set which shows a color is $C = \{''Black'', ''Blue'', ''Red'', ''Purple''\}$ and c is the element $c \in C$.

$$d_c = \sqrt{(R_{(m,n)} - R^c_{ave})^2 + (B_{(m,n)} - B^c_{ave})^2} \tag{4}$$

R^c_{ave} and B^c_{ave} within Eq.(4) are called on reference points. The reference points are initially determined by using a frame negotiated by both the transmitter and the receiver. An example of sets of received light

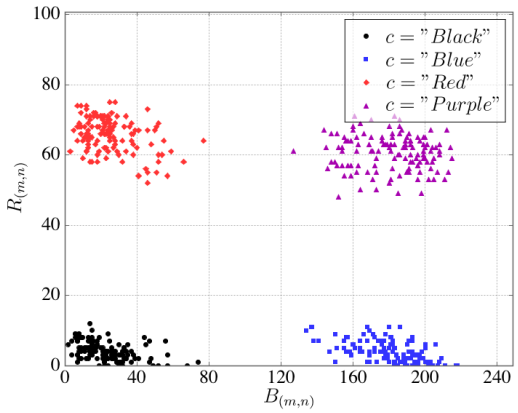

Figure 6: An Example of Cell State Values, $R_{(m,n)}$ and $B_{(m,n)}$

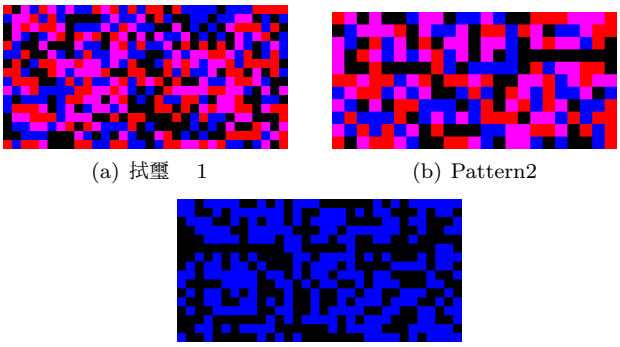

(a) 拭璽 1 (b) Pattern2

(c) Pattern3

Figure 7: Luminescence Patterns by the LCD

intensities, $(B_{(m,n)}, R_{(m,n)})$, are shown in Fig.6. We can found that the sets of intensities are concentrated on four points corresponding to four colors.

4. Experiments

4.1. Luminescence Patterns of the Frame

The luminescence patterns of frame is assumed three patterns shown in Fig. 7. The frame construction of each pattern is shown in Table 3. As shown in Table 3, these three patterns use the almost equivalent LCD pixels for information transmission. Because the number of boxes of Pattern 1 is twice as many as one of Pattern 2, Pattern 1 transmits information twice as many as Pattern 2. On the other hand, since the boxes of Pattern 1 have half LCD pixels by comparing with Pattern 2, Pattern 1 is more influenced from adjacent boxes. Moreover, because the luminescent colors of Pattern 1 are twice as many as one of Pattern 3, Pattern 1 can transmit twice information bits comparing with Pattern 3.

Table 3: Details of Luminescence Patterns by the LCD

Display pattern	Pattern 1	Pattern 2	Pattern 3
The number of colors	4 (black, blue, red, purple)	4 (black, blue, red, purple)	2 (black, blue)
The number of boxes per frame ($M \times N$)	512 (16×32)	253 (11×23)	512 (16×32)
The number of pixels per box ($c_h \times c_w$)	225 (15×15)	441 (21×21)	225 (15×15)
The number of total pixels	115,200	111,573	115,200

Table 4: Parameters of the Turbo Code

Constraint length	3
Generator matrix	(7,5)
Coded rate	0.50
Word length	Information:1522[bit] Code:3048[bit]
Decoding	10[time]

In this experiment, since four corner boxes are used for the position detection, the number of boxes which can transmit information are $M \times N - 4$. Because each box of Pattern 1 and 2 can transmit 2 bits, the amount of information bits per frame is 1016 [bit/frame] by Pattern 1 and 498 [bit/frame] by Pattern 2, respectively. In Pattern 3, one frame can transmit 508 [bit/frame] because this pattern uses only two colors.

4.2. Introduction to FEC

As well known, Forward Error Correction (FEC) codes are useful for reliable communication. Although FEC codes decrease a bit rate, reliability of communications increases. In this paper, we adopt a Turbo code as a FEC code. The specification of the Turbo code is shown in Table 4.

4.3. Conditions of Experiments

Assumptions of this experiments are shown in Table 5. We set four experimental conditions namely ExA, ExB, ExC and ExD, as shown in Table 6. ExB, ExC, and ExD have an almost the equal information transmission rate. ExA can achieve a twice as much information transmission rate as ExB, ExC and ExD.

4.4. Experimental Results

Fig.8 shows the BER performance vs. communication distance which is the distance between the LCD and the USB camera. The results of ExA and ExD exhibited almost the equal BER characteristic. It means that CSK have large capability because ExA can transmit information twice as many as ExD. Next, since ExB utilized the turbo code, as compared with ExA, BER

Table 6: Experimental Conditions

	ExA	ExB	ExC	ExD
Display Pattern	Pattern1	Pattern1	Pattern2	Pattern3
FEC	Uncoded	Turbo encoded	Uncoded	Uncoded
Bit rate	5080[bit]	5080[bit]	2490[bit]	2540[bit]
Symbol rate	2540[symbol]	2540[symbol]	1245[symbol]	2540[symbol]
Code Rate	1.00	0.50	1.00	1.00
Start code	508[symbol]	508[symbol]	506[symbol]	508[symbol]

Table 5: Experimental Assumptions

Environment	indoors,830[Lux]
Communication distance	100-250[cm]
Resolution of the camera	640×480
Position detection code length, K	15[bit]
Frame rate	5.0[fps]
Number of trials	1000[time]

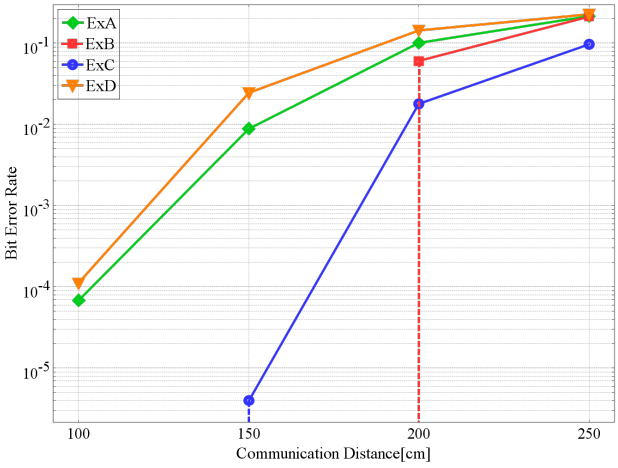

Figure 8: BER Performance using CSK

has been improved when the communication distance was less than 200[cm]. We have can also find that the BER characteristic of ExC was better than one of ExA. It is because the area of boxes of ExC is larger than that of ExA and influence from adjacent boxes might be reduced in ExC.

5. Conclusions

In this paper, we have constructed the prototype of a parallel transmission ISC system using CSK. We evaluated system performance by experiments. As a result, we shown that CSK and FEC (Turbo code) were very effective for ISC.

References

[1] H. Sugiyama, S. Haruyama, and M. Nakagawa, "Experimental Investigation of Modulation method for Visible-Light Communications," IEICE Technical Report, OCS2005-19, May. 2005 (in Japanese).

[2] T. Yamazato, "What Visible Light Communication (VLC) can do, what VLC cannot do.", IEICE Technical Report, RCS2011-49,
June. 2011 (in Japanese).

[3] J. Amano, T. Wada, K. Mukumoto, " An Evaluation of a Parallel Transmission Visible Light Communication System employing an LDPC code, "
Proc. International Symposium on Information Theory and its Applications(ISITA 2012), pp. 566-570, 2012

Gadjah Mada University – Shizuoka University Joint Workshop on Telecommunications
Gadjah Mada University, Yogyakarta, Indonesia, December 2–7, 2013

A Study on Color Error for Color Shift Keying in Parallel Transmission Visible Light Communications Systems

Tin Nguyenthuong†, Tadahiro Wada†, Kaiji Mukumoto‡

†Graduate School of Engineering,
Shizuoka University
3-5-1 Johoku, Hamamatsu, 432-8561, JAPAN
Email: {f0330298,tetwada}@ipc.shizuoka.ac.jp

‡Division of Technical Service,
Shizuoka University
3-5-1 Johoku, Hamamatsu, 432-8561, JAPAN
Email: tekmuku@ipc.shizuoka.ac.jp

Abstract

In this paper, we deal with Visible Light Communication(VLC) Systems. VLC is a communication system using visible light and have some advantages. Color Shift Keying is a candidate technique to increase transmission rate of VLC. The paper provides evaluation of color error on VLC using CSK. The evaluation is carried out from the view points of experiments and theoretical analysis.

1. Introduction

Visible light communication (VLC) is a communication system using the visible light as a carrier. Range of wavelength of it is 380nm-800nm. VLC has many advantages as follows:

- Not be limited by radio law. The radio waves are limited by the Radio Law, and it is defined as electromagnetic waves below 3[THz] in Japan. However, the wavelength of visible light is 400-800[THz] in frequency band, that it is outside the control of the Radio Law.
- Little effect on precision equipments and human bodies. Because VLC does not use the radio waves, it can be used in environments that are strictly limited to usage of radio waves such as hospitals, trains and planes.
- High operability and security. Because we can see the visible light by naked eyes, we are able to control it easily. Therefore, VLC has the strong security and high operability.

On the other hand, the VLC still exists some disadvantages:

- Because wavelength of visible light is short, VLC does not have effect on diffraction, scattering and reflection. Therefore, it can not transmit information when meeting a shield.
- VLC is much affected by noise such that natural lights, artificial lights and so on.

With the light source which are used in the VLC, the light emitting diode (LED) has been noticed. Comparing with a fluorescent lamp and an incandescent lamp, it has a lot of advantages, such as low power consumption, long life, height of the visibility, small size and lack of heat generation. Therefore, it is widely applied in a variety of locations in traffic-light apparatus, electrical scoreboards, etc.

Moreover, PIN photodiode, avalanche photodiode and image sensor are the typical light-receiving devices in VLC. The PIN photodiode and the avalanche photodiode are the general light-receiving elements. They are possible to detect the intensity-modulated signal to GHz. The image sensor has very high spatial resolution, which means that the number of pixels of the image sensor is the number of maximum channels. Therefore image sensor communication allows parallel communication. Moreover, this scheme has very strong tolerance for disturbance by eliminating another light sources from the received image. However, the frame rate of the standard image sensor is 30-60[fps], which is too slow to use it as the receiver. Nevertheless, image sensor communication has been developed more popularly than PIN photodiode, because image sensor communication has above-mentioned unique features and most cellular phones are equipped with an image sensor as a digital camera.

Red, green and blue are the three primary colors in the LED. They are also able to produce different colors if we change the mixing ratio of the light from them. In 1960, the red LED was born, and then the green LED was invented. However, it was difficult to develop the blue LED, because it needed a high technology. In 1990s, the blue LED was invented. After it was born, the color LEDs are widely used in various applications. For example, many of the huge screen on the wall surfaces of the tall building started to use LEDs.

In our laboratory, researches on VLC have been done. In most of the researches, one color of LEDs

is considered. However, comparing with one color, the usage of three colors is expected to transmit more information. Therefore, we consider to use three colors for transmissions, which is called as Color Shift Keying (CSK). We evaluated color error rate of CSK in view of theoretical analysis and experimental results.

2. Experiments

2.1. The system configuration

In order to obtain experimental data, we configure the systems shown in Figure 1.

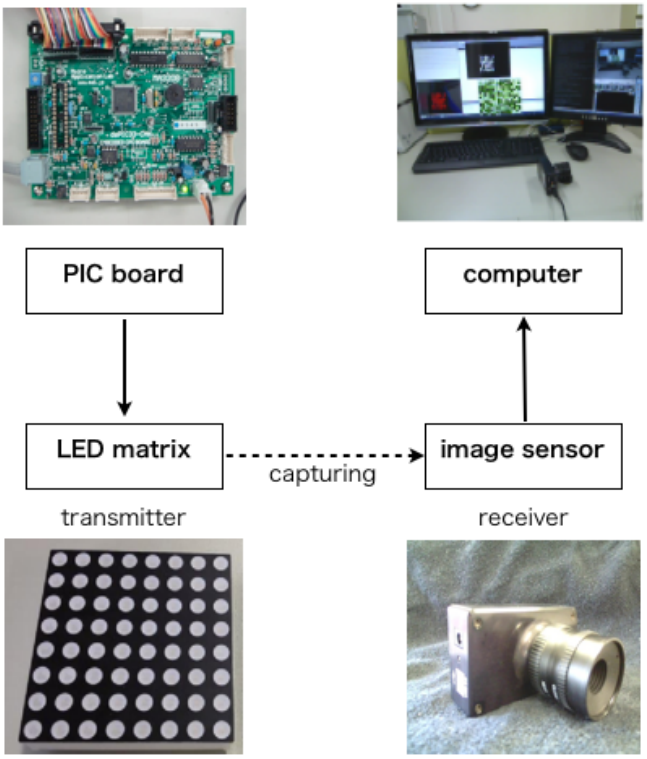

Figure 1: The system configuration

At first, from a micro computer driven by Peripheral Interface Controller (PIC), signal is fed to an LED matrix. Next, the LED matrix displays lighting patterns according to the signal. Then, an image sensor installed on an USB camera captures the display of the LED matrix. Lastly, the captured image is fed to a computer and image-processed to obtain the transmitted data.

2.2. Experiment results

In the transmitter, the numbers of samples of Red, Green and Blue are 2070, 2090 and 3240, respectively, as shown in Table 1. The distance between the USB camera and the LED matrix is 200cm.

Table 1: The samples of transmitter

Color	Numbers
Blue	2070
Green	3090
Red	3240
Total	8400

At the receiver, even when sending one color, we obtained three colors of luminance intensity, Red, Green and Blue. The luminance intensity ranges of them is 0-255.

Figure 2 shows the method to determine the color error rate when transmitting Blue. It is similar to the cases that we transmit Green and Red.

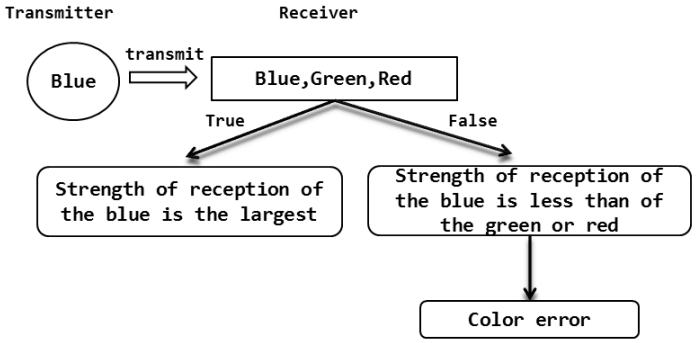

Figure 2: Detection of color error when transmitting Blue

Table 2 shows the probability of color errors by obtaining from the experiments.

Table 2: The probability of color error by experiments

	Reception		
Transmission	Blue	Green	Red
Blue	—	0	0
Green	1.78×10^{-2}	—	0
Red	3.12×10^{-2}	0	—

From Table 2, when sending the Blue, no color error occurs. However, when sending the Green and Red, we can see that color errors to Blue occur.

3. The mathematical model of luminance intensity

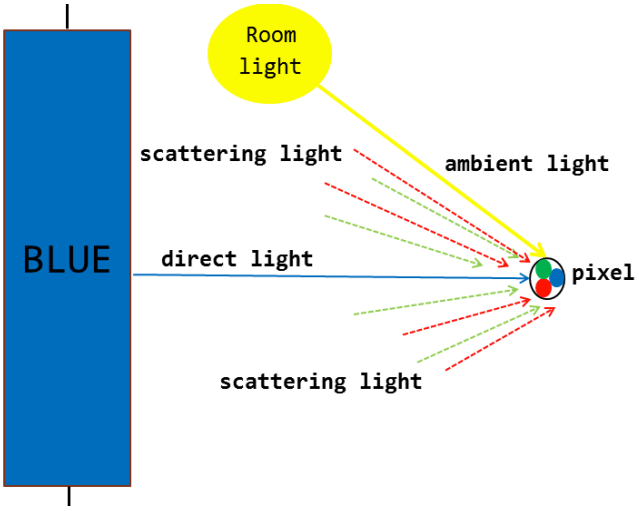

Figure 3: State of the lights which arrive at pixel of the receiver

3.1. Way of thinking about luminance strength

Making a mathematical model of luminance intensity is important to recognize physical meaning of reception and to enable analysis easily. In figure 3, the reception of lights are roughly described when a "Blue" color LED light is front of a pixel of the receiver. Note that other LED lights, "Red", "Green" and also "Blue", exist in the neighborhood of the Blue light.

As mentioned earlier, even when we send a blue color light, we obtain the three of luminance intensity, Red, Green, and Blue at the receiver. In this case, the front "Blue" color light is a direct light. And neighboring lights, Red, Green and also Blue, can be considered as scattering lights. Furthermore, illumination lamps are also affected and can be considered as an ambient light.

From this figure, we can see that, at the pixel of the receiver, the Blue component consists of the direct light, the scattering lights, and the ambient lights. However, the Green and Red components consist of only the scattering and ambient lights. Therefore, we use Nakagami-Rice distribution to approximate for the luminance intensity of "Blue", and Rayleigh distribution to approximate for that of "Green" and "Red".

Both Nakagami-Rice and Rayleigh distributions are described in Appendix.

3.2. Results of approximation

Figures 4, 5 and 6 show probability density function of luminance intensity when sending Blue, Green, Red, respectively, and approximation results of them. The horizontal axis shows the luminance intensity of reception, and the vertical axis shows the probability density function(PDF). The PDF of the luminance intensity can be obtained by the experiments shown in the previous section.

In order to obtain estimates of the approximation, ML estimation is used for Rayleigh distribution to statistically obtain average and variance from the experimental data. However, because it is difficult to obtain the estimates for Nakagami-Rice distribution, simple average and unbalanced variance of the experimental data are calculated to obtain the estimates.

We can see that the shape of graphs of experimental data and graphs expressed by approximation are nearly similar. In figure 4, since the characteristic which represents the intensity of the Blue does not overlap with the intensity of the others, the color error rate is less when transmitting blue. On the other hand, in figures 5 and 6, the characteristic which represents the intensity of Green and Red overlap significantly with other intensities. Therefore, when transmitting Green and Red, the color error rate tends to be high.

3.3. Probability of color error rate by theoretical analysis

By an appropriate approximation of the luminance intensity, we can easily and mathematically estimate color error rates. Here we derive equation of the error rate by using Nakagami-Rice distribution and Rayleigh distribution.

As expressed in Appendix, probability density function of Nakagami-Rice distribution is as follow,

$$P_N(r) = \frac{r}{\sigma_1^2} e^{-\frac{r^2+A^2}{2\sigma_1^2}} I_0\left(\frac{rA}{\sigma_1^2}\right). \tag{1}$$

Probability density function of Rayleigh distribution is as follow,

$$P_R(r) = \frac{r}{\sigma_2^2} e^{-\frac{r^2}{2\sigma_2^2}}. \tag{2}$$

Let a random variable r_1 follow the Nakagami-Rice distribution and a random variable r_2 follow the Rayleigh distribution. Probability that r_2 is greater than r_1 can be expressed is as follow,

$$\begin{aligned} P &= \int_0^\infty P_N(r_1) \int_{r_1}^\infty P_R(r_2) dr_2 dr_1. \\ &= \frac{1}{\sigma_1^2} e^{-\frac{A^2}{2\sigma_1^2}} \frac{\sigma_1^2\sigma_2^2}{\sigma_1^2+\sigma_2^2} e^{-\frac{A^2\sigma_2^2}{2\sigma_1^2}(\sigma_1^2+\sigma_2^2)}. \end{aligned} \tag{3}$$

We use this equation to find the probability of color error rate. The result is as shown in Table 3.

Table 3: The probability of color error by theoretical analysis

	Receiver		
Transmitter	Blue	Green	Red
Blue	—	2.96×10^{-3}	7.1×10^{-5}
Green	2.83×10^{-2}	—	3.51×10^{-3}
Red	1.84×10^{-2}	1.72×10^{-4}	—

By comparing the results between Table 2 and Table 3, we can find:

- When sending the blue, the error rate is low.
- There is no significantly different between the results of the error rate by the experimental results and theoretical analysis. Therefore, it is reasonable when using Rayleigh distribution and Nakagami-Rice distribution to approximate.

4. Conclusion

This research, we examined color error rate in parallel transmission visible light communication when using CSK. Firstly, we found the probability of color error rate by experimental results. Next, we determined the mathematical model of the luminance intensity of reception characteristic and found the probability of color error rate by theoretical analysis. Finally, we compared the results of probability of color error rate which are found by experimental results and theoretical analysis.

References

[1] S.Stein, J.J.Jones, Modern Communication Principles, McGRAW HILL, 1967.

A. Rayleigh distribution

Rayleigh distribution is the distribution of the amplitude $x+jy$ whose coordinates x, y are independent, with identically distributed $N(0,\sigma)$[1]. Probability density function $f(x)$ of the random variable x is given by the following equation,

$$f(x) = \frac{1}{\sqrt{2\pi}\sigma}\exp\left(-\frac{x^2}{2\sigma^2}\right). \quad (4)$$

Similarly, the probability density function of the random variable y is $f(y) = \frac{1}{\sqrt{2\pi}\sigma}\exp\left(-\frac{y^2}{2\sigma^2}\right)$.

Here, we have $r = |x+jy| = \sqrt{x^2+y^2}$. By setting $x = r\cos\phi$, $y = r\sin\phi$, and the probability density function $f(x,y)$ is given by the following equation,

$$\begin{aligned} f(r,\phi) &= f(x,y) = f(x)f(y)\left|\begin{matrix}\frac{\partial x}{\partial r} & \frac{\partial x}{\partial \phi}\\ \frac{\partial y}{\partial r} & \frac{\partial y}{\partial \phi}\end{matrix}\right| \\ &= \frac{r}{2\pi\sigma^2}\exp\left(-\frac{r^2}{2\sigma^2}\right). \end{aligned} \quad (5)$$

By integrating over from 0 to 2π with relating to ϕ, the probability density function $f(r)$ with the random variable r is given by the following equation,

$$f(r) = \int_0^{2\pi} f(r,\phi)d\phi = \frac{r}{\sigma^2}\exp\left(-\frac{r^2}{2\sigma^2}\right). \quad (6)$$

B. Nakagami-Rice distribution

We give the probability density functions $f(x)$ and $f(y)$ as follow,

$$f(x) = \frac{1}{\sqrt{2\pi}\sigma}\exp\left(-\frac{(x-A)^2}{2\sigma^2}\right). \quad (7)$$

$$f(y) = \frac{1}{\sqrt{2\pi}\sigma}\exp\left(-\frac{y^2}{2\sigma^2}\right). \quad (8)$$

We focus on the magnitude of r which is expressed as $r = |x+jy| = \sqrt{x^2+y^2}$. By setting $x = r\cos\phi$ and $y = r\sin\phi$, probability density function, $f(r,\phi)$, is given by the following equation,

$$\begin{aligned} f(r,\phi) &= f_x f_y\left|\begin{matrix}\frac{\partial x}{\partial r} & \frac{\partial x}{\partial \phi}\\ \frac{\partial y}{\partial r} & \frac{\partial y}{\partial \phi}\end{matrix}\right| \\ &= \frac{r}{2\pi\sigma^2}\exp\left(-\frac{A-2Ar\cos\phi+r^2}{2\phi^2}\right) \end{aligned} \quad (9)$$

By integrating over from 0 to 2π with relating to ϕ, the probability density function $f(r)$ with the random variable r is given by the following equation,

$$\begin{aligned} f(r) &= \int_0^{2\pi} f(r,\phi)d\phi \\ &= \frac{r}{\sigma^2}\exp\left(-\frac{A^2+r^2}{2\sigma^2}\right) I_0\left(\frac{rA}{\sigma^2}\right) \end{aligned} \quad (10)$$

Here, $f(r)$ is defined as the probability density function called Nakagami-Rice distribution,

where $I_o()$ means Modified Bessel function of the first order,

$$I_0(z) = \frac{1}{2\pi} \int_0^{2\pi} e^{z \cos\theta} d\theta. \tag{11}$$

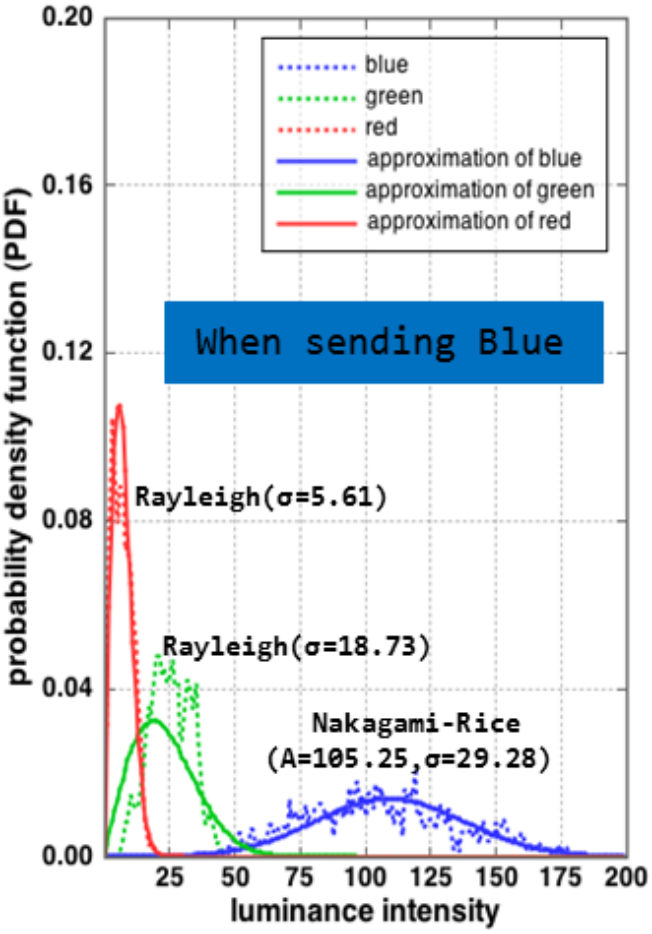

Figure 4: The probability density function of luminance intensity when sending Blue

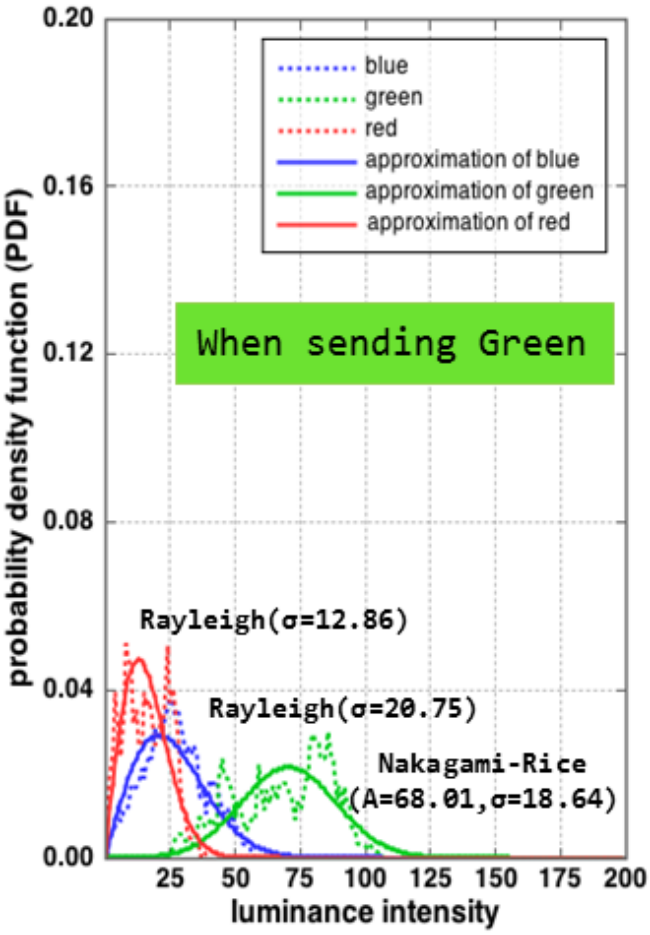

Figure 5: The probability density function of luminance intensity when sending Green

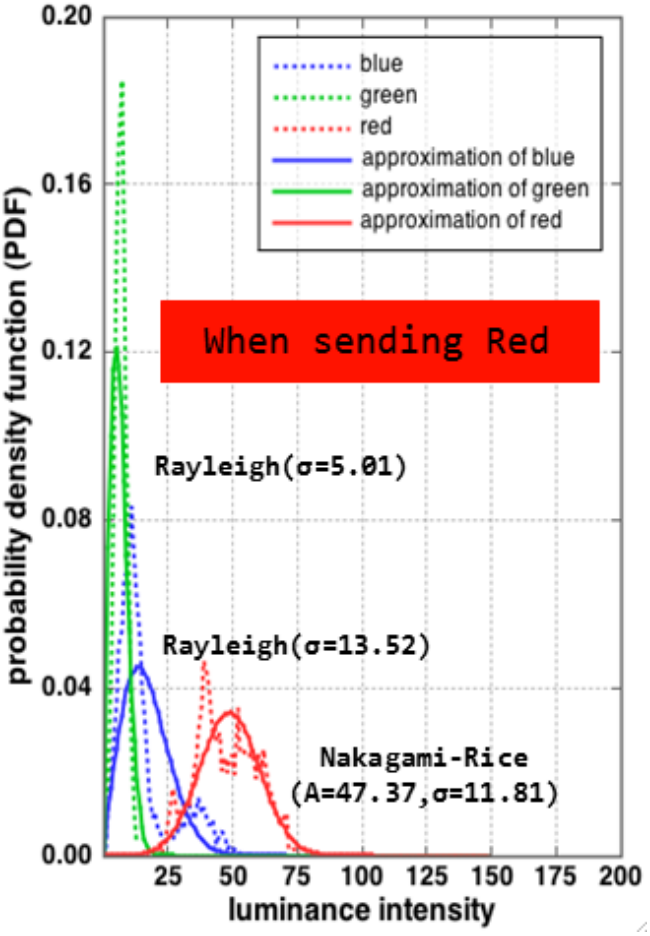

Figure 6: The probability density function of luminance intensity when sending Red

Contempo: A Home Care Model to Enhance the Wellbeing of Elderly Pople

Kurnianingsih-*IEEE Member*, Lukito Edi Nugroho, Widyawan, Lutfan Lazuardi, Ridi Ferdiana, Selo

***Abstract*— Fast growing population of elderly people has recently been a serious issue in many developing countries and it becomes a global concern in the world. Most elderly people require assistance in their daily life, including in maintaining their wellbeing, taking care of their health, or responding to emergency medical situations. The need for caring for elderly people, particularly to maintain their wellbeing, has been growing significantly. The objective of this research is to seek improvements in quality of life that can enhance the wellbeing of elderly people through innovations in information technology. This research is also expected to be a significant contribution for dealing with ageing population as a common issue in developing countries. This paper deals with a pervasive health care technologies and ambient environment, which propose a model of Connected Technologies for Home Care for Elderly People (Contempo) to enhance the wellbeing of elderly people. A model of wellbeing assessment is also proposed to examine the proposed model of Contempo.**

I. INTRODUCTION

The population of aging people has recently been gaining attention from many countries. Due to the unique demography profile, developing countries tend to have more elderly people compared to developed countries. United Nations data predicted that by the year 2019 elderly Indonesian's ratio will reach about 7% of the population and will rise from 7% to 14% in 2041 [1].

A major concern for elderly people is their health care. Healthcare for elderly becomes a very crucial issue in many developing countries, because if it is neglected, poor and sick old people will indeed become burdens to their families and the government. Continuous urbanization in which people from rural move to urban area has made most elderly people will eventually live in urban areas. Elderly people are at high risk for disease and disability. The problem of rush, bustle of activity, and crowded health services in urban areas are the factors that sometimes make elderly people become difficult to go out of their home to meet health professionals for routine clinical check-up. Their disability to access public health services brings up a problem in their medical care. Additionally, most elderly people are still unwilling to enter nursing homes. They prefer to have the convenience and comfort of staying at home. Contempo which implement the concepts of pervasive computing technologies and ambient environments is a solution to deal with this problem. Contempo can be defined as a dwelling that connects the residents, household appliances, environments, sensor and services, medical care givers, family member and allow them to be remotely monitored or accessed. Such connected home health care which equipped an automated stand-alone surveillance method and fully integrated within the environment is a real and urgent need, particularly for elderly people who likes living autonomously. The monitoring can be done remotely by health service providers such as hospitals. Having the capability of remote health care services can reduce human resources and response time in critical situations and finally enhance the wellbeing of elderly people.

Enhancing the wellbeing of elderly people in this research project will be concerned on the technological perspective through Contempo, including metrics and evaluation criteria which can be tested by elderly people. In this sense, we aim at proposing a Contempo model, which is equipped with an automated stand-alone surveillance method and is fully integrated with the environment. We also aim at proposing a wellbeing assessment model as a tool to assess Contempo model, which is a technology solutions for immediate and convenient medical and health services for elderly community in order to enhance the wellbeing of elderly people. Finally, this research project is also expected to be a significant contribution for dealing with ageing population as a common issue in developing countries.

The structure of this paper is as follows. Section 2 gives a description about related research work. Section 3 describes a proposed model. Section 4 presents challenges. Conclusion is discussed in Section 5.

II. RELATED RESEARCH WORK

This research project deals with elderly people relevants to regional common issues of population ageing [1]. The issue of rapidly aging population in many countries has been published by JICA on a Japanese study report [2, 3]. In response to the aging population, Indonesia as one of developing countries has adopted a National Action Plan [4], which focuses on establishing and ensuring necessary support for the elderly.

Lots of health problems faced by elderly people such as chronic desease, disability, and fall make elderly need asisstant living. Many inventions [5,6,7] have been developed to overcome elder's health problems. Wireless Sensor Network (WSN) and Radio Frequency Identification (RFID) in health care system has become a tremendous effort as communication tools in health care [8,9] However,

Kurnianingsih is with the Dept. of Electrical Engineering and Information Technology, Universitas Gadjah Mada, Yogyakarta, Indonesia and also with Dept. of Electrical Engineering, Politeknik Negeri Semarang, Indonesia (e-mail: kurnia.s3te13@mail.ugm.ac.id).

Lukito Edi Nugroho, Widyawan, Ridi Ferdiana, and Selo are with the Dept. of Electrical Engineering and Information Technology, Universitas Gadjah Mada, Yogyakarta, Indonesia (e-mail: lukito@ugm.ac.id; widyawan@ugm.ac.id; ridi@ugm.ac.id; selo@ugm.ac.id).

Lutfan Lazuardi is also with the Dept. of Public Health, Universitas Gadjah Mada(e-mail: lutfan.lazuardi@ugm.ac.id).

improving quality of life is one of the main concern for the pursuit of wellbeing of elderly people.

Many researchers have work in wellbeing projects [10-13]. The four domains of the framework of wellbeing has been categorized as an individual wellbeing,family wellbeing. community wellbeing and societal wellbeing [10]. Indicators as 'satisfaction', 'anxiety' and 'happiness' are used by UK government to measure people''s 'individual' and 'psychological'[11, 12].

Home is the best environment for elderly people to get convenience healthcare. By utilizing WSN and RFID, medical caregivers also can remotely monitor the elderly activities and physiological parameters. Elderly's disability to access public health services and elderly's preference to have the convenience and comfort of staying at home are a strong justification for developing a Contempo. It can provide constant monitoring of their health and activities despite their incapabilities and preference, which in turn will enhance their wellbeing.

III. THE PROPOSED MODEL

In this section, an architecture of a proposed model of Contempo to enhance the wellbeing of elderly people is proposed, as shown in Figure 1. Contempo is an ambient and pervasive system which is equipped an automated stand-alone surveillance method and fully integrated within the environment. It can provide constant monitoring the activities and physiological parameters of elderly person, recognizes changes in their health status, and has the capability to alert health professionals medical care and family members.

The proposed model of Contempo, as shown in Figure 2, consists of three main system, namely Reflective Sensing System, Historical Alert System, Diagnostic Support System. This three main system of Contempo will work in harmony simultaneously in order to enhance the wellbeing of elderly people, particularly elderly people with dissabilities or/and elderly people with chronic deseases.

A. Reflective Sensing System (RSS)

RSS will provide automatically reflection of sensing gathered from vital sign sensors, activity daily sensors, fall detection and tracking sensors, and ambient environment sensors. Sensor will send data of the elderly in real time about health status and environment surrounding the elderly as inputs to RSS. Output from this system will be sent automatically to home appliances or/and personal health appliances (particularly for elderly with chronic desease).

B. Alert System (AS)

AS will provide alert to medical care and family members related to elderly health status in emergency condition.

C. Diagnostic Support System (DSS)

DSS will provide medical diagnostic to doctors to be monitored and analyzed. The result of analyzing, doctor will give resume of diagnostic as a feed back manually to the system to improve the elderly health status and treatment.

We define alert system of Contempo into five categories:

- *Category 1: Wellness Improvement Condition*

Condition that elderly has significant improvement on wellness. We will define wellness of elderly by indexing based on physiology of elderly and activity of elderly.

- *Category 2: Critical Activity Condition*

Condition that elderly needs special attention because of doing critical activity. Critical activity leads to possibility of having accidents such as position in bathroom, going to outside home.

- *Category 3: Minor Condition*

Condition that elderly needs more convenience from environment and some asisstances.

- *Category 4: Major Condition*

Condition that elderly in critical condition and needs some medical asisstance, such as falls which not resulting injury, elderly remains awake.

- *Category 5: Emergency Condition*

Condition that elderly in emergency condition and need asisstance from emergency units. Emergency conditions such as fall in the elderly and resulting serious injury.

Alert condition category 1 till category 3 will be sent only to care giver and family member. Alert condition category 4 will be sent to doctor, care giver, and family member. Alert condition category 5 will be sent to emergency unit, doctor, care giver, and family member.

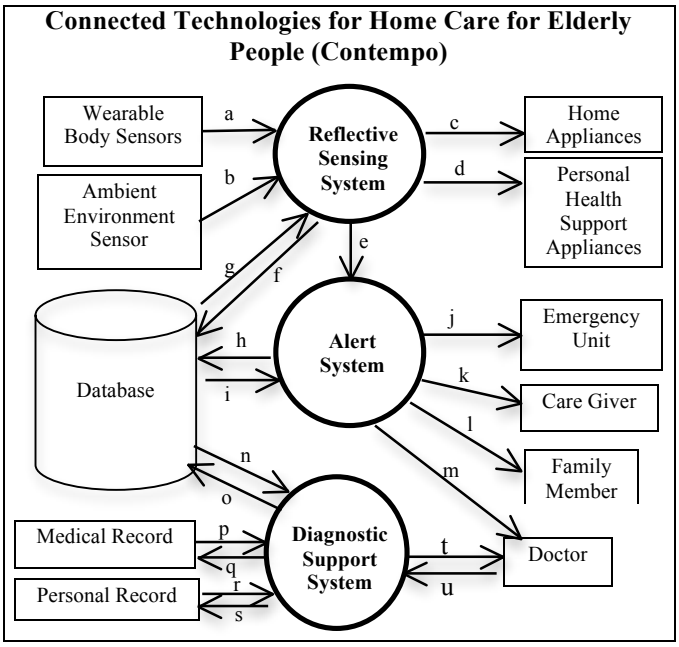

Figure 1. A Proposed Model of Contempo

The flows in connected home health care, as described below.

a. Wearable_Body_Sensor_Data

Wearable_Body_Sensor_Data consists of data from vital sign sensors, activity daily monitoring sensors, fall detection sensor, and tracking sensors. Vital sign will monitor physiological function of elderly, which includes data of blood pressure, heart rate, respiratory rate, and body temperature. Activity daily monitoring sensors will monitor elderly's activity, which includes sitting, lying, and standing. We will classify the state of activity into two categories namely active state and passive state. Active state is a state where the elderly in a active circumstance such as sitting position and standing position. Both sitting position and standing position are states where elderly is doing activities. Lying position will be defined as a passive circumstance where elderly is not doing activities, in this case elderly is in an idle activity. Falls often happen to elderly that can cause injury and fatal damaged, even death. Fall detection will have to be able to accurately predict a fall of elderly so that some fast preventive measures can be taken to prevent any serious injury from occurring. Elderly tracking system will be able to track the location of elderly. When something happened to elderly in dangerous condition such as fall, the system can detect the position of the person and will give alert to emergency unit, doctor, care giver, and family member.

b. Ambient_Environment_Data

Awaring context of environment for connected home health care is a crucial matter in the design of solutions for inhouse safety. Context information related to elderly wellbeing such as location and health status will be obtained by sensor infrastructure such as lighting, temperature, and density. The information can then be further processed and combined with wearable body sensor data to give appropriate condition of elderly health status.

c. Trigger_Data

The processing result of Reflective_Sensing_System will produce Trigger _Data reflectively to Home Appliances to do some action to home appliances.

d. Trigger_Data

The processing result of Reflective_Sensing_System will produce Trigger_Data to Personal_Health_Appliances to do some action reflectively to elderly's themselves.

e. Trigger_Data

The processing result of Reflective_Sensing_System will produce Trigger_Data to Historical_Alert_System to do some action related to alert condition of elderly.

f. Sensing_Data

The processing result of Reflective_Sensing_System will produce Sensing_Data, which will be saved in database.

g. Sensing_Parameter

Sensing_Parameter is a historical data taken from database to be processed in Reflective_Sensing_System to trigger Home_Appliances and Personal_Health_Appliances.

h. Historical_Alert

Historical_Alert is data as a result from Historical_Alert_System and will be saved in database.

i. Historical_Data

Historical_Data is data taken from processed database as an input to Historical_Alert_System.

j. Emergency_Alert

The output of Historical_Alert_System will be sent as an alert to emergency unit if elderly is in emergency condition only.

k. Alert

The output of Historical_Alert_System will also be sent as an alert to care giver if elderly is in wellness improvement condition, critical activity condition, minor condition, major condition, and emergency condition.

l. Alert

The output of Historical_Alert_System will also be sent as an alert to family if elderly is in wellness improvement condition, critical activity condition, minor condition, major condition, and emergency condition.

m. High_Alert

The output of Historical_Alert_System will also be sent as an alert to doctor if elderly is in major condition and emergency condition.

n. Historical_Data

Historical_Data is data taken from processed database as an input to Diagnostic_Decision_Support processing system.

o. Diagnostic_Data

Diagnostic_Data is the result of processed Diagnostic_Decision_Support that will be saved in Database. There are three inputs to Diagnostic_Decision_Support processing system: Medical_Record_Data, Personal_Health_Record_Data, and Resume_of_Doctor_Diagnosis.

p-q Medical_Record_Data

Medical Record (MR) contains information about elderly/patient's health compiled and maintained by each of healthcare providers. Medical_Record_Data consists of elderly health information including personal identification; anamnese; laboratory, radiological, and other test record; medication record.

r-s Personal_Health_Record_Data

Personal Health Record (PHR) contains information about elderly/patient's health compiled and maintained by elderly themselves. Personal_Health_Record_Data consists of medical record information, which comes from healthcare providers, and patient/elderly's additional information, which comes from individual such as preferences.

t. Diagnosis_Data

The result of Diagnostic_Decision_Support will be sent to the Doctor as a Diagnosis Data. Doctor then will monitor and analyze it.

u. Resume_of_Doctor_Diagnosis

Doctor's analysis manually will be sent as a Resume_of_Doctor_Diagnosis to improve processing in Diagnostic_Decision_Support. The information related to elderly's health status will periodically update by system and doctor.

This Contempo model will be tested and assessed to measure level of wellbeing. We also proposed a wellbeing assessment model, as shown in Figure 2, to test a proposed Contempo model. Wellbeing assessment can be measure qualitatively, including satisfaction, anxiety, happiness [11, 12]. We propose three components to assess wellbeing, namely physical health, behaviour, and environment.

A. Physical Health

There are four variables to measure physical health periodically such as body temperature, blood pressure, heart rate, and respiration. Body temperature will be measured quantitively in Celcius degree. Bood pressure will be measured quantitively in mmHg. Heart rate will be measured quantitively in pulse/minutes. Respiration will be measured quantitively in breaths/minutes.

B. Behaviour

There are two variables to measure behaviour periodically such as duration of active state and event of fall. Active state will be defined as a sitting or standing position while doing activities. We will measure and analyze the duration of active state done by elderly in a day. Event of fall will be measured every day and will checked the history of fall.

C. Environment

There are three variables to measure environment periodically such as lighting, temperature, and density.

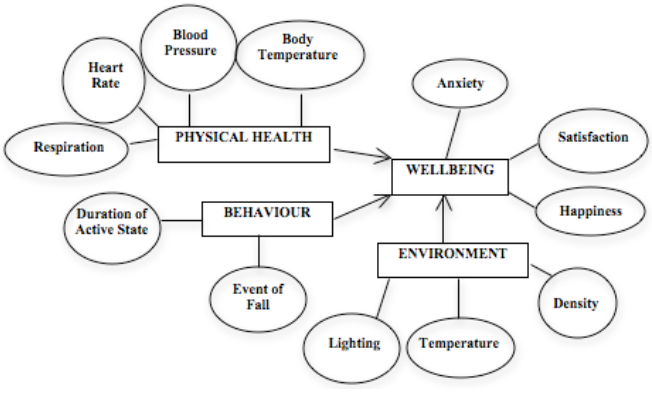

Figure 2. A Proposed Model of Wellbeing Assessment

IV. CHALLENGES

Many healthcare services projects have developed deals with aspects of well being through the concepts of pervasive computing technologies and ambient intelligent. Technological enhancements can be beneficial to promoting people's wellness. Since health care for elderly people is becoming an important issue in developing countries due to rapid growth of elderly people population, development of Contempo system to enhance the quality of health and wellbeing of elderly people is of significant importance. Elderly's disability to access public health services and elderly's preference to have the convenience and comfort of staying at home are a strong justification for developing a Contempo system. There are some challenges in promoting wellbeing of elderly through Contempo systems, such as (1) how to integrate three main sub systems of Contempo to become an effective and comprehensive system, (2) how determine parameters for wellbeing index, and (3) how to develop knowledge base to determine the appropriate clinical decision support system. Such Contempo system, which equipped an automated stand-alone surveillance method and fully integrated within the environment is expected to be able to provide constant monitoring of their health and activities despite their incapabilities and preference, which in turn will enhance their wellbeing.

REFERENCES

[1] World Health Organization and US National Institute of Aging, Global Health and Aging, October 2011.

[2] K. Oizumi, H. Kajiwara, and N. Aratama, Facing up the Problem of Population Aging in Developing Countries, JICA, December 2006

[3] JICA, Aging Population in Asia: Experience of Japan, Thailand, and China, March 2007.

[4] United Nations, Permanent Mission of The Republic of Indonesia to The United Nations New York, New York, 29 April 2011.

[5] D. Popescu, R. Dobrescu, A. Maciuca, and R. Marcu, "Smart Sensor Network For Continuous Monitoring at Home of Elderly Population with Chronic Desease", IEEE 20th Telecommunication Forum TELFOR 2012, Serbia, Nov 20-22, 2012, pp. 603-606.

[6] R.A. Ramlee, D.H.Z. Tang, and M.M Ismail, "Smart Home System for Disabled People Via Wireless Blutooth", 2012 IEEE International Conference on System Engineering and Technology, Bandung, September 11-12, 2012.

[7] W. Putchana, S. Chivapreecha, and T. Limpiti, "Wireless Intelligent Fall Detection and Movement Classification Using Fuzzy Logic", IEEE The 2012 Biomedical Engineering International Conference ((BMEiCON-2012)

[8] N. S. R. K. Prasad and A. Rajesh, "RFID-based hospital real time patient management system," International Journal of Computer Trends and Technology, Vol. 3, Issue 3, 2012, pp. 509-517.

[9] P.Dillon and T. Znati, "Towards an architecture for mobile healthcare," 37th Annual IEEE Conference on Local Computer Network, Florida, 22-25 Oct 2012, pp. 260-263.

[10] V.L. Placa, A. McKnaught, and A. Knight, "Discourse on wellbeing in research and practise", International Journal of Wellbeing, Vol 3, 2013, pp. 116-125.

[11] Stratton, A., (2010). Happiness index to gauge Britain's national mood. *The Guardian*, 15 November, p. 20.

[12] Office for National Statistics (ONS). (2012). Analysis of experimental subjective well-being data from the annualpopulation survey, April to September 2011. Office for National Statistics (ONS).

[13] Hsinchun Chen, "Smart Health and Wellbeing", IEEE Journal on Intelligent System, 2011.

Gadjah Mada University – Shizuoka University Joint Workshop on Telecommunications
Gadjah Mada University, Yogyakarta, Indonesia, December 2–7, 2013

Development of Embedded Gateway for Wireless Sensor Network and Internet Protocol Interoperability

Guntur Dharma Putra, Sigit Basuki Wibowo, Bimo Sunarfri Hantono, Widyawan

Department of Electrical Engineering and Information Technology,
Universitas Gadjah Mada
Jalan Grafika 2, Yogyakarta, INDONESIA
Email: guntur.dharma@mail.ugm.ac.id

Abstract

Wireless Sensor Network (WSN) usage for buildings and household has been increasingly popular because it offers many benefits, such as home automation and home surveilliance. Therefore, in order to increase WSN flexibility usage, remote controlling which enables administration is needed. In fact, generally WSN is controlled by a coordinator (sink node) which is located near the WSN area itself. This research proposes integration of WSN and Internet Protocol (IP), that enables remote controlling and administration through the Internet Protocol stack. This research utilizes the wireless local area network or commonly known as WiFi. One of main components on this WiFi network is Access Point (AP) that acts as node coordinator. Furthermore, AP also serves as a gateway that connects multiple devices, that is connected to the AP, to the Internet. Therefore, this research will develop a software which is going to be implemented to the AP so that the AP has a capability as a gateway for both WiFi network and several WSN protocols to the Internet.

1. Introduction

Wireless Sensor Network (WSN) is a form of distributed autonomous node network which is used for monitoring physical or environment condition such as temperature, sound, vibration, and humidity. Furthermore, it is possible to add an additional function to every node, for instance input/output port which allows actuator controlling that bounds with another electronic or electric device.

WSN usage in a building or household has been increasingly popular since it offers many benefits. A popular example of WSN usage in a household is home surveillance, which allows realtime home monitoring in every corner of the house. Thus, the householders should not be worried about their house security, because the WSN has made the home security much more secure and better. Another example is home automation, a process of automatization of any regular routine activities at home. For instance, turning on lamps when the environment gets dark and turning on the air conditioner when the house owner is about to go back home.

Generally, WSN is controlled by a sink node near the sensor's network area. Thus, the problem arrises if there is a need of remote controlling which is required when the controller is far from WSN area. The possible solution of this problem is the use of Internet Protocol (IP) because it offers wider area and it is accessible anywhere.

However, most WSN does not use the IP stack, but their own proprietary communication protocol, such as ZigBee and IQRF. Therefore, there is a need of a gateway which enables the WSN from multiple vendors to be remotely accessible from the internet.

1.1. Research Objective

This research objectives is to carry out a research about development of a software which will be implemented in an household wireless Access Point to serve as a gateway that is able to integrate WiFi network and a couple of WSN protocols with the internet.

2. Tools and Materials

This research employs TP-LINK MR3020 with OpenWRT installed as an OS for the WiFi Gateway. However, the developed software is not device-specific. It could run on any WiFi router or even desktop computer. This software requires LAMP stack, Python, and USB to serial driver in order to operate. OpenWRT OS has more capability than the default router firmware, it is actually based on Linux kernel [6] and optimized for embedded device. OpenWRT can also serves an web server with LAMP Stack installed. Furthermore, it needs Python with PySerial library and

I would like to thank both of my thesis supervisors, S B Wibowo and B S Hantono.

USB to serial driver in order to communicate with WSNs.

Two kind of WSN will be utilized in this research. The first WSN is IQRF technology. IQRF consist of [4] IQRF sensor nodes, development board for uploading the program, and evaluation board for testing and deployment. In order to work, IQRF needs to be programmed, and the program will run on top of IQRF OS. In this research, IQRF is used to measure environment temperature. However, IQRF sensor nodes support many features and it is not only limited for temperature measurement.

In addition to IQRF, this research will also utilize ZigBee using XBee Series 1, Arduino Uno, and Relay shield. This second part is used to simulate home automation and remote controlling. A coordinator will be connected to the WiFi router using XBee Explorer USB cable and the nodes are Arduino Uno with Relay shield and XBee plugged in.

3. Methodology

3.1. Architecture Design

The architecture design that will be adopted in this research is illustrated in Figure 1, and 2 alleges architecture design in block diagram. The figure illustrates a system which contains two distinct WSN with its own different protocols and a local wireless network (WiFi). WSN protocols employed in this research are IQRF and ZigBee. The research execution will be divided into three Work Package (WP).

3.2. Working Plan

WP 1: Software Design
This part covers literature review which is mostly about the Operating System for the desired embedded device. The next step is the design of software that would be implemented in the wireless Access Point (AP). This implemented software has to be efficiently working to overcome the wireless AP's computational limitation.

WP 2: Software Implementation
This Work Package carries out software implementation. Firstly, ensure that both WSNs are connected to the internet as previously planned. Secondly, assure that WiFi network still runs smoothly after the developed software has been implemented to the Access Point. Supplementary additional features can also be added in this step.

This software utilizes Python programming language with PySerial library in order to read serial port for communicating with the WSNs coordinator. For instance, the code listing for reading IQRF temperature is listed in Listing 1.

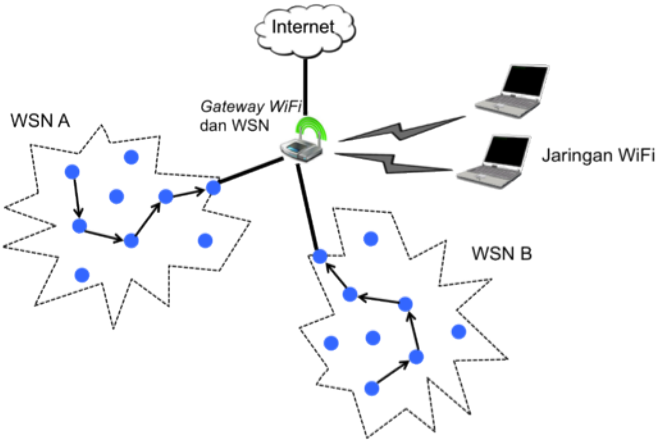

Figure 1: WSN and IP architecture with single wireless Access Point.

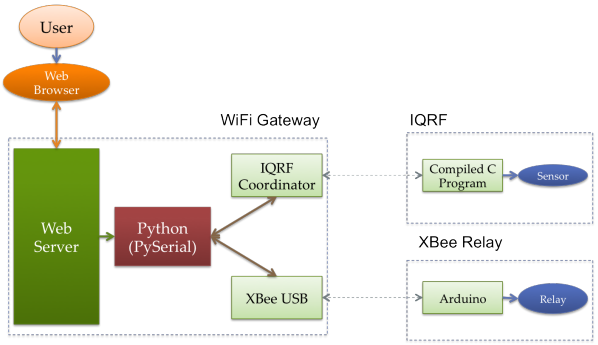

Figure 2: System design in block diagram.

```
# Importing PySerial library (serial)
    to read serial port
import serial,sys

# xbee is a variable that refers to
    serial port:
#       path:           /dev/ttyUSB0
#       baud rate:      4800
xbee = serial.Serial('/dev/ttyUSB0',
    4800)

# write char 'g' and get the returned
    temperature
xbee.write("g")
print xbee.read(10)

# close port
xbee.close()
```

Listing 1: Python code to read IQRF temperature.

The Python source will be executed by the web application that is written using PHP programming lan-

guage. This web application will be called using AJAX in order to get continous update from the IQRF temperature. The PHP code snippet is shown on Listing 2.

```
<?php
$command = 'python /root/iqrf.py';

echo substr(exec($command), 0, 2);

?>
```

Listing 2: PHP code to execute Python script.

WP 3: Integration and Overall System Testing
If both WiFi and two proprietary WSN protocols are able to connect to the internet, this part will only cover entire system tesing. The testing process will also be increased from laboratory scale to test bed scale. Testing in the test bed scale is carried out to ensure that the system will run according to the desired scheme.

4. Result

This research produces a prototype of web application which enables users to control WSNs from several vendors. As seen in Figure 3, this research is conducted by using IQRF Wireless Sensor Network and XBee. IQRF is used to measure the local environment temperature, while XBee is connected to an Arduino Relay for controlling the relay remotely with ZigBee communication protocol.

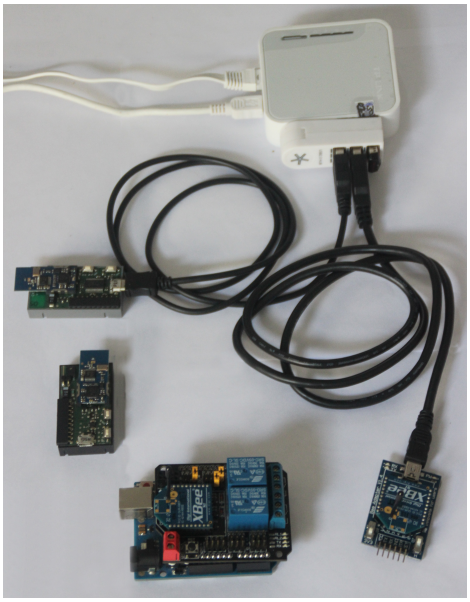

Figure 3: WiFi Router as a gateway is connected to WSNs.

Figure 4 shows the web application screenshot. The web page allows relay controlling and temperature monitoring in a single page. User management and scheduling is also included in this web application.

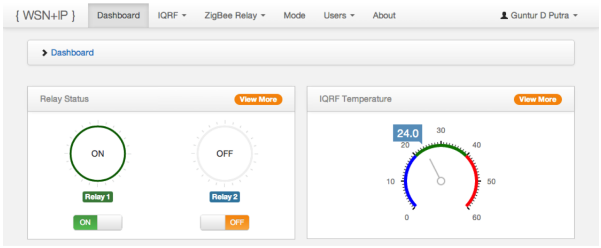

Figure 4: Web application screenshot.

5. Conclusion

This research proposes an approach of software delopment that is intended for developing a software for embedded home router to integrate Wireless Sensor Network and Internet Protocol. This software will run on the top of OpenWRT operating system. By using this software, users could remotely control WSN from both desktop or mobile web browser anywhere as long as there is a connection to the gateway.

The software developed from this research is not device-specific. It could run on any WiFi router or even desktop computer. However, this software requires LAMP stack, Python, and USB to serial driver in order to operate.

Since this device consumes lesser energy than conventional dekstop computer does and supports task automation, this device is suitable to be implemented in a green building.

References

[1] Spinar, R., et al., "Demo Abstract: Efficient Building Management with IP-based Wireless Sensor Network", , 6th European Conference on Wireless Sensor Networks. Cork, Ireland 11-13 February 2009.

[2] Adam Dunkels, Thiemo Voigt, Niclas Bergman, and Mats Jonsson "The Design and Implementation of an IP-based Sensor Network for Intrusion Monitoring", Swedish National Computer Networking Workshop, Sweden, 2004.

[3] Sigit B. Wibowo, and Widyawan, "Wireless Sensor Network and Internet Protocol Integration with COTS", 2013 AUN/SEED-Net Regional Conference in Electrical and Electronics Engineering, Bangkok, Thailand, 2013.

[4] Online document, http://www.iqrf.org/, IQRF, accessed in March 2013.

[5] Widyawan, et al., "iHome: Low-Cost Domotic for Residential Houses", 5th AUN/SEED-Net Regional Conference on Information and Communications Technology (RCICT), Manila, The Philippines, 2012.

[6] Online document, https://openwrt.org/, accessed in March 2013.

[7] Online document, http://www.digi.com/technology/rf-articles/wireless-zigbe, accessed in March 2013.

Gadjah Mada University – Shizuoka University Joint Workshop on Telecommunications
Gadjah Mada University, Yogyakarta, Indonesia, December 2–7, 2013

The Impact of Nonlinear Fiber Propagation on the Integrated LTE (Long Term Evolution) and RoF (Radio over Fiber) over Transmission Varying Span on High Mobility Scenarios

Fakhriy Hario Partiansyah[1,2], Adhi Susanto[1], and I Wayan Mustika[1]

[1]Department of Electrical and Information Engineering,
Faculty of Engineering Gadjah Mada University
Yogyakarta, Indonesia
Email: susanto@te.ugm.ac.id,wmustika@ugm.ac.id

[2]Department of Electrical Engineering,
Faculty of Engineering Brawijaya University
Malang, Indonesia
Email: fakhriy08@ub.ac.id

Abstract

In the high way of metropolitan area, demands tilted use communication voice and data mobility access on high mobility condition. The problem in providing broadband communication (LTE) on high mobility access is not widespread due to the large inter- carrier interference, terrestrial obstacles effect Doppler and multipath fading. Radio over- Fiber (RoF) techniques have been considered as an alternative for wireless interface structure between eNB and RN in order to avoid severe multipath fading. The aim of this research is propose to investigation achieved condition throughput, degradation Error Vector Magnitude (EVM) LTE-RoF over varying transmission span respectively 5-60 Km using modulation QPSK, 16-QAM and 64-QAM by simulating. Research also investigation effect of reducing the overall system throughput for 30 Km/H and 120 Km/H cases.

1. Introduction

In recent years, vehicular networks have attracted a considerable attention from the research community and the automotive industry aiming to provide not only safety and efficiency in the transportation systems but also leisure and infotainment to the driver and the passengers. However, these networks are challenging as they have some specific characteristics, such as high velocity of vehicles and the dynamic network topology, that need to be taken into account in designing any solution for Vehicle-to-Vehicle (V2V) and Vehicle-to-Infrastructure (V2I) communications [1].

Though, as ubiquitous broadband internet access be-comes more and more essential, providing broadband wireless internet on high speed mobility in highway has not been widespread due to several obstacles. First, high speed of mobile station (MS) and high carrier frequency result in large Doppler frequency shift and severe inter carrier interference (ICI) in orthogonal frequency division multiplexing (OFDM) systems, which is the mainstream modulation technique for next-generation communication systems. Secondly, all kinds of signal shadowing and blocking due to the terrestrials, such as hills, buildings and tunnels. [1],[2]. Future generation technology, the integration of microwave and optical networks is a solution for increasing capacity and mobility as well as decreasing costs in the access network using RoF architecture.

Radio-over-Fiber technology is use of optical fiber links to distribute RF signals from BS to Remote Antenna Unit (RAU). In the communication system, RF signal processing functions such as frequency upconversion, carrier modulation, and multiplexing, is performed into the antenna. RoF makes it possible to centralize the RF signal processing function in one head end, then to use optical fiber, which offers low signal loss between 0.3 dB/km for 1550 nm and 0.5 dB/km for 1310 nm wavelength [3].

Distortion in the RoF system is nonlinearity distortion mostly caused by nonlinear character of laser diode. There are chromatic dispersion of optical fiber and noise awakened by transmitter device which still require to be considered. With the consideration, hence writer feels important to do performance evaluation of OFDM system which is integrated with radio over fiber system. Laser are inherently nonlinear, the very basic lasing operation involves several nonlinear mechanisms such as the threshold current, stimulated emission and the spontaneous emission. The stimulated emission is a self multiplying mechanism that occurs under positive optical feedback conditions. Spontaneously emitted photons lack coherency and therefore not desirable. However, only when the driving currents is large than the threshold current, the stimulated emission becomes dominant compared to the spontaneous emission process.

However, there have been several projects attempting to provide broadband wireless network on metro area. An extended survey of broadband internet ac-

I would like to thank my lab members, Professor YYY and Professor ZZZ.

cess approaches on train was presented in [5]. The previous research is presents a comprehensive theoretical and experimental analysis of the full system with a directly modulated LTE-RoF link [4], the system is theoretically and experimentally demonstrated as the high-speed interface between e NodeB and a relay node. The LTE signals under test comprise three different modulation schemes, namely, quaternary phase-shift keying (QPSK), 16- quadratic-amplitude modulation (QAM), and 64-QAM, which are modulated on to orthogonal frequency-division multiplexing (OFDM) at 2.6 GHz. The aims to optimize the physical layer connectivity for the third generation partnership programlong-term evolution employing RoF technologies [5]. Additional research on LTE-RoF [6], proposed LTE4V2X, a novel framework for a centralized vehicular network organization using LTE. In the continuity to this work, this paper presents new performances evaluation of LTE4V2X in highway scenarios in order to evaluate the impact of high mobility. They are studied performances against a decentralized organization protocol.

The main goal of this research is the impact of nonlinear fiber propagation on RoF-LTE integrated to achieve high data rate / throughput and EVMs with varying transmission span fiber on high mobility case. The characteristics of the proposed architecture can be summarized as follows. Line-of-sight (LOS) deployment can greatly avoid ICI induced by Doppler frequency to overcome the signal blocking by the terrestrials.

2. Nonlinear Fiber

The terms linear and nonlinear in optics, mean intensity independent and intensity-dependent phenomena respectively. Nonlinear effects in optical fibers occur due to (1) change in the refractive index of the medium with optical intensity and, (2) inelasticscattering phenomenon. The power dependence of the refractive index is responsible for the Kerr-effect. Depending upon the type of input signal, the Kerr-nonlinearity manifests itself in three different effects such as Self-Phase Modulation (SPM), Cross-Phase Modulation (CPM) and Four-Wave Mixing (FWM). At high power level, the inelastic scattering phenomenon can induce stimulated effects such as Stimulated Brillouin-Scattering (SBS) and Stimulated Raman-Scattering (SRS). The intensity of scattered light grows exponentially if the incident power exceeds a certain threshold value. The difference between Brillouin and Raman scattering is that the Brillouin generated phonons (acoustic) are coherent and give rise to a macroscopic acoustic wave in the fiber, while in Raman scattering the phonons (optical) are incoherent and no macroscopic wave is generated.

The nonlinear effects depend on transmission length. The longer the fiber link length, the more the light interaction and greater the nonlinear effect. As the optical beam propagates along the link length, its power decreases because of fiber attenuation. The effective length (L_{eff}) is that length, up to which power is assumed to be constant [6]. The optical power at a distance z along link is given as

$$P(z) = P_{in} \exp(-\alpha Z)), \tag{1}$$

where P_{in} is the input power (power at $z = 0$)and is coefficient of attenuation. For a actual link length (L) effective length is defined as [6]:

$$P_{in}L_{eff} = \int_{z=0}^{L} p(Z)dz. \tag{2}$$

$$L_{eff} = \frac{1 - exp(-\alpha Z)}{\alpha}. \tag{3}$$

Since communication fibers are long enough so that $L \geq \frac{1}{\alpha}$ This results in $L_{eff} \approx \frac{1}{\alpha}$

2.1. Self Phase Modulation (SPM)

The higher intensity portions of an optical pulse encounter a higher refractive index of the fiber compared with the lower intensity portions while it travels through the fiber. In fact time varying signal intensity produces a time varying refractive index in a medium that has an intensity-dependant refractive index. The phase (ϕ) introduced by a field E over a fiber length L is given by [6]:

$$(\phi) = \frac{2\pi}{\lambda}\eta L, \tag{4}$$

where λ is wavelength of optical pulse propagating in fiber of refractive index η, and ηL is known as optical path length. For a fiber containing high-transmitted power n and L can be replaced by η_{eff} and Ł$_{eff}$ respectively[6]

$$(\phi) = \frac{2\pi}{\lambda}\eta_{eff}L_{eff}. \tag{5}$$

2.2. Cross Phase Modulation (CPM)

SPM is the major nonlinear limitation in a single channel system. The intensity dependence of refractive index leads to another nonlinear phenomenon known as cross-phase modulation (CPM). When two or more optical pulses propagate simultaneously, the cross-phase modulation is always accompanied by SPM and occurs because the nonlinear refractive index seen by an optical beam depends not only on the intensity of that beam but also on the intensity of the other copropagating beams [9]. The effective refractive index of a nonlinear medium can be expressed in terms of the input power (P) and effective core area (A_{eff}) as [6]:

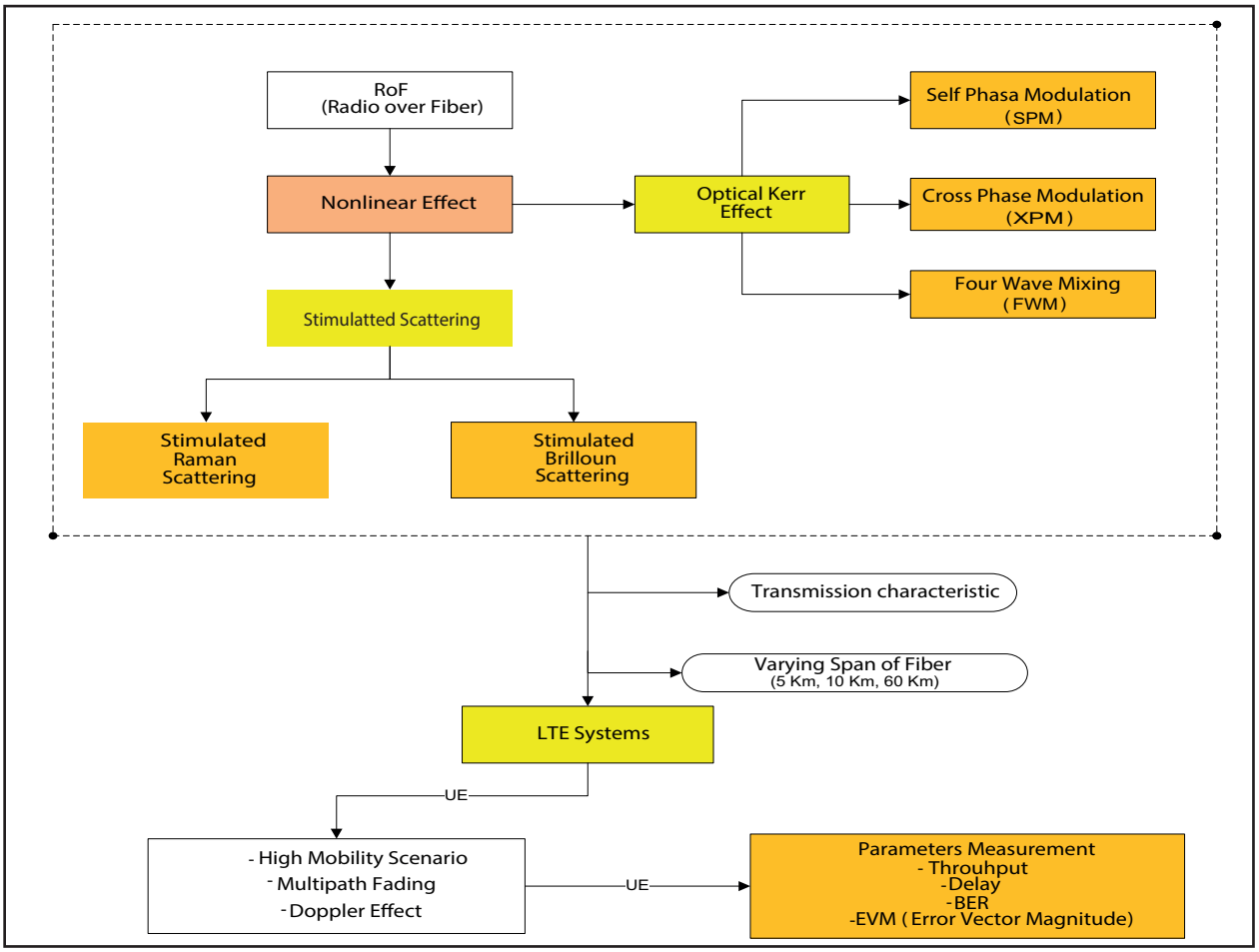

Figure 1: Block Diagram Research Integrated LTE-RoF scheme.

$$\eta_{eff} = \eta_l |\eta_{\eta l} \frac{P}{A_{eff}}. \tag{6}$$

The nonlinear effects depend on ratio of light power to the crosssectional area of the fiber. If the first-order perturbation theory is applied to investigate how fiber modes are affected by the nonlinear refractive index, it is found that the mode shape does not change but the propagation constant becomes power dependent.

$$k_{eff} = k_l + k_{nl} P, \tag{7}$$

where kl is the linear portion of the propagation constant and k_{nl} is nonlinear propagation constant. The phase shift caused by nonlinear propagation constant in traveling a distance L inside fiber is given as [6]:

$$\phi_{nl} = \int_0^L (k_{eff} - k_l) dz. \tag{8}$$

Using equations (8) and (2) nonlinear phase shift becomes

$$\phi_{nl} = k_{nl} P_{in} Leff. \tag{9}$$

2.3. Four Wave Mixing (FWM)

The origin of FWM process lies in the nonlinear response of bound electrons of a material to an applied optical field. In fact, the polarization induced in the medium contains not only linear terms but also the nonlinear terms. The magnitude of these terms is governed by the nonlinear susceptibilities of different orders. The FWM process originates from third order nonlinear susceptibility $(X^{(3)})$. If three optical fields with carrier frequencies ω_1, ω_2 and ω_3, copropagate inside the fiber simultaneously, $(X^{(3)})$ generates a fourth field with frequency [6]: ω_4, which is related to other frequencies by a relation

$$\omega_4 = \omega_1 \pm \omega_2 \pm \omega_3. \tag{10}$$

$$\text{Energy} : \omega_1 + \omega_2 = \omega_3 + \omega_4. \tag{11}$$

$$Momentum : \beta_1 + \beta_2 = \beta_3 + \beta_4. \tag{12}$$

2.4. Stimulated Brilloun Scattering (SBS)

Stimulated Brillouin scattering (SBS) is a nonlinear optical process when the input power exceeds the threshold in a fiber. Since SBS was observed as the nonlinear phenomena in the 1964 for the first time, it has been extensively investigated. SBS is shown through the Stokes light of which wave frequency relative to the incident light down, the frequency shift is determined by the nonlinear medium. Because of the low threshold of inherent power, the narrow line-width gain and high conversion efficiency characteristics of SBS, fiber amplifier (FBA) and lasers (FBL) based on SBS are important in many applications. Only can the long fiber length and high pulse light input power satisfy the need of long distance and large scale structural monitoring. The Brillouin of the stokes wave is given by [9]:

$$V_B = \frac{\omega_A}{2_\pi} = \frac{2_n}{\lambda_p}, \tag{13}$$

where V_A is refraqtive index of the fiber, W_A is the freq of the acoustic wave and λ_p is the pump wave length. Estimatis Brillouin threshold for long fibers 20 km for α=0.2 dB/Km at $1.55\mu m$. For telecom fibers $A_{eff} = 50-75\mu m^2$. Threshold power $P_{th} \sim 1mW$ is relatively small. The Brillouin for pump light is approximated by

$$P_{th} = \frac{21A_{eff}}{gBL_{eff}}. \tag{14}$$

Brillouin gain $gB = 5\chi 10^{-}11m/W$ is nearly independent of the pump wavelength.

2.5. Stimulated Raman Scattering (SRS)

Stimulated Raman scattering (SRS) is important as a phenomenon which can cause signal distortion in long haul, low-loss telecommunications fibres and as an effect upon which wavelength shifting devices, known as fibre Raman lasers, are based . Narrow linewidth pump laser light is converted to a broad Stokes spectral output. The conversion efficiency from pump to Stokes wave- lengths is strongly influenced by the input power, the fibre length, the intrinsic Raman gain and the loss distribution over the range of wavelengths corresponding to the Stokes output.

The Raman gain y_i that is coupling the first and the channel can be expressed using triangular Raman gain as follows [5]:

$$y_i = \frac{i\Delta_v Y_p}{1.5X10^{13}}, \tag{15}$$

For $i\Delta_v < 1.5x10^{13}$

Y_p= Peak Raman gain coefficient with a value $6x10^{-12}$ and Δ_v= channel sampling frequency [5].

Raman threshold is defined as the input pump power at which Stokes power becomes equal to the pump power at the fiber output[5]:

$$P_s(L) = P_pLP_o \exp(-\alpha L), \tag{16}$$

for $P_o = I_oA_{eff}$ Assuming a Lorentzian shape for the Raman-gain spectrum, Raman threshold is reached when (Smith, Appl. Opt. 11, 2489, 1972)

$$P_{th} = \frac{16A_{eff}}{grL_{eff}}. \tag{17}$$

3. Conclusion

This research is propose to investigate the impact of performance integrated LTE-RoF system from nonlinear fiber propagation phenomena and effect reducing the overall system. Goal of the measurement is to achieve value of throughput, BER, delay and EVM on high mobility and terrestrial condition.

References

[1] Guillaume Remy, Sidi-Mohammed Senouci, Francois Jan, Yvon Gourhant, Impact of High Mobility in Highway Scenarios, Laboratory, University of Bourgogne, France, IEEE 2011.

[2] W. P. Ng, T. Kanesan, Z. Ghassemlooy C. Lu, Theoretical and Experimental Optimum System Design for LTE-RoF Over Varying Transmission Span and Identifi cation of System Nonlinear Limit, Volume 4, Number 5, October 2012.

[3] havamaran Kanesan, Zabih Ghassemlooy, Optimization of Optical Modulator for LTE RoF in Nonlinear Fiber Propagation, IEEE Photonics Technology Latters Vol 24, No 7, April 2012.

[4] G. Remy, S.-M. Senouci, F. Jan, and Y. Gourhant, Lte4v2x: Lte for a centralized vanet organization, in Submitted to IEEE Globecom 2011,Houston, Texas.

[5] Xiaorui Li, Huaping Gong *, Shuhua Li, Jianfeng Wang, "Experimental Investigation on Pulse Light Stirn ulated Brillouin Scattering in the Optical Fiber." Institute of Optoelectronic Technology, China Jiliang University, Hangzhou, China,2011.

[6] S. P. Singh and N. Singh,"Nonlinear Effects in Optical Fibers :Origin Management and Application,"Progress In Electromagnetics Research, PIER 73, 249275, 2007,Department of Electronics and Communication University of Allahabad Allahabad-211002, India.

[7] R.Herschel, C.G Schaffer, Radio over Fiber systems for Next Generation Wireless Access, International Scientist Workshop, Hamburg, Germany 2011.

[8] M. Cherif, S.-M. Senouci, and B. Ducourthial, Vehicular network selforganizing architectures, in Proc. IEEE GCC 2009.

[9] S. W. Peters, A. Y. Panah, K. T. Truong, and J. R. W. Heath, BRelay Architectures for 3GPP LTE-Advanced,[EURASIP]. Wireless Commun. Netw., vol. 2009, pp. 618787-1618787-14, 2009.

[10] K. Dimou, W. Min, Y. Yu, M. Kazmi, A. Larmo, J. Pettersson, W.Muller, and Y. Timner, BHandover within 3GPP LTE:Design principles and performance,[in Proc. IEEE 70th VTC, 2009, pp. 1 4.

[11] M. Zhou, Principle, Technology and Challenge of Radio over Fiber (RoF) based Broadband Access for Metro and Inter-city Trains, in Asia Communications and Photonics Conference and Exhibition, 2009, pp. 1 10.

[12] S. P. Singh and N. Singh nonlinear effect in optical fibers origin management and application, Progress In Electromagnetics Research, PIER 73, 249275, 2007.

[13] Reza Abdole, Razali Ngah, Vida Vakilin, Tharek A. Rahman, Application of Radio over Fiber in mobile communication, Asia Pacific Conference, December 4-6, 2007

Controllability and Observability Analysis of the Gain Scheduling Based Linearization for UAV Quadrotor

***Abstract*—This paper presents the gain scheduling based linearization of simplified quadrotor non-linear model as well as the test for the system controllability and observability for various equilibrium point. The simplified non-linear model of quadrotor is linearized at some equilibrium points to get the linear state equation. Then, the controllability and observability test is done to the linearized model for various equilibrium points. The system behavior is then tested by using the state feedback controller to confirm the result.**

***Keywords*—Quadcopter, non-linear control system, linearization, gain scheduling, LQR.**

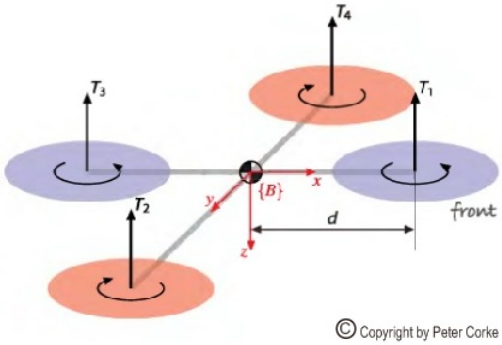

Fig. 1. Quadcopter axis

I. Introduction

Quadcopter is one of many type of Unmanned Aerial Vehicle that becoming popular and having much attentions from various group recently, especially the researchers and hobbiest in aeromodeling. Several factors that contribute to its popularity are its reliability in maneuvering, its ability to be flown indoors, and easier to model and control [1], [6].

One of the most important problem on the quadcopter stems from the fact that quadcopter is essentially not a stable system, both in stabilization and trajectroy following. Therefore, a special considerations are needed in designing the control system for the purpose of estabilizing or maneuvering. Existing control theories in controlling quadcopter are widely varied. The most commonly used is the conventional PID control, mainly due to its simple structure are easy enough to be designed and implemented in varied systems including quadcopter [1].

The drawback of PID Controller is it has the constant gain which may be optimum just for some specific condition. In order to get better result, the controller has to be adaptive so that it can adjust the controller gain to adapt to the position and attitude change of the quadrotor. Many people have tried to design this adaptive control such as Gaikwad [2] with auto-tuning PID Loop Shaping and Liu [4] who design self-adaptive PID based on the least-square method.

One of the challenge in designing controller for quadrotor is that the system is non-linear so that we have to linearize it first. The basic limitation of the controller design via standard linearization is the fact that the control is guaranteed to work only in the neighborhood of a single equilibrium point. Gain scheduling is a technique to design controller of non-linear system by linearize the system at several equilibrium points, design the controller at each point, and implement the family of linear controllers as a single controller with varying gain or parameter[3].

In this paper, we linearize the simplified model of quadrotor based on Peter Corkes model [1] using the Gain Scheduling linearization at some equilibrium point. Then, we test the controllability and observability of the system for various equilibrium points. After that, using the linearized state equation, we find the state feedback controller and use it to control the altitude and attitude of the quadrotor non-linear model.

II. Project Overview

A. Notation Explanation

In this section, we explain the derivation of state-space equation of quadcopter system. The linearization is performed in order to formulate the transfer function of the quadcopter plant. Based on the Corke's model [1], the model is shown at figure 1. We use 12 states for this state-space model, its position in world frame is denoted as $\epsilon_1 = \begin{bmatrix} x & y & z \end{bmatrix}$, its roll, pitch, yaw angles denoted as $\epsilon_2 = \begin{bmatrix} \phi & \theta & \psi \end{bmatrix}$, its velocity due to x-axis, y-axis, z-axis denoted as $\epsilon_3 = \begin{bmatrix} \dot{x} & \dot{y} & \dot{z} \end{bmatrix}$

, and its angular velocity due to x-axis, y-axis, z-axis denoted as $\boldsymbol{\epsilon}_4 = \begin{bmatrix} \dot{p} & \dot{q} & \dot{r} \end{bmatrix}$. The state variable and its system input is $x = \begin{bmatrix} \boldsymbol{\epsilon}_1^T & \boldsymbol{\epsilon}_2^T & \boldsymbol{\epsilon}_3^T & \boldsymbol{\epsilon}_4^T \end{bmatrix}^T$, $u = \begin{bmatrix} \omega_1^2 & \omega_2^2 & \omega_3^2 & \omega_4^2 \end{bmatrix}^T$. Hence,

$$x = \begin{bmatrix} x_1, & ..., & x_{12} \end{bmatrix}^T$$

$$u = \begin{bmatrix} u_1, & ..., & u_4 \end{bmatrix}^T$$

.

B. Translational and Rotational Analysis

Based on Newton's second law of translational motion [6], we have this equation:

$$\boldsymbol{F} = m\dot{\boldsymbol{v}} + (\boldsymbol{\omega} \times m\boldsymbol{v}) \tag{1}$$

where $\boldsymbol{\omega} = \boldsymbol{\epsilon}_4$ and $v = \boldsymbol{\epsilon}_3$.

From fig.1, we could get the forces which is worked on the quadcopter

$$\boldsymbol{F} = \boldsymbol{F}_g - \boldsymbol{F}_{thrust} \tag{2}$$

$$\boldsymbol{F} = \begin{bmatrix} 0 \\ 0 \\ mg \end{bmatrix} - {}^W\boldsymbol{R}_B \begin{bmatrix} 0 \\ 0 \\ T \end{bmatrix}$$

Therefore, equation 2 can be expressed as

$$\dot{\boldsymbol{v}} = \frac{1}{m}\left[g \begin{bmatrix} 0 \\ 0 \\ 1 \end{bmatrix} - {}^W\boldsymbol{R}_B \begin{bmatrix} 0 \\ 0 \\ T \end{bmatrix} \right] - \begin{bmatrix} \dot{p} \\ \dot{q} \\ \dot{r} \end{bmatrix} \times \begin{bmatrix} \dot{x} \\ \dot{y} \\ \dot{z} \end{bmatrix}$$

where m is the mass of quadcopter, T is vertical thrust of quadcopter against gravity and ${}^W\boldsymbol{R}_B$ is the rotation matrix from body-frame to world-frame or inertial-frame.

$${}^W\boldsymbol{R}_B = \begin{bmatrix} c_\theta c_\psi & s_\phi s_\theta c_\psi - c_\phi s_\psi & c_\phi s_\theta c_\psi + s_\phi s_\psi \\ c_\theta s_\psi & s_\phi s_\theta s_\psi + c_\phi c_\psi & c_\phi s_\theta s_\psi - s_\phi c_\psi \\ s_\theta & s_\phi c_\theta & c_\phi c_\theta \end{bmatrix}$$

$$\dot{\boldsymbol{v}} = \frac{1}{m}\left[\begin{bmatrix} -T(c_\phi s_\theta c_\psi + s_\phi s_\psi) \\ -T(c_\phi s_\theta s_\psi - s_\phi c_\psi) \\ mg - T(c_\phi c_\theta) \end{bmatrix} - {}^W\boldsymbol{R}_B \begin{bmatrix} (\dot{q}\dot{z} - \dot{r}\dot{y}) \\ (\dot{r}\dot{x} - \dot{p}\dot{z}) \\ (\dot{p}\dot{y} - \dot{q}\dot{x}) \end{bmatrix} \right]$$

Assume $\dot{p}, \dot{q}, \dot{r}, \dot{x}, \dot{y}, \dot{z} \approx 0$, then

$$\ddot{x} = -\frac{1}{m}T(c_\phi s_\theta c_\psi + s_\phi s_\psi) \tag{3}$$

$$\ddot{y} = -\frac{1}{m}T(c_\phi s_\theta s_\psi - s_\phi c_\psi) \tag{4}$$

$$\ddot{z} = g - \frac{1}{m}T(c_\phi c_\theta) \tag{5}$$

Using rigid body rotational law, we have

$$\boldsymbol{\Gamma} = I\dot{\boldsymbol{\omega}} + (\boldsymbol{\omega} \times I\boldsymbol{\omega}) \tag{6}$$

where, I is moment of inertia of quadcopter

$$I = \begin{bmatrix} I_x & 0 & 0 \\ 0 & I_y & 0 \\ 0 & 0 & I_z \end{bmatrix}.$$

Then, equation 6 can be written as

$$I\dot{\boldsymbol{\omega}} = \begin{bmatrix} \tau_x \\ \tau_y \\ \tau_z \end{bmatrix} - \left[\begin{bmatrix} \dot{p} \\ \dot{q} \\ \dot{r} \end{bmatrix} \times \begin{bmatrix} I_x\dot{p} \\ I_y\dot{q} \\ I_z\dot{r} \end{bmatrix} \right]$$

and

$$\tau_x = db(\omega_4^2 - \omega_2^2)$$

$$\tau_y = db(\omega_1^2 - \omega_3^2)$$

$$\tau_z = k(\omega_1^2 - \omega_2^2 + \omega_3^2 - \omega_4^2)$$

$$T = b(\omega_1^2 + \omega_2^2 + \omega_3^2 + \omega_4^2)$$

Thus, we have these equations for angular acceleration of quadcopter

$$\ddot{p} = \frac{db}{I_x}(\omega_4^2 - \omega_2^2) - \frac{I_z - I_y}{I_x}\dot{q}\dot{r} \tag{7}$$

$$\ddot{q} = \frac{db}{I_y}(\omega_1^2 - \omega_3^2) - \frac{I_x - I_z}{I_y}\dot{p}\dot{r} \tag{8}$$

$$\ddot{r} = \frac{k}{I_z}(\omega_1^2 - \omega_2^2 + \omega_3^2 - \omega_4^2) - \frac{I_y - I_x}{I_z}\dot{p}\dot{q} \tag{9}$$

We also derive the roll, pitch and yaw (RPY) rates which is a function of angular velocity, using $inverted\ Wronskian\ matrix$, denoted as

$$W^{-1} = \frac{1}{c_\theta}\begin{bmatrix} c_\theta & s_\phi s_\theta & c_\phi s_\theta \\ 0 & c_\phi c_\theta & -s_\phi c_\theta \\ 0 & s_\phi & c_\phi \end{bmatrix}$$

and the relation between RPY rates and angular velocity expressed by matrix

$$\begin{bmatrix} \dot{\phi} \\ \dot{\theta} \\ \dot{\psi} \end{bmatrix} = W^{-1}\begin{bmatrix} \dot{p} \\ \dot{q} \\ \dot{r} \end{bmatrix}$$

So, the roll, pitch and yaw rates is

$$\dot{\phi} = \dot{p} + s_\phi t_\theta \dot{q} + c_\phi t_\theta \dot{r} \tag{10}$$

$$\dot{\theta} = c_\phi \dot{q} + s_\phi \dot{r} \tag{11}$$

$$\dot{\psi} = \frac{s_\phi}{c_\theta}\dot{q} + \frac{c_\phi}{c_\theta}\dot{r} \tag{12}$$

C. Linearization

The non-linear model of quadrotor will be linearized at the equilibrium point in order to make the system more amenable. In order to do the linearization, we have to find the equilibrium point of the system or can be written as

$$0 = f(X(\boldsymbol{\alpha}, \boldsymbol{\beta}, \boldsymbol{\gamma}, \boldsymbol{\delta})).$$

So, the equations can be modified as follow

$$\dot{x}_1 = \dot{x} = x_7 = 0 \tag{13}$$

$$\dot{x}_2 = \dot{y} = x_8 = 0 \tag{14}$$

$$\dot{x}_3 = \dot{z} = x_9 = 0 \tag{15}$$

$$\dot{x}_4 = \dot{\phi} = x_{10} + s_{x_4} t_{x_5} x_{11} + c_{x_4} t_{x_5} x_{12} = 0 \quad (16)$$

$$\dot{x}_5 = \dot{\theta} = c_{x_4} x_{11} + s_{x_4} x_{12} = 0 \quad (17)$$

$$\dot{x}_6 = \dot{\psi} = \frac{s_{x_4}}{c_{x_5}} x_{11} + \frac{c_{x_4}}{c_{x_5}} x_{12} = 0 \quad (18)$$

$$\dot{x}_7 = \ddot{x} = -\frac{1}{m} T(c_{x_4} s_{x_5} c_{x_6} + s_{x_4} s_{x_6}) = 0 \quad (19)$$

$$\dot{x}_8 = \ddot{y} = -\frac{1}{m} T(c_{x_4} s_{x_5} s_{x_6} - s_{x_4} c_{x_6}) = 0 \quad (20)$$

$$\dot{x}_9 = \ddot{z} = g - \frac{1}{m} T(c_{x_4} c_{x_5}) = 0 \quad (21)$$

$$\dot{x}_{10} = \ddot{p} = \frac{db}{I_x}(u_4 - u_2) - \frac{I_z - I_y}{I_x} x_{11} x_{12} = 0 \quad (22)$$

$$\dot{x}_{11} = \ddot{q} = \frac{db}{I_y}(u_1 - u_3) - \frac{I_x - I_z}{I_y} x_{10} x_{12} = 0 \quad (23)$$

$$\dot{x}_{12} = \ddot{r} = \frac{k}{I_z}(u_1 - u_2 + u_3 - u_4) - \frac{I_y - I_x}{I_z} x_{10} x_{11} = 0 \quad (24)$$

From equation 19 and 20, we get

$$s^2 x_5 + t^2 x_4 = 0$$

The only solution for this equation is $x_4 = 0$ and $x_5 = 0$. Combining the results with equation 16, 17, and 18 we get $x_{10} = 0$, $x_{11} = 0$ and $x_{12} = 0$. Lets assume the equilibrium point is located at some certain position in Cartesian coordinate (x, y, z) and at some yaw angle position defined by $x = \alpha$, $y = \beta$, $z = \gamma$ and $\psi = \delta$. So, the complete list of the state variables value in this equilibrium, $X(\alpha, \beta, \gamma, \delta)$, can be written as $x_1 = \alpha$, $x_2 = \beta$, $x_3 = \gamma$, $x_4 = 0$, $x_5 = 0$, $x_6 = \delta$, $x_7 = 0$, $x_8 = 0$, $x_9 = 0$, $x_{10} = 0$, $x_{11} = 0$ and $x_{12} = 0$.

The state equation for the linearized model is given by

$$\dot{x} = \boldsymbol{A}x + \boldsymbol{B}u$$
$$y = \boldsymbol{C}x + \boldsymbol{D}u.$$

We can find the matrix $\boldsymbol{A}$ and $\boldsymbol{B}$ by using this equation

$$\boldsymbol{A} = \begin{bmatrix} \frac{\partial f_1}{\partial x_1}|_{X(\alpha,\beta,\gamma,\delta)} & \cdots & \frac{\partial f_1}{\partial x_{12}}|_{X(\alpha,\beta,\gamma,\delta)} \\ \vdots & \ddots & \vdots \\ \frac{\partial f_{12}}{\partial x_1}|_{X(\alpha,\beta,\gamma,\delta)} & \cdots & \frac{\partial f_{12}}{\partial x_{12}}|_{X(\alpha,\beta,\gamma,\delta)} \end{bmatrix}$$

$$\boldsymbol{B} = \begin{bmatrix} \frac{\partial f_1}{\partial u_1}|_{X(\alpha,\beta,\gamma,\delta)} & \cdots & \frac{\partial f_1}{\partial u_4}|_{X(\alpha,\beta,\gamma,\delta)} \\ \vdots & \ddots & \vdots \\ \frac{\partial f_{12}}{\partial u_1}|_{X(\alpha,\beta,\gamma,\delta)} & \cdots & \frac{\partial f_{12}}{\partial u_4}|_{X(\alpha,\beta,\gamma,\delta)} \end{bmatrix}$$

And then, we get

$$\boldsymbol{A}_{(12\times12)} = \left[\begin{array}{ccc|c} & \boldsymbol{O}_{(6\times6)} & & \boldsymbol{I}_{(6\times6)} \\ \hline \boldsymbol{O}_{(2\times3)} & \boldsymbol{N}_{(2\times2)} & \boldsymbol{O}_{(2\times1)} & \boldsymbol{I}_{(6\times6)} \\ & \boldsymbol{O}_{(4\times6)} & & \end{array}\right] \quad (25)$$

$$\boldsymbol{B}_{(12\times4)} = \begin{bmatrix} \boldsymbol{O}_{(8\times4)} \\ \boldsymbol{M}_{(4\times4)} \end{bmatrix} \quad (26)$$

where $\boldsymbol{O}$ is zero matrix and $\boldsymbol{I}$ is identity matrix. While $\boldsymbol{N}$ and $\boldsymbol{M}$ can be defined as

$$\boldsymbol{N}_{(2\times2)} = \begin{bmatrix} -gs_\delta & -gc_\delta \\ gc_\delta & -gs_\delta \end{bmatrix},$$

$$\boldsymbol{M}_{(2\times2)} = \begin{bmatrix} -\frac{b}{m} & -\frac{b}{m} & -\frac{b}{m} & -\frac{b}{m} \\ 0 & -\frac{db}{I_x} & 0 & \frac{db}{I_x} \\ \frac{db}{I_y} & 0 & -\frac{db}{I_y} & 0 \\ \frac{k}{I_z} & -\frac{k}{I_z} & \frac{k}{I_z} & -\frac{k}{I_z} \end{bmatrix}.$$

Constants which are used is defined as

$$g = 9,81\ {}^{m}/_{s^2}$$
$$i_x = 0.0820\ kg.m^2$$
$$i_y = 0.0845\ kg.m^2$$
$$i_z = 0.1377\ kg.m^2$$
$$b = 1.2953 \times 10^{-5}\ kg.m$$
$$d = 0.165\ m$$
$$k = 1.0368 \times 10^{-7}\ kg.m^2$$
$$m = 4.34\ kg$$

The output of this quadrotor model is defined by the vector $y = \begin{bmatrix} x & y & z & \psi \end{bmatrix}^T$, so the matrix $\boldsymbol{C}$ and $\boldsymbol{D}$ can be written as

$$\boldsymbol{C}_{(4\times12)} = \begin{bmatrix} \boldsymbol{I}_{(3\times3)} & \boldsymbol{O}_{(3\times9)} \\ \boldsymbol{O}_{(1\times3)} & \boldsymbol{L}_{(1\times3)} \end{bmatrix} \quad (27)$$

where

$$\boldsymbol{L}_{(4\times12)} = \begin{bmatrix} 0 & 0 & 1 & 0 & 0 & 0 & 0 & 0 & 0 \end{bmatrix}.$$

So, the linearized model of this quadrotor is

$$\dot{x} = \boldsymbol{A}_{12\times12}x + \boldsymbol{B}_{12\times4}u$$
$$y = \boldsymbol{C}_{12\times1}x.$$

D. Controlability and Observability

Before designing any controller or observer any further, we have to check the controllability and observability of the system. Let us define the controllability matrix as

$$P_c = \begin{bmatrix} \boldsymbol{B} & \boldsymbol{AB} & \boldsymbol{A^2B} & \cdots & \boldsymbol{A^{n-1}B} \end{bmatrix}$$

.

With n defines the order of the system. In our case, the matrix can be written as

$$P_{c(12\times48)} = \left[\begin{array}{cccccc} \boldsymbol{B} & \boldsymbol{AB} & \boldsymbol{A^2B} & \cdots & \boldsymbol{A^{11}B} \end{array} \right]$$

$$P_{c(12\times48)} = \left[\begin{array}{c|c|c|c|c} \boldsymbol{O}_{(8\times4)} & \boldsymbol{O}_{(2\times4)} & \boldsymbol{O}_{(6\times4)} & R_{(2\times4)} & \\ & \boldsymbol{M}_{(4\times4)} & R_{(2\times4)} & \boldsymbol{O}_{(10\times4)} & \boldsymbol{O}_{(12\times36)} \\ \boldsymbol{M}_{(4\times4)} & \boldsymbol{O}_{(6\times4)} & \boldsymbol{O}_{(4\times4)} & & \end{array} \right] \quad (28)$$

where

$$R_{(2\times4)} = \left[\begin{array}{cccc} -\frac{gc_\delta db}{I_y} & \frac{gc_\delta db}{I_x} & \frac{gc_\delta db}{I_y} & -\frac{gc_\delta db}{I_x} \\ -\frac{gs_\delta db}{I_y} & -\frac{gc_\delta db}{I_x} & \frac{gs_\delta db}{I_y} & \frac{gc_\delta db}{I_x} \end{array} \right].$$

This controllability matrix has unique form. From the configuration of the matrix element above, we can conclude that the rank of the controllability matrix will always be the same with the order of the system (n=12) regardless of the value of $\alpha, \beta, \gamma, \delta, g, \epsilon, \lambda, \kappa$ and ρ. We can conclude that the system is controllable.

By definition, the matrix observability can be written as

$$P_{o(48\times12)} = \left[\begin{array}{cccccc} \boldsymbol{C} & \boldsymbol{CA} & \boldsymbol{CA^2} & \cdots & \boldsymbol{CA^{11}} \end{array} \right]^T$$

$$P_{o(48\times12)} = \left[\begin{array}{c} \boldsymbol{\chi}_{1(4\times12)} \\ \boldsymbol{\chi}_{2(4\times12)} \\ \boldsymbol{\chi}_{3(4\times12)} \\ \boldsymbol{\chi}_{4(4\times12)} \\ \boldsymbol{O}_{(32\times12)} \end{array} \right] \quad (29)$$

where

$$\boldsymbol{\chi}_{1(4\times12)} = \left[\begin{array}{cc} \boldsymbol{I}_{(3\times3)} & \boldsymbol{O}_{(3\times9)} \\ \boldsymbol{O}_{(1\times3)} & \boldsymbol{L}_{(1\times9)} \end{array} \right]$$

$$\boldsymbol{\chi}_{2(4\times12)} = \left[\begin{array}{cccc} \boldsymbol{O}_{(4\times6)} & \boldsymbol{I}_{(3\times3)} & \boldsymbol{O}_{(4\times2)} & \boldsymbol{Z}_{(4\times1)} \\ & \boldsymbol{O}_{(1\times3)} & & \end{array} \right]$$

$$\boldsymbol{\chi}_{3(4\times12)} = \left[\begin{array}{ccc} \boldsymbol{O}_{(4\times3)} & \boldsymbol{N}_{(2\times2)} & \boldsymbol{O}_{(4\times7)} \\ & \boldsymbol{O}_{(2\times2)} & \end{array} \right]$$

$$\boldsymbol{\chi}_{4(4\times12)} = \left[\begin{array}{ccc} \boldsymbol{O}_{(2\times9)} & \boldsymbol{N}_{(2\times2)} & \boldsymbol{O}_{(4\times1)} \\ & \boldsymbol{O}_{(2\times2)} & \end{array} \right]$$

and

$$\boldsymbol{Z}_{(4\times1)} = \left[\begin{array}{cccc} 0 & 0 & 0 & 1 \end{array} \right]^T$$

This observability matrix has unique form. From the configuration of the matrix element above, we can conclude that the rank of the observability matrix will always be the same with the order of the system $(n = 12)$ regardless of the value $\alpha, \beta, \gamma, \delta, g, \epsilon, \lambda, \kappa$ and ρ. We can conclude that the system is observable.

What makes this result interesting is the fact that the controllability and observability dont depend on the equilibrium point we have chosen in the beginning, which is at $x = \alpha$, $y = \beta$, $z = \gamma$, and $\psi = \delta$. Even, the property of matrix $\boldsymbol{A}$ and $\boldsymbol{B}$ depend only on the yaw angle value. So, we can conclude that the system can be controlled by more advance adaptive controller technique such as gain scheduling without concerning the controllability and observability of the system. For gain scheduling, the controller matrix K will depend on the value of yaw angle ψ and will be both controllable and observable for all value of possible ψ.

III. Control System Design

We are now able to design controller of quadrotor using the matrix $\boldsymbol{A}$, $\boldsymbol{B}$, and $\boldsymbol{C}$ we have found. Let us verify the controllability of this linearized model by using state feedback regulator.

A. Linear Quadratic Regulator

Linear quadratic regulator is a control method using state feedback law $u = -Kx$ [5] to minimize the cost function defined as

$$J(u) \int_0^\infty x^T Q x + u^T R u \, dt \quad (30)$$

where Q is weight matrix for state energy and R is weight matrix for input energy. The matrix K can be derived from equation

$$K = R^{-1}(\boldsymbol{B}^T S + N^T). \quad (31)$$

While the matrix S is solution for the Riccati equation

$$\boldsymbol{A}^T S + S\boldsymbol{A} - (S\boldsymbol{B} + N)R^{-1}(\boldsymbol{B}^T S + N^T) + Q = 0. \quad (32)$$

In order to solve for matrix K, we have to give numerical value for so that we get all numerical values of matrix A and B. For simplicity, lets choose the weight matrix Q and R as follow

$$Q = qI_{12\times12}$$
$$R = rI_{12\times12}.$$

Where $q = 10000000000$ and $r = 0.0000000001$. We choose small value for weight matrix R because we dont want to minimize the energy of input signal. In order to make the quadrotor able to maintain its altitude, we have to give great amount of energy for input signal. We choose the value for $\delta = 0.5$. The matrix K we get from the LQR is

$$K_{(4\times12)} = \xi \times \left[\begin{array}{ccc} \boldsymbol{U}_{(4\times4)} & \boldsymbol{V}_{(4\times4)} & \boldsymbol{W}_{(4\times4)} \end{array} \right] \quad (33)$$

where ξ is a constant, its value is 1.0×10^{10} and

$$\boldsymbol{U}_{(4\times4)} = \left[\begin{array}{cccc} -0.6205 & -0.3390 & -0.5000 & 0.0000 \\ 0.3390 & -0.6250 & -0.5000 & -3.8392 \\ 0.6205 & 0.3390 & -0.5000 & 0.0000 \\ -0.3390 & 0.6250 & -0.5000 & 3.8392 \end{array} \right],$$

$$\boldsymbol{V}_{(4\times6)} = \left[\begin{array}{cccc} 3.8392 & 0.5000 & -0.9007 & -0.4921 \\ 0.0000 & -0.5000 & 0.4921 & -0.9007 \\ -3.8392 & 0.5000 & 0.9007 & 0.4921 \\ 0.0000 & -0.5000 & -0.4921 & 0.9007 \end{array} \right],$$

$$\boldsymbol{W}_{(4\times6)} = \begin{bmatrix} -0.5000 & 0.0000 & 0.7071 & 0.5000 \\ -0.5000 & -0.7071 & 0.0000 & -0.5000 \\ -0.5000 & 0.0000 & -0.7071 & 0.5000 \\ -0.5000 & 0.7071 & 0.0000 & -0.5000 \end{bmatrix}.$$

B. Simulation

We use matrix which has been mentioned above to produce input signal based on the state feedback law $u = -Kx$. Here, we present the result for quadrotor attitude and altitude control using state feedback controller we get by using the linearized model property of quadrotor.

In figure 2, we get the graph of quadrotor altitude with initial condition $z = 0$ to the steady state condition $z = -5$. While, in figure 3, we have the graph of quadrotor yaw angle with initial condition $\psi = 0$ and steady state condition $\psi = 0.5$. We can see that the state feedback controller we get from the linearized model of the quadrotor works well. We dont see any overshoot and the system dont need much time to reach the stability. Changing the value of variable $\delta = 1$, we get the result in figure 4 and figure 5.

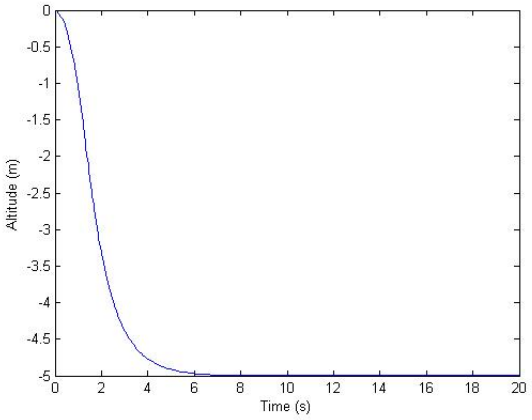

Fig. 2. Altitude Z, for $\delta = 0.5$

IV. Conclusion

In this paper, we get the linearized model of quadrotor simplified model and show that the system is controllable and observable regardless of the value of reference position in Cartesian coordinate as well as the reference yaw angle. We use the simplified model of quadrotor based on Peter Corkes model then linearize it to get the linearized state equation at some equilibrium point. Then, we test the controllability and observability of the linearized system and show that the system is controllable and observable regardless of the value of the equilibrium point we choose. We then test the system behavior by

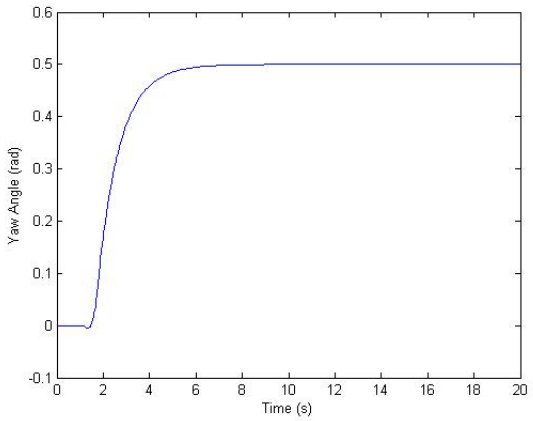

Fig. 3. Attitude Yaw, for $\delta = 0.5$

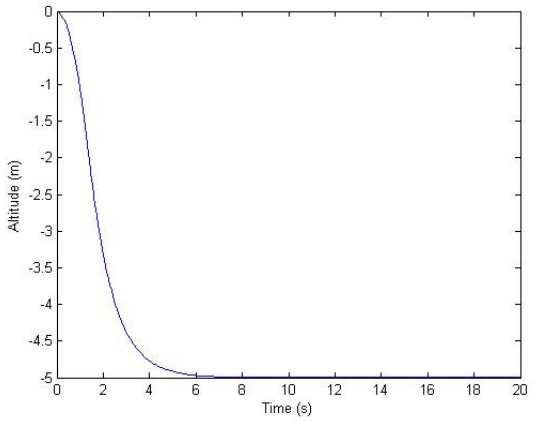

Fig. 4. Altitude Z, for $\delta = 1$

using the state feedback controller and series of experiment confirm our results. The result we get from this paper show that the simplified model of quadrotor can be controlled by more advance adaptive controller technique such as gain scheduling and will be still controllable and observable for all possible equilibrium point.

Acknowledgement

The authors would like to thanks to Japan International for Cooperation Agency (JICA) for their kind support in providing the Collaborative Grant for Researches Alumnae.

References

[1] P. I. Corke, *Robotics, vision and control: fundamental algorithms in MATLAB*, ser. Springer tracts in advanced robotics. Berlin: Springer, 2011, no. v. 73.

[2] S. Gaikwad, S. Dash, and G. Stein, "Auto-tuning PID using loop-shaping ideas," vol. 1. IEEE, 1999, p. 589593. [Online]. Available: http://ieeexplore.ieee.org/lpdocs/epic03/wrapper.htm?arnumber=806712

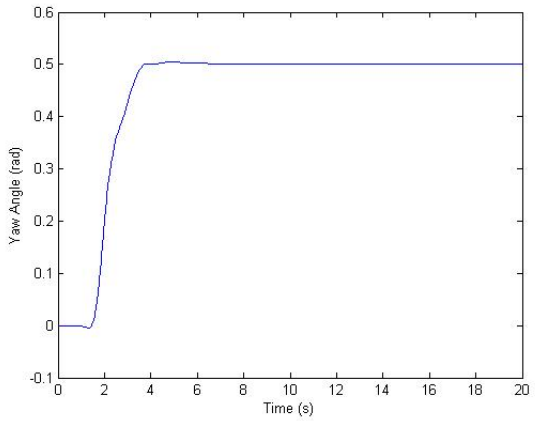

Fig. 5. Attitude Yaw, for $\delta = 1$

[3] H. K. Khalil, *Nonlinear systems*, 2nd ed. Upper Saddle River, NJ: Prentice Hall, 1996.

[4] X. Liu, T. Huang, X. Tang, and H. Xin, "Design of self-adaptive PID controller based on least square method." IEEE, Oct. 2009, p. 527529. [Online]. Available: http://ieeexplore.ieee.org/lpdocs/epic03/wrapper.htm?arnumber=5402780

[5] K. Ogata, *Modern control engineering*, 5th ed., ser. Prentice-Hall electrical engineering series. Instrumentation and controls series. Boston: Prentice-Hall, 2010.

[6] P. Pounds, R. Mahony, and P. Corke, "Modelling and control of a quad-rotor robot," in *Australasian Conference on Robotics and Automation 2006*. Auckland, New Zealand: Australian Robotics and Automation Association Inc., 2006. [Online]. Available: http://eprints.qut.edu.au/33767/

Gadjah Mada University – Shizuoka University Joint Workshop on Telecommunications
Gadjah Mada University, Yogyakarta, Indonesia, December 2–7, 2013

Particle Swarm Optimization Algorithm for Optimal Deployment of Wireless Sensor Network by Taking Into Account of Barrier Position and Attenuation

Masjudin, I Wayan Mustika, Widyawan

Graduate School of Engineering,
Gadjah Mada University
Jl. Grafika No. 2, Kampus UGM, Sleman, Yogyakarta Indonesia
Email: masjudin_s2te_11@mail.ugm.ac.id, {wmustika, widyawan}ugm.ac.id

Abstract

Connectivity is an important part in the deployment of Wireless Sensor Network (WSN). Proper placement of the sensor nodes can reduce the complexity problems in WSN such as routing, data fusion, communication between nodes and etc. This paper studies the optimal deployment of sensor nodes by taking into account the position of barriers and damping effect based on particle swarm optimization algorithm. The research uses two scenarios, the first scenario uses single barrier and the second one uses two barriers. The results show that the sensor node deployment in indoor environment without barrier has the best connectivity compared to that of with barrier. The position of the obstacle also affects the connectivity of the sensor nodes.

1. Introduction

Connectivity is an important part in the deployment of Wireless Sensor Network (WSN). Proper placement of the sensor nodes can reduce the complexity problems in WSNs as, for example, routing, data fusion, communication, etc [1]. In addition, optimal placement of the sensor nodes can extend the node life time and maintain the connectivity among nodes. The existence of wall material in indoor environment could change the routing path and thus affect the data transmission delay between nodes or from node to sink. Propagation attenuation is influenced by the condition of the track around. Attenuation decreases signal quality at the receiver. Study of the radio wave propagation in mobile radio communication shows that the magnitude of the damping rates of propagation is dominated by a percentage of the concrete walls in indoor environment. This suggests a strong correlation between propagation attenuation with propagation constant of a space [2].

There are several algorithms used by researchers to get a good spread of sensor nodes. Obstacle-Resistant Deployment algorithm (ORRD) is used for the deployment of sensor nodes in the area with obstacles. This study involves the robot moving direction and deploy sensors to limit certain areas, and be able to handle the presence of the barrier with regular shape or not. This algorithm is able to deploy sensor nodes using minimal number of sensors with the full area coverage [3].

Subsequent research using Particle swarm optimization algorithm to new mobility control algorithm is to maximize the wireless nano sensor node lifetime and improve the network performance. Simulation results show that the proposed optimization algorithm improves the network coverage by better utilization of neighbor nodes. The results also demonstrate that the algorithm increases nano sensor lifetime [4]. Implementation of the PSO algorithm is also applied to the deployment of sensors to provide fault tolerance in WSN in order prolong its lifetime, to reduce its complexity and to increase the quality of service (QoS) for WSNs applications. Simulation results show that, the proposed algorithm outperforms random deployment in terms of coverage [5].

Particle swarm optimization algorithm is also suitable to be applied on the deployment of sensor nodes without any obstructions in the path (Line Of Sight) which shows the results of the sensor nodes to form a network with good connectivity [6].

This paper will discuss the spread of simulated sensor nodes to see the influence of the barrier position and attenuation against sensor node connectivity in wireless sensor network based algorithm Particle Swarm Optimization (PSO). PSO algorithm is chosen because it has several advantages, such as easy to implement and have fewer functions and operating parameters to be determined [7].

The structure of this paper is as follows: Section II describes the model of wave propagation, Part III particle swarm optimization algorithm is then followed by a test scenario in Section IV and the test results in

Section V. Finally, it is concluded in Section VI.

2. Radio Wave Propagation Model

Radio wave propagation for wireless applications in the space that has a barrier or bulkhead as in the building have different propagation models with space without barriers (Line Of Sight). Attenuation will occur for propagation with barrier. Attenuation effect decreases signal quality at the receiver. Power received in a room with a barrier no longer affected by the distance as in space without obstructions (LOS), but also by the attenuation barrier. On testing wave propagation in space by a barrier, assuming the barrier has a certain attenuation value, and the transmit power received by the base (there are no reflections or wave interference) the attenuation in decibels equation can be formulated as the following equation:

$$L = 32.44 + 20\log f + 20\log d + (\Sigma X), \qquad (1)$$

where :
L : damping of space
f : frequency (MHz)
d : distance between transmitter and receiver (Km)
X : damping value of obstacle / barrier.

In this study, distance (d) is the distance between the sensor nodes in the network, at get the Euclidean distance formula :

$$d = \sqrt{(x_1 - x_2)^2 + (y_1 - y_2)^2} \qquad (2)$$

Strong magnitude of the received signal at the receiver by calculating power loss can be calculated by the following formula :

$$Pr = Pt + Gt + Gr - (32.44 + 20\log f + 20\log d + (\Sigma X)) \qquad (3)$$

with :
P_t : power transmit
G_t : gain of transmitter antenna
G_r : gain of receiver antenna

3. Particle Swarm Optimization

Particle Swarm Optimization is one of the optimization methods inspired by the behavior of herd animals such as fish movements (school of fish), animal herbivor (herd), and birds (flock) of each object are then reduced to a particle animals. This algorithm was introduced by Eberhart and Kennedy in 1995 [8]. The distinctive feature of PSO is the particle velocity settings heuristic and probabilistic. If a particle has a constant speed so if the position of a particle is visualized trail will form a straight line. With the external factors that distort the line and then move the particles in the search space is expected to lead particles, approached, and eventually reach the optimum point. External factors in question include the best position ever visited by a particle, the whole particle best position (assumed to know the best position of each particle every other particle), as well as to explore the creativity factor.

The standard procedure for applying PSO algorithm is as follows:

- Initialize a population of particles with random positions and velocities in a search space dimension.
- Evaluate the desired optimization fitness function in the variable d on each particle.
- Comparing the fitness evaluation with its particle P_{best}. If there is a better value than the value its P_{best}, then P_{best} is set equal to the value and location of the i-th particle at the location of the existing particles (Xi) in d-dimensional space.
- Identification of particles in the environment with the best results so far.
- Update the particle velocity and new position.
- Return to step b until the criteria are met, usually stopping at a pretty good fitness value or until the maximum number of iterations.

Other parameters are known in PSO algorithm is constriction factor, this parameter was introduced by Clerc in order to guarantee a search in PSO algorithm to converge faster [9]. Value constriction factor (K) obtained from the following equation :

$$K = \frac{2}{|2 - \varphi - \sqrt{\varphi^2 - 4\varphi}|}, \quad \varphi = \varphi_1 + \varphi_2, \quad \varphi > 4 \qquad (4)$$

The equation for update the particle velocity and new position as in point (e) by inserting the following constriction factor:

$$v_{id}^{k+1} = K.v_{id}^{k} + c_1.r_1((p_{\text{best}})_k^{id} - x_{id}^{k}) + c_2.r_2((p_{\text{best}})_k^{id} - x_{id}^{k}) \qquad (5)$$

$$x_{id}^{k+1} = x_{id}^{k} + v_{id}^{k+1} \qquad (6)$$

with the provisions of :

$$x_{id}^{k+1} = \begin{cases} x_{id}^{k} + v_{id}^{k+1} & x_{\min} < x_{id}^{k} + v_{id}^{k+1} < x_{\max} \\ x_{\max} & x_{id}^{k} + v_{id}^{k+1} > x_{\max}, \\ x_{\min} & x_{id}^{k} + v_{id}^{k+1} < x_{\min}, \end{cases} \qquad (7)$$

with :
$x_{\min}$ = lower limit problem
$x_{\max}$ = upper limit problem

In this study, PSO parameters used are :

1. Swarm
   Swarm is a collection of particles that make up the population. The recommended size of the swarm range 20-60. Swarm size is too small does not give you many options and solutions particles tend to get stuck at a local optimum solution. While the size of the swarm are too large to provide a global optimum solution, but slows down the process of computing. In this study swarm size used was 30.

2. Particle
   Particle is a member or an individual part of the swarm. A particle will represent a solution. In this study, the position of the particle is a solution of the sensor nodes are randomly generated in a room with a size of 500 x 500 m^2. Coordinate the generation constrained with an upper limit of 500 problems and lower limit 0 in order that the solutions obtained are in the scope of the distribution area. Visualize the particles in 2D coordinates to represent the position of the sensor nodes (x,y)

3. Fitness Function
   The fitness function is an important part of the PSO algorithm. The fitness function is determined according to the research objectives. The focus of this research is to develop a system to design the sensor node deployment in space by taking into account the connectivity barrier is maintained between the sensor nodes on the network. Fitness function in the design of sensor node deployment is determined based on the received power and the number of connections or the number of neighboring nodes are detected at a sensor node with the following provisions :

   - Power received that would otherwise require to connect at -110 dB, greater than the limit of acceptability in the datasheet IQRF -110 dBm or -140 dB. This is because the area of distribution of the measured area is only 500 meters while IQRF transmit power range of 700 meters (1.2 kbps)
   - The deployment is designed to form a network with full connection limits (full mesh) but the connection part (partial mesh) is also allowed because the sensor nodes are used multihoop, because it influences the number of connections into account in the fitness function. In the event of a full connection in the network (full mesh) then the number of connections by $n \cdot (n-1)$ with n the number of sensor nodes

   Based on the foregoing, the fitness function can be mathematically formulated in equation :

$$F_{Xi} = \sum_{0}^{j-1} P_{rk}(x_{id}) - \sum 2^{n(id)-1} \cdot C \quad (8)$$

   with :
   $F(Xi)$= fitness function of particle Xi
   P_{rk} = power receive connected of particle i node d
   n = number of neighboring nodes detected on particle i node d
   C = constant (30)

4. Learning Rate
   Learning rate used in this study φ_1=1,3 and φ_2=2,8 in accordance with the general limitations which are used in the constriction factor φ>4, to balance the cognitive part and the social part of PSO

4. Testing Scenario

The process of testing in this study observe the following :

- Transmit power is included varies according to transmit power range IQRF TR 52B i.e -25 dB, -28 dB, -31 dB and -34 dB with the number of sensor nodes 10, the area of 500 × 500m^2, and used band frequency 868 MHz
- The distribution area is divided by a barrier into 1, 2 and 3 space with the location of the barrier can be set so that the change of the space distribution area of sensor nodes can also be changed
- The value of damping (attenuation) is used in the form of a barrier wall with 6 dB attenuation values, 0.5 inch glass barrier with the attenuation of 2 dB and a wooden barrier with the attenuation of 2.35 dB

Parameters tested at this stage is :

- Testing the influence of the position and number of obstructions in the distribution area to area coverage and network connectivity

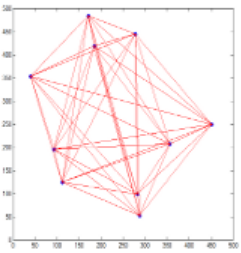

(a) without barrier

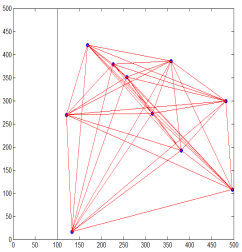

(b) brick wall

Figure 1: Comparison of the results of deployment without barrier with single barrier (barrier coordinates x = 100)

- Testing the effect of different barrier against area coverage and network connectivity
- Assessment of the effect of transmit power to the area coverage and network connectivity

5. Test Result

- The scenario with single Barrier
  Deployment of sensor nodes in the area tested with a single barrier with barrier location coordinates on the x-axis and shifted by a certain amount. Location coordinates barrier removal is intended to look at the influence of placement or position of the barrier on PSO algorithm in sensor nodes deployement. Coordinates barrier placed sequentially on the x-axis = 100, 250, and 400. While the transmit power used is -25 dB, -28 dB, -31 dB, and -34 dB. The test results showed the sensor nodes deployment more sensor nodes spread over a wider area than a smaller area. Large emittance will cover a wider area than the smaller emittance. Insulation material existence which gives the damping has a significant influence on connectivity and sensor coverage area. Different types of barriers also affect the connectivity of the network. This is because the value of the different attenuation of the barrier like a wall of wood with brick walls have different attenuation values that influence the emitted transmitter signal attenuation is also different.

Fig.1 shows the differences in the results of the deployment of sensor nodes with no barriers and obstacles given area using -25 dB transmit power. Both networks can form a full network (full mesh), but the area coverage in the area of sensor nodes with single barrier narrower. For scenarios with the location of the barrier on the x-axis = 100 area with a brick barrier wall, wood and glass still showed results similar deployment.

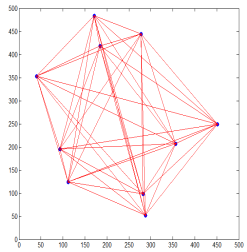

(a) without barrier

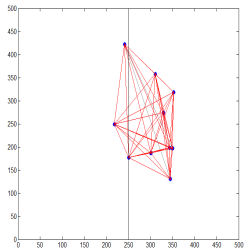

(b) brick wall

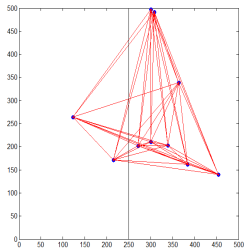

(c) wall of wood

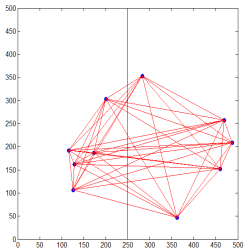

(d) wall of glass

Figure 2: Comparison of the results with the deployment location of the barrier and the different types of barrier

Fig.2 illustrates the results of the deployment of sensor nodes with the transmit power and the same type of barrier to the scenario in Fig.1, but the location of the barrier in the slide to the x-axis = 250. Different barrier locations will provide solutions of different sensor node deployment, although with the same power and the same initial coordinates. This shows the position of the sensor node deployment barriers also affect and Noteworthy. Deployment of sensor nodes in a room with a barrier wall shows the coverage area is small and there are 3 (three) nodes that are not connected in full are marked with gray lines. This indicates the received power is less than -110 dB, but the node is still connected via another node. While in the area of distribution of a given barrier walls of wood and glass, the network can be formed in full (full mesh), but the area coverage in a sensor network with a wooden barrier narrower when compared to sensor networks in the distribution area with a glass barrier. This is due to the damping value is smaller than the value of the glass timber damping. Most of the wall attenuation values resulting in greater attenuation of the transmit power range resulting in a network coverage area into small.

Fig.3 shows the results of the deployment of sensor nodes with -28 dB transmit power, smaller than the emittance of such a scenario in Fig.1 and Fig.2 that

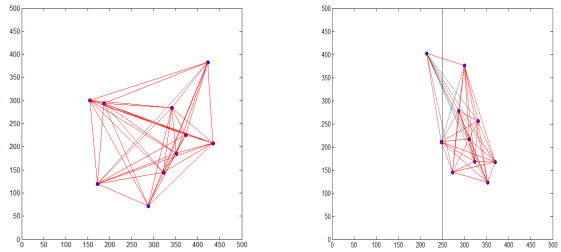

(a) without barrier (b) brick wall

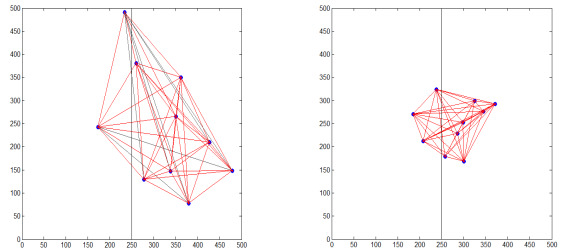

(c) wall of wood (d) wall of glass

Figure 3: comparison of the results with the deployment of smaller emittance

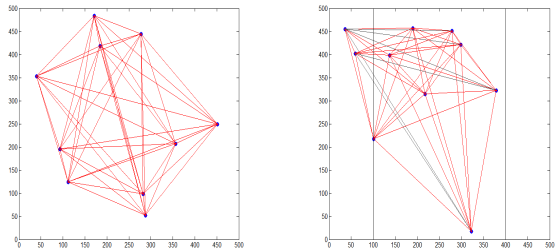

(a) without barrier (b) brick wall

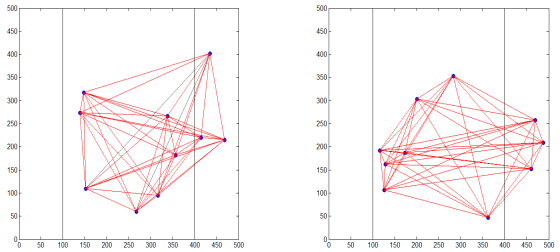

(c) wall of wood (d) wall of glass

Figure 4: Comparison of the results of the deployment of sensor nodes with two barrier

use transmit power -25 dB.

Area coverage of sensors to be smaller and more nodes are not full connected form. Areas with a glass barrier can form a full connections (full mesh) but the coverage area is smaller when compared to scenarios that use transmit power -25 dB. Smaller transmit power will result in wireless sensor networks with smaller coverage areas and fewer connections. From the deployment results of which are shown, sensor nodes deployment is affected by the transmit power, the location of the barrier and the barrier types that have different attenuation values.

- Scenarios with Two Barrier

Testing scenarios using two barrier different transmit power is -25 dB, -28 dB, -31 dB, and -34 dB. To simplify the calculation, using the restriction barrier type scenario is similar to the same space (barrier equal to x_1 and x_2, e.g. wall of wood and wall of wood or brick walls and brick walls) so that the total value of attenuation barrier is a multiple of the value of the attenuation barrier. At best deployment testing results obtained at -25 dB transmit power usage. Just as in the scenario of the barrier, the results of deployment may include a wider area or the maximum number of connections compared to the use of smaller emittance.

Fig.4 shows the results of the deployment of sensor nodes transmit power and -25 dB in the area with two barriers, each of which is placed on the axis $x_1 = 100$ and $x_2 = 400$. Deployment area with no barrier to form a network with full connection (full mesh) and area coverage, while the distribution area of the barrier brick wall to form a partial mesh networks with many nodes that are not connected in full. Area distribution of the barrier wall of wood forming tissues with narrower scope area and there are nodes that are not connected in full. Area distribution of the barrier wall of glass to form a network with full connection but narrower than the distribution area without barrier. If we compare it with the distribution area of the single barrier as shown in Fig 1-3, the number of barriers also affect the results of deployment. In the area with two barrier with the same type of barrier, nodes are connected in full amount less. Suppose the deployment results in the distribution area of the barrier wall of wood that in scenario single barrier can form a full mesh network, in a scenario with two barriers can not form a full mesh network, although the transmit power and position coordinates of the beginning of each sensor node.

Results of sensor node deployment such as in Fig. 5 shows the results of deployment with different barrier positions namely $x_1 = 225$ and $x_2 = 275$. Different barrier positions when compared to the scenario in Fig. 4 shows the influence of the position of the barrier to the results of the sensor node deployment. Deployment results with the same power and the same initial koordi-

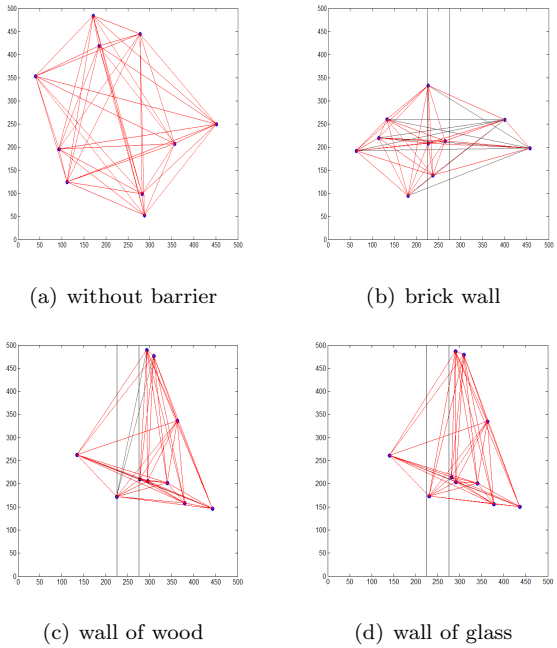

(a) without barrier (b) brick wall

(c) wall of wood (d) wall of glass

Figure 5: comparison of the results of the deployment of sensor nodes with different barrier positions

nant position would be different if the barrier position changed. Different types of barriers will also provide different solutions. Deployment best results obtained on deployment with the highest transmit power and -25 dB in the area without barrier. While the results are less good deployment in get on deployment with small emittance (-34 dB) and the area with the type of barrier brick wall. In the sensor node deployment, deployment results will be affected by the transmit power, the location of the barrier, barrier types and number of barrier.

6. Conclusion

Deployment of sensor nodes in a room with a barrier based on PSO algorithm can form a network with good connectivity. Deployment results show the effect of transmit power, position and attenuation barrier as well as the number of barriers to coverage area and the connectivity of sensor nodes in the network. The existence of a barrier that provides the damping effect of the transmit power make WSN coverage area becomes narrower and connections that occur are not as good as in areas without barrier. System design developed sensor node deployment has several limitations such as uneven sensor deployment, the lack of variation of the barrier in the same room for two-barrier example, using the first barrier and the second barrier walls using wood, as well as the application has not shown that the shortest path can taken at the time of data transmission

References

[1] W. Y. Poe, J. Schmitt, Node deployment in large wireless sensor networks: Coverage, energy consumption, and worst-case delay, ACM,2009.

[2] Indrawati, Amir D, Analisa korelasi konstanta propagasi terhadap redaman propagasi gelombang radio dalam ruang pada komunikasi bergerak, jurnal litek volume 6 nomor 1, hal 11-14, 2009.

[3] C.Y. Chang, C.C. Tsun, C.Y. Chieh, C. H. Ruey, Obstacle resistant deployment algorithm for wireless sensor networks, IEEE vehicular technology 58:6:2925-2941, 2009.

[4] M. Abbasi, M.S.A Latiff, A. Modirkhazeni, M.H. Anisi, Optimization of wireless sensor network coverage based on evolutionary algorithm, IJCCN International Journal of Computer Communications and Networks, Volume 1, 2011.

[5] M. Abbasi, M.S.A. Latiff, Mobility control to improve nanosensor network lifetime based on particle swarm optimization, International Journal of Computer Applications (0975-8887), Volume 30: No.4, 2011.

[6] Z. Saharuna, Widyawan, S. Sumaryono, Deployment jaringan sensor nirkabel berdasarkan algoritma particle swarm optimization, Universitas Gadjah Mada, 2012.

[7] R.L. Haupt, S.E. Haupt, Practical genetic algorithm, 2nd Ed. Hoboken, New Jersey: John Wiley & Sons, Inc. 2004.

[8] R.C. Eberhart, Y.H. Shi, Comparison between genetic algorithm and particle swarm optimization, Evolutionary programming VII: Proc. 1998.

[9] M. Clerc, J. Kennedy, The particle swarm explosion, stability, and convergence in a multidimensional complex space, IEEE Trans. Evolutionary Computation, 6(1):58-73, 2002.

Gadjah Mada University – Shizuoka University Joint Workshop on Telecommunications
Gadjah Mada University, Yogyakarta, Indonesia, December 2–7, 2013

A Game-Theoretic Framework with Utility Improvement for Joint Base Station and Resource Selection in LTE Heterogeneous Networks

Agus Nurcahyo†, Wayan Mustika†, Widyawan†, and Koji Yamamoto††

† Department of Electrical Engineering and Information Technology
Universitas Gadjah Mada, Indonesia
†† Graduate School of Informatics, Kyoto University, Japan
Email: †agus_s2te_11@mail.ugm.ac.id, {wmustika, widyawan}@ugm.ac.id

Abstract

In the present paper, a game theoretic framework with utility improvement in an orthogonal frequency-division multiple access (OFDMA) cellular network is proposed. Inspired by the cognitive radio technology, each mobile node selects the most appropriate base station and resource blocks for uplink transmission in a decentralized manner in order to improve the throughput performance and manage the interference. A utility function is defined for each mobile node, which takes into account the cross- and co-tier interference, and incentive to choose the base station based on the link quality. Such a self-organization scheme can be modeled as a potential game, which is guaranteed to converge to a Nash equilibrium. The simulation results show that the proposed utility improves system capacity in LTE heterogeneous networks.

1. Introduction

Picocells have been proposed as a promising solution for increasing the coverage and capacity of next-generation cellular systems, which will benefit both end-users and network operators. Pico base stations, which are known as pico eNBs (PeNBs) in 3GPP Long-Term Evolution (LTE) terminology, are cost-efficient, low-power, and short-range cellular base stations. They are designed to serve a small coverage area, and they can reuse the licensed spectrum in indoor or outdoor environments [1].

By embedding low-power cellular base stations inside a macrocell coverage, a heterogeneous network (HetNet) is constructed, and thus the benefit in offloading the macrocell traffic and enhancing the system capacity can be obtained [2]. Recently, the concept of HetNet has been extensively discussed for application in LTE and LTE-Advanced [3]. In co-channel operation of HetNet, the spectrum resources can be effectively reused, thereby improving the spectral efficiency. However, densely deployed picocells in an existing macrocell network could introduce excessive uplink interference from macro user equipments (MUEs) to pico eNBs. Therefore, mitigating the cross- and co-tier interference is an indispensable task in HetNet deployment.

In [4] and [5], the feasibility of co-channel operation and interference coordination strategies in HetNets were investigated. In the study reported in [6–8], the authors showed that the interference in HetNets can also be managed by resource partitioning, range expansion and power control techniques. In addition, the authors of [9] proposed a cognitive radio resource management scheme for an OFDMA network. This scheme can be used to mitigate the interference while providing quality-of-service (QoS) guarantee in HetNets.

The other techniques for mitigating the interference and enhancing the system capacity in co-channel operation of HetNets are self-organization and access control mechanisms. Self-organization refers to the ability of an autonomous entity to join to the network, learn the surrounding environment, and allocate the resource accordingly, without the assistance of a network operator. Access control refers to the connectivity rights of the users for using a low-power base station. Two approaches of access control are identified: closed access and open access. These techniques are mainly discussed in [10–12]. Our previous work in [13] showed that network convergence can be guaranted in the proposed scheme.

As a contribution to this work, a game theoretic framework with utility improvement in an orthogonal frequency-division multiple access (OFDMA) cellular network is proposed. Inspired by the cognitive radio technology, each UE acts as an autonomous entity and attempts to choose the most appropriate strategy combination of eNB and resource blocks (RBs) to maximize its respective utility. The performance of the proposed scheme is analyzed using a game-theoretic approach by defining a utility function for each UE, which takes into account the cross- and co-tier interference, and incentive to choose eNB based on the link quality. In general, the best response strategy, which is defined as the best of strategy of a player in response to the current

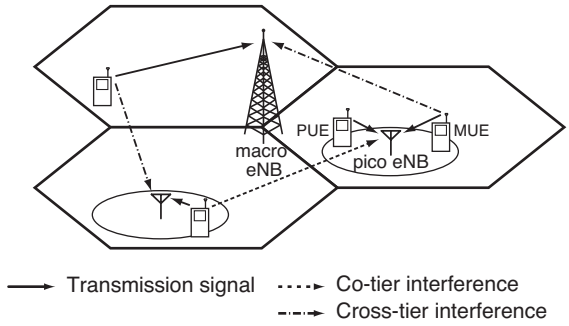

Figure 1: System model for uplink transmission of HetNet with cross- and co-tier interference scenario.

strategies of the other players, may not converge to a Nash equilibrium (NE). However, when the joint base station and resource selection can be formulated as a potential game, the best response strategy of players is guaranteed to converge in a finite number of steps to the NE [14]. The NE, which is the most widely-used solution concept in a non-cooperative game, corresponds to a steady-state condition that can be used in analyzing the performance of the proposed scheme. Thus, in order to improvement performance utility, we consider weighting value in cros and co-tier interference. Finaly, a weight value in the utility function is adjusted.

The remainder of this paper is structured as follows. The system model of a LTE HetNet is described in Section 2. Section 3 describes the proposed self-organization scheme for joint base station and resource block selection based on potential game approach. The evaluation of the effectiveness of the proposed scheme is presented in Section 5. Finally, the conclusion is presented in Section 6.

2. System Model

We consider the uplink transmission in an HetNet with cross- and co-tier interference, as shown in Fig. 1. Cross-tier interference refers to the interference between different network tiers, i.e., interference between picocell tier and macrocell tier or vice versa. In addition, interference may occur between neighboring picocells, which is known as co-tier interference. In the LTE OFDMA system, the system bandwidth W is divided into K RBs, in which an RB is defined as the smallest time-frequency resource unit that can be allocated to a UE. P outdoor pico eNBs are randomly deployed in each sector of macro eNBs. There are U_{M} macro UEs (MUEs) and U_{P} pico UEs (PUEs) that are randomly distributed in each sector of macro eNBs and in each picocell, respectively. Thus, the total number of UEs in three sectors of the macrocell site can be calculated as $N = 3(U_{\mathrm{M}} + PU_{\mathrm{P}})$.

The co-channel operation of macro- and picocells is considered such that interference occurs when the UEs in different cells transmit using the same RB. Each sector of the macro eNBs can reuse all the spectrum resources in order to improve the spectrum utilization. As a consequence, each MUE also experiences significant interference from the other MUEs and PUEs in the nearby sectors. Furthermore, perfect synchronization of OFDMA network is assumed.

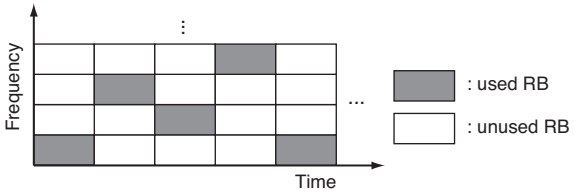

Figure 2: Frame structure of the resources in an LTE OFDMA system. A UE utilizes multiple RBs for uplink transmission; the used RBs are represented by the shaded blocks.

3. Potential Game Approach for Joint Base Station and Resource Selection

3.1. Game Theoretic Framework

We model the self-organization scheme as a strategic non-cooperative game that has three major components: players, strategies, and utilities. The players are UEs (MUEs and PUEs), which are assumed to have cognitive radio capabilities. The strategy of UE i is the combination of eNB and subset of RBs, $s_i = (b_i, \mathcal{R}_i) \in \mathcal{S}_i$, where $b_i \in \mathcal{B}$ is the eNB that is selected by UE i from the set of eNBs $\mathcal{B}$. The set of eNBs consists of the sectors of macro eNB and pico eNBs. $k_i^{(l)} \in \mathcal{R}_i$, $1 \leq l \leq L$, is an element of the subset of RBs $\mathcal{R}_i$ selected by UE i and $|\mathcal{R}_i| = L$, $\forall i \in \mathcal{N}$, is the number of elements in the subset of RBs $\mathcal{R}_i$. It is assumed that the number of elements in $\mathcal{R}_i$ (L) is predefined at the initial assignment. As shown in Fig. 2, a UE utilizes $L = 5$ RBs for transmission. The utility of UE i is a function of cross- and co-tier interference, and incentive to choose eNB based on the link quality.

In general, the strategic form game can be mathematically defined as $\Gamma = \left\{\mathcal{N}, \{\mathcal{S}_i\}_{i\in\mathcal{N}}, \{u_i\}_{i\in\mathcal{N}}\right\}$. The finite set of players and the set of strategies associated with player i are denoted as $\mathcal{N}$ and $\mathcal{S}_i$, respectively. The utility function, $u_i : \mathcal{S} \rightarrow \mathbb{R}$, maps each possible combination of the strategies of all players, $\mathcal{S} = \prod_{i\in\mathcal{N}} \mathcal{S}_i$, to a real value $\mathbb{R}$. The utility function, which can be used by the players to measure their respective utility, represents the degree of satisfaction of player i as a function of the strategy chosen

by player i, s_i, and the strategy of the other players, $\boldsymbol{s}_{-i} = (s_1, \ldots, s_{i-1}, s_{i+1}, \ldots, s_N)$.

3.2. Proposed Joint Base Station and Resource Selection based on Potential Game Approach

The most widely-used solution concept in a non-cooperative game is the Nash equilibrium, which represents a steady-state condition resulting when none of the players deviate from their respective strategies because if they deviate from their strategies, their respective utility would not increase [15]. A set of pure strategy profiles of all players, $\boldsymbol{s}^\star = (s_i^\star, \boldsymbol{s}_{-i}^\star) \in \mathcal{S}$, is a Nash equilibrium if and only if the following condition is satisfied:

$$u_i(s_i^\star, \boldsymbol{s}_{-i}^\star) \geq u_i(s_i', \boldsymbol{s}_{-i}^\star), \forall s_i' \neq s_i^\star, \forall s_i' \in \mathcal{S}_i, \ \forall i \in \mathcal{N}. \quad (1)$$

A potential game [16] is a type of non-cooperative game where the convergence to a pure strategy Nash equilibrium can be guaranteed as long as sequential play based on the best response strategy is adopted. The best response of player i to the strategy profile $\boldsymbol{s}_{-i}$ at time $t+1$, $s_i^{(t+1)}(\boldsymbol{s}_{-i})$, is the strategy that satisfies the following condition [14]

$$s_i^{(t+1)}(\boldsymbol{s}_{-i}) \in \arg\max_{s_i' \in \mathcal{S}_i} u_i(s_i', \boldsymbol{s}_{-i}^{(t)}), \quad (2)$$

where $(s_i^{(t)}, \boldsymbol{s}_{-i}^{(t)}) \in \mathcal{S}$ represents the strategy profile at time t.

A strategic game is called an exact potential game if there exists a potential function $P : \mathcal{S} \to \mathbb{R}$ with the following properties

$$P(s_i', \boldsymbol{s}_{-i}) - P(s_i, \boldsymbol{s}_{-i}) = u_i(s_i', \boldsymbol{s}_{-i}) - u_i(s_i, \boldsymbol{s}_{-i}), \quad (3)$$

where $s_i' \in \mathcal{S}_i$, $\forall i \in \mathcal{N}$. From (3), it can be inferred that the information related to the improvement path of a game can be modeled using the potential function if the improvement in the utility of a player as a result of deviating from the player's strategy is equal to the improvement in the potential function. In general, the best response strategy does not always converge to a Nash equilibrium. However, when a game can be modeled as a potential game with a finite set of strategies, the best response strategy of all players will terminate in a finite number of steps to a Nash equilibrium, regardless of the initial condition of the game and the order of the sequential play [14].

In this paper, UEs, which are assumed to have cognitive radio capability, are able to dynamically sense the available spectrum, measure the interference received and estimate their interference contributions on their neighbors, and intelligently tune their transmission parameters by selecting the most appropriate combination of eNB and the subset of RBs in order to improve the throughput performance. As shown in Fig. 3,

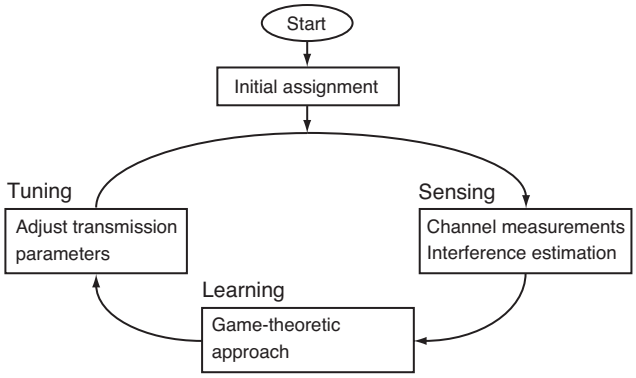

Figure 3: Self-organization cycle of the proposed scheme.

the proposed scheme consists of three main phases that resemble the cognitive cycle [17]: sensing phase, learning phase, and tuning phase.

In the sensing phase, the UE i observes its surrounding environment and obtains the information required for the learning purpose, such as the channel gain to the neighboring eNBs. The control messages are transmitted on a common control channel where the information of the channel gains of the UEs is exchanged through this channel. In order to reduce the signaling overhead during this phase, a local information exchange based on interference power threshold is considered. Thus, UE i exchanges the control message to the neighboring eNBs within a radius of information exchange, where the radius is determined by the interference power threshold I_{th}. We note that the amount of information exchange during this phase depends on the interference power threshold I_{th}. Decreasing I_{th} will allow UEs to learn more potential interferers since the radius of information exchange increases. However, since the radius of information exchange increases, the complexity of the proposed system will increase due to an increase of information exchange during this phase.

In the learning phase, a game theoretic approach is used to model and analyze the interactions among UEs, in which the outcome of these interactions can be predicted and the set of strategies that satisfies the utilities of all UEs can be identified. Using this approach, each UE tries to evaluate its utility for every strategy combination of eNB and the subset of RBs, given the current strategies of the other UEs. The proposed utility function for each UE in the LTE HetNet

can be represented as follows:

$$u_i(s_i, \boldsymbol{s}_{-i}) = \sum_{x=1}^{L}\sum_{y=1}^{L}\left(- \sum_{j=1, j\neq i}^{N} G_{b_i,j} p_j h_{b_i,j} \delta_{k_i^{(x)} k_j^{(y)}} - \sum_{j=1, j\neq i}^{N} G_{b_j,i} p_i h_{b_j,i} \delta_{k_j^{(y)} k_i^{(x)}} \right) + \alpha G_{b_i,i}\, p_i h_{b_i,i}. \quad (4)$$

where $G_{b_i,j}$ denotes the link gain between the UE j and eNB that is selected by the UE i, p_j denotes the transmit power of UE j in each selected RB, x and y are the index of elements of subset of RBs selected by UE i and j, and $\delta_{k_i^{(x)} k_j^{(y)}}$ is the interference function that indicates whether or not the elements of the set of selected RBs by the UE i and j are the same: if $k_i^{(x)} = k_j^{(y)}$, $\delta_{k_i^{(x)} k_j^{(y)}} = 1$; otherwise, $\delta_{k_i^{(x)} k_j^{(y)}} = 0$. Assuming that the total transmit power of UE i is divided equally among the selected RBs, a radius function from UE i to eNB that is selected by UE j, denoted by $h_{b_j,i}$, indicates whether or not UE i and eNB that is selected by UE j are on the same radius of information exchange:

$$h_{b_j,i} = \begin{cases} 1, & G_{b_j,i} p_i \geq I_{\text{th}}, \\ 0, & G_{b_j,i} p_i < I_{\text{th}}, \end{cases} \quad (5)$$

where p_i denotes the transmit power of UE i in each selected RB and $G_{b_j,i}$ denotes the link gain between UE i and eNB that is selected by UE j.

The first two terms in the proposed utility function take into account the total interference received by eNB that is selected by UE i and the interference that is potentially generated by UE i. The last term depends only on the strategy chosen by UE i, which captures the incentive to make a handoff to eNB based on the link quality with an incentive factor α.

Given the proposed utility function u_i, we formulate the potential function as

$$P(s_i, \boldsymbol{s}_{-i}) = \sum_{i=1}^{N}\left[\sum_{x=1}^{L}\sum_{y=1}^{L}\left(-\frac{1}{2}\sum_{j=1, j\neq i}^{N} G_{b_i,j} p_j h_{b_i,j} \delta_{k_i^{(x)} k_j^{(y)}} - \frac{1}{2}\sum_{j=1, j\neq i}^{N} G_{b_j,i} p_i h_{b_j,i} \delta_{k_j^{(y)} k_i^{(x)}} \right) + \alpha G_{b_i,i}\, p_i h_{b_i,i}\right]. \quad (6)$$

The proof to show that the proposed utility function u and potential function P are an exact potential game is given in the Appendix.

The last part of the learning phase is the best response strategy as explained in (2). In the best response strategy, the UE selects the most appropriate strategy combination of eNB and RBs in response to the strategies of the other UEs.

In the tuning phase, the UE adjusts its transmission parameters such as eNB and the subset of RBs according the result of the learning phase. This can be done by updating its strategy combination of eNB and the subset of RBs, and informs all neighboring UEs about the selected strategy by sending the control message on the common control channel. The selected strategy is the strategy that maximizes the utility of the corresponding UE, given the current strategies of the other UEs.

4. Utility Improvement

Utility improvements is obtained by multiplying a weight value with the potential interference create and interference received in the proposed function. so in order to seek improved system performance, the utility improvement function is proposed to evaluate the utility function.

$$u_i(s_i, \boldsymbol{s}_{-i}) = \sum_{x=1}^{L}\sum_{y=1}^{L}\left(-n_r \sum_{j=1, j\neq i}^{N} G_{b_i,j} p_j h_{b_i,j} \delta_{k_i^{(x)} k_j^{(y)}} - n_c \sum_{j=1, j\neq i}^{N} G_{b_j,i} p_i h_{b_j,i} \delta_{k_j^{(y)} k_i^{(x)}} \right) + \alpha G_{b_i,i}\, p_i h_{b_i,i}. \quad (7)$$

Evaluation of the utility is done by running the game until the nash equilibrium conditions and take the last value of the game. the game will be repeated with a combination of values of different n_{c} andn_{r}. Each game is complete will take the last system throughput value, and compare these values to get the highest value would indicate an improvement in the utility function

5. Performance Evaluation

5.1. Simulation Model

We consider a network with 19 cell sites, each of which has three hexagonal sectors as shown in Fig. 4. The inter-site distance (ISD) is 500 m, which is in accordance with the 3GPP simulation assumption case 1 [2]. Tri-sector antenna with 120° beamwidth at each sector of macro eNBs is assumed [18]. In each sector of macro eNBs, 10 MUEs are randomly and uniformly distributed. Thus, 30 MUEs exist in a macrocell site during network setup. Outdoor pico eNBs are randomly deployed in each sector of macro eNBs, which are equipped with omnidirectional antennas. 2 PUEs are randomly distributed inside the picocell coverage area. The performance statistics of three central sectors are observed, while the other sectors of different

Table 1: Simulation parameters

Parameters	Values
Cellular layout of macrocell	Hexagonal grid, 19 cell sites 3 sectors per site
Cellular layout of picocell	Circular cell, 1 sector per cell
Macrocell picocell radius	288.68 m (ISD = 500 m), 40 m
Macro path loss	$128.1 + 37.6 \log_{10}(d_{\mathrm{m}}[\mathrm{km}])$ dB[2]
Pico path loss	$140.7 + 36.7 \log_{10}(d_{\mathrm{p}}[\mathrm{km}])$ dB[2]
Shadowing standard deviation	8 dB (macro), 10 dB (pico)
Macro eNBX	$A_{\mathrm{H}}(\theta) = -\min\left[12\left(\frac{\theta}{\theta_{3\,\mathrm{dB}}}\right)^2, A_{\mathrm{m}}\right]$ $\theta_{3\,\mathrm{dB}} = 70°$and $A_{\mathrm{m}} = 20\,\mathrm{dB}$
standard deviation	
Pico eNB antenna	Omnidirectional
Antenna gain eNB	14 dBi (macro), 5 dBi (pico)
Antenna gain UE	0 dBi
UE power class	23 dBm
Thermal noise density	−174 dBm/Hz
Number of pico eNBs (PeNBs)	4 PeNBs/sector
Number of UEs	10 MUEs/sector, 2 PUEs/pico eNB
Min. distance macro eNB-MUE	35 m
System/RB bandwidth	10 MHz (System), 180 kHz (RB)
bandwidth	
Number of RBs	50
Carrier frequency	2 GHz
Incentive factor α	1.0
Traffic model	Full buffer
Number of topologies	500

cell sites are considered only as the interference contributors.

To enhance the spectrum utilization, co-channel operation of HetNet is considered; and thus, all spectrum resources can be reused in every sector of macrocells and in each picocell. We consider 10 MHz system bandwidth, which constitutes a total of 50 RBs. With respect to the strategy space, each UE utilize 5 RBs ($L = 5$) for uplink transmission. At the initial assignment, these RBs are randomly selected under the condition that interference between MUEs in the same sector of macro eNB, which is known as intra-tier interference, is avoided. For the sake of simplicity, we assume that the effect of fast fading is averaged out. Furthermore, it is assumed that the total transmit power is divided equally among the selected RBs. The other relevant parameters used in the simulation are summarized in Table 1.

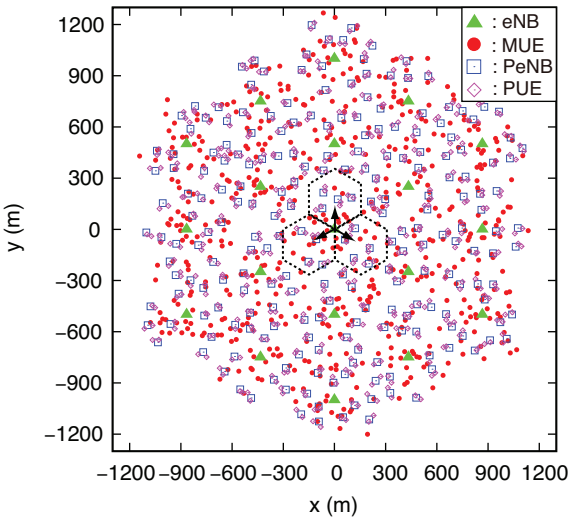

Figure 4: Simulation model of HetNet with 19 macrocell sites.

5.2. Simulation Results

Figure 5 shows the evaluation of the utility function with system throughput at the end of each game with different combinations of n_{c} and n_{r}. The highest value of throughput system showed the best combination of n_{c} and n_{r}. As show figure 5 the best performance is achieved when n_{c} and n_{r} are set to 2 and 6. Thus, the optimal utility function can be formulate as

$$u_i(s_i, \boldsymbol{s}_{-i}) = \sum_{x=1}^{L}\sum_{y=1}^{L}\left(-6\sum_{j=1,j\neq i}^{N} G_{b_i,j}p_j h_{b_i,j}\delta_{k_i^{(x)}k_j^{(y)}} - 2\sum_{j=1,j\neq i}^{N} G_{b_j,i}p_i h_{b_j,i}\delta_{k_j^{(y)}k_i^{(x)}}\right) + \alpha G_{b_i,i}\, p_i h_{b_i,i}. \quad (8)$$

Figure 6 and 7 shows the impact of the interference power threshold I_{th} during sensing phase on the convergence of system throughput. The system throughput represents the sum of the throughput of all UEs

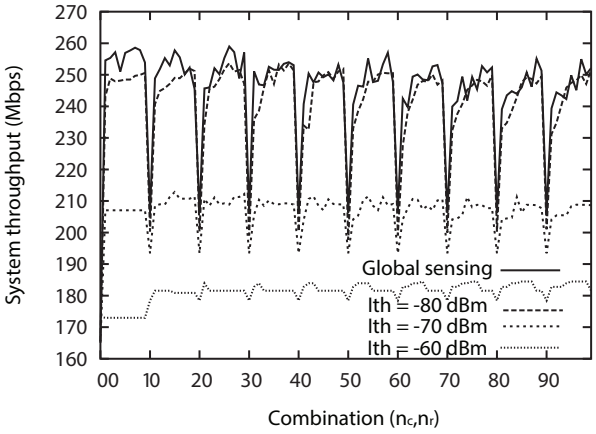

Figure 5: System throughput in each game with combination n_{c} and n_{r}.

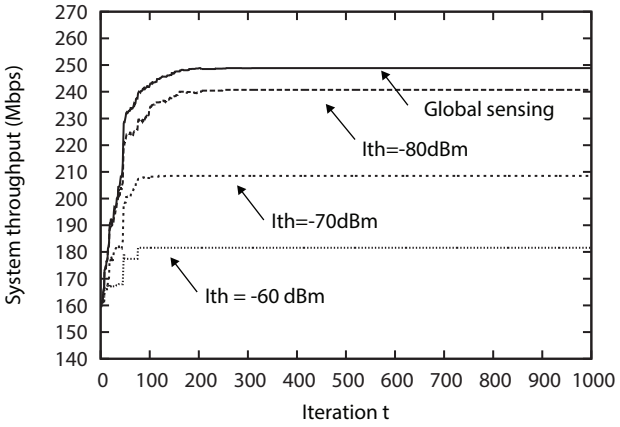

Figure 6: Impact of parameter I_{th} on the convergence of system throughput.

(MUEs and PUEs) in the central macrocell site and the throughput of UE i that utilizes L RBs can be calculated as

$$T_i = W_{\mathrm{RB}} \sum_{l=1}^{L} \log_2(1 + \gamma_{k_i^{(l)}}), \tag{9}$$

where W_{RB} is the RB bandwidth and $\gamma_{k_i^{(l)}}$ is the received SINR on RB l. Starting with the initial assignment ($t = 0$) where each UE connects with its initial eNB (either macro eNB or pico eNB) and randomly selects the subset of RBs for transmission, each UE sequentially goes through the phases of the self-organization cycle shown in Fig. 3. In the final phase, the UE updates its strategy so as to maximize its own utility, and this eventually improves the system throughput. After some iteration steps, the steady-state condition, which also indicates the convergence to a Nash equilibrium, is reached. At this point, no UE can improve its own utility by choosing another strategy combination of eNB and subset of RBs that is different than its best one.

From Figure 6 and 7 we also see that the system throughput at the convergence state decreases as I_{th} increases. In other words, there is a trade-off between the system throughput at the convergence state and the radius of information exchange, which is determined by the value of I_{th}. Using the global information during the sensing phase, which is referred to as global sensing, the upper bound of the system throughput at the convergence state is achieved. However, this is impractical in a large network since the UE has to exchange the information to all eNBs in the network.

Figure 7 shows the system throughput improved when compared with figure 6. This proves the utility evaluation to obtain the optimal utility function can improve the capacity system.

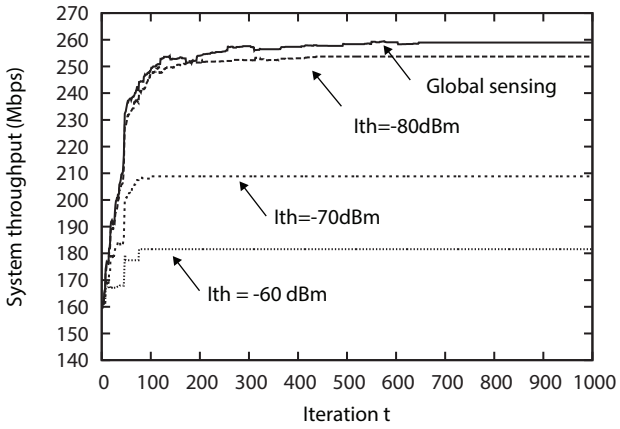

Figure 7: Impact of parameter I_{th} on the convergence of system throughput using optimal utility function.

6. Conclusion

A game theoretic framework with utility improvement in an orthogonal frequency-division multiple access (OFDMA) cellular network is proposed in this paper. Inspired by the cognitive radio technology, each mobile node selects the most appropriate base station and resource blocks for uplink transmission in a decentralized manner in order to improve the throughput performance and manage the interference. The proposed a game theoretic framework with utility improvement can be modeled as a potential game, which is demonstrated to converge to a Nash equilibrium as long as distributed sequential play based on the best response strategy is adopted. The simulation results show that the proposed scheme improves the system capacity.

References

[1] V. Chandrasekhar, J. Andrews, and A. Gatherer, "Femtocell networks: A survey, " *IEEE Commun. Mag.*, vol. 46, no. 9, pp. 59–67, Sep. 2008.

[2] 3GPP TR 36.814 v9.0.0, "Evolved Universal Terrestrial Radio Access (E-UTRA); Further advancement of E-UTRA physical layer aspects (Release 9)," Mar. 2010.

[3] S. Brueck, "Heterogeneous networks in LTE-Advanced," *Proc. 8th International Symposium on Wireless Communication Systems (ISWCS '2011)*, pp.171–175, Aachen, Germany, Nov. 2011.

[4] H. Claussen, "Performance of macro- and co-channel femtocells in a hierarchical cell structure, " *Proc. 18th IEEE International Symposium on Personal, Indoor, and Mobile Radio Communications (PIMRC '07)*, vol. 1, pp. 1–5, Athens, Greece, Sep. 2007.

[5] Y. Li, M. Peng, and W. Hu, "Adaptive heterogeneous interference coordination algorithm in uplink LTE-Advanced systems," *Proc. 23rd IEEE International Symposium on Personal Indoor and Mobile Radio Communications (PIMRC '12)*, pp. 536–540, Sydney, Australia, Sep. 2012.

[6] R. Madan, J. Borran, A. Sampath, N. Bhushan, A. Khandekar, T. Ji, "Cell association and interference coordination in heterogeneous LTE-A cellular networks," *IEEE J. Sel. Areas Commun.*, vol. 28, no. 9, pp.1479–1489, Dec., 2010.

[7] C.-S. Chiu and C.-C. Huang,"An interference coordination scheme for picocell range expansion in heterogeneous networks," *Proc. IEEE VTC '12-Spring*, Yokohama, Japan, May 2012.

[8] D. López-Pérez, I. Guvenc, G. de la Roche, M. Kountouris, T.Q.S. Quek, J. Zhang, "Enhanced Inter-cell Interference coordination challenges in heterogeneous networks," *IEEE Wireless Commun.*, vol. 18, no. 3, pp.22–30, Jun., 2011.

[9] S.-Y. Lien, C.-C. Tseng, K.-C. Chen, and C.-W. Su, "Cognitive radio resource management for QoS guarantees in autonomous femtocell networks," *Proc. IEEE ICC '10*, Cape Town, South Africa, May 2010.

[10] D. López-Pérez, A. Ladányi, A. Jüuttner, and J. Zhang, "OFDMA femtocells: A self-organizing approach for frequency assignment," *Proc. IEEE PIMRC '09*, pp. 2202–2207, Tokyo, Japan, Sep. 2009.

[11] D. Choi, P. Monajeni, S. Kang, and J. Villasenor, "Dealing with loud neighbors: The benefit and tradeoff of adaptive femtocell access," *Proc. IEEE GLOBECOM '08*, New Orleans, LA, USA, Dec. 2008.

[12] D. Das and V. Ramaswamy, "Co-channel femtocell-macrocell deployments — Access control," *Proc. IEEE VTC '09-Fall*, Anchorage, Alaska, USA, Sep. 2009.

[13] I. W. Mustika, Agus Nurcahyo, Widyawan, Koji Yamamoto "A Game-Theoretic Framework for Joint Base Station and Resource Selection in LTE Heterogeneous Networks," *Proc. APCC '13*, Bali, Indonesia, September 2013.

[14] M. Voorneveld, "Best-response potential games," *Economic Letters*, vol. 66, pp. 289–295, Mar. 2000.

[15] D. Fudenberg and J. Tirole, *Game Theory*. MIT Press, 1991.

[16] D. Monderer and L. S. Shapley, "Potential games," *Journal of Games and Economic Behavior*, vol. 14, pp. 124–143, May 1996.

[17] J. Mitola, "Cognitive radio: An integrated agent architecture for software defined radio," Doctor of Technology Dissertation, Royal Institute of Technology (KTH), Stockholm, Sweden, 2000.

[18] 3GPP TR 36.942 v10.1.0, "Evolved Universal Terrestrial Radio Access (E-UTRA); Radio frequency (RF) system scenarios (Release 10)," Sep. 2010.